

**UCSF**

**UC San Francisco Electronic Theses and Dissertations**

**Title**

Characterization of the human intervertebral disc with magnetic resonance imaging

**Permalink**

<https://escholarship.org/uc/item/0gd5b6s5>

**Author**

Chiu, Elaine Jannine

**Publication Date**

1998

Peer reviewed|Thesis/dissertation

Characterization of the Human Intervertebral Disc  
with Magnetic Resonance Imaging

by

Elaine Jannine Chiu

DISSERTATION

Submitted in partial satisfaction of the requirements for the degree of

DOCTOR OF PHILOSOPHY

in

Bioengineering

in the

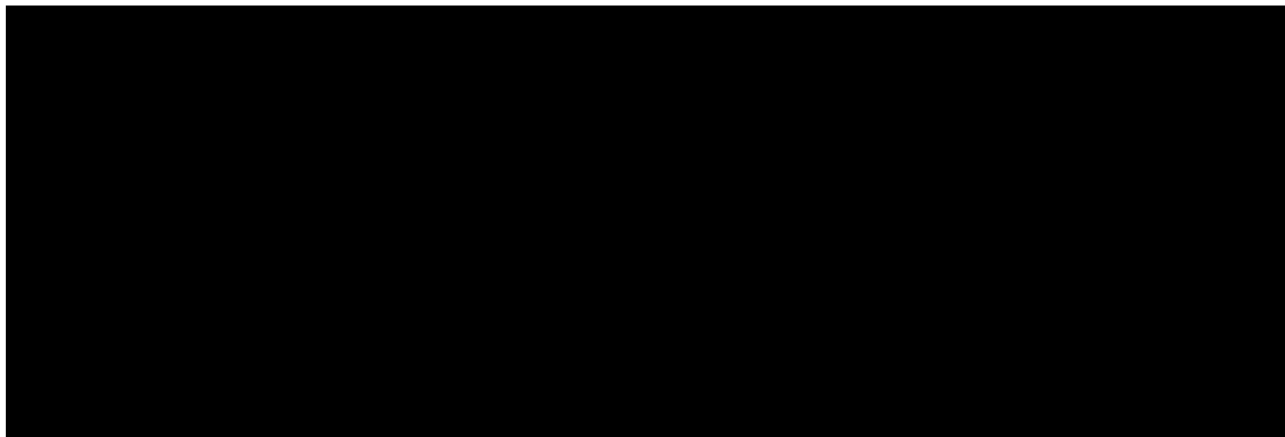
GRADUATE DIVISIONS

of the

UNIVERSITY OF CALIFORNIA SAN FRANCISCO

and

UNIVERSITY OF CALIFORNIA BERKELEY



Date

University Librarian

Degree Conferred: .....

copyright 1998

by

**Elaine Jannine Chiu**

I wish to dedicate this dissertation  
to the memory of my grandmother

**Pearl K. Lowe,**

who was always there when we needed her,  
always supportive and loving,  
brilliant and energetic to the end,  
creative and resourceful.

May I accomplish half of what you did in life, Grandma.

I miss you, and your spirit lives on with me.



## ACKNOWLEDGEMENTS

I am extremely grateful to the following people for all their help and support during this Ph.D. period of my life. I wish to say "**Thank You**" to...

**Thomas and Louise Chiu**...for supporting me through this period of career and life changes...for giving me enough space to figure out what I needed to do in life...

**Jamila and Dolly Champsi**...for encouraging me from the time that I left medicine to start this Ph.D. to the time now that I'm writing and returning for clinical research...  
for letting me crash at their place whenever I was too tired to go home...  
for letting me raid the frig. for that homemade dahl...

**Frank Ashford**...for helping with the computers, the MTS, the specimen cutting...  
the technical factors around the orthopedic biomechanics lab., even on  
the off-hours that I sometimes had to work...

**Moira Heilman**...for helping me build so many lab. fixtures, compression devices and other projects...for sharing her extraordinary mechanical talents in helping design those projects and find the parts...for keeping me from killing myself with the lathe...

**Evelyn Proctor and Niles Bruce**...for holding my hand when I first started scanning, showing me which buttons to push...

**Margaret Lobo**...for showing me what the realities of research life are...for doing the "Money, Money, Money" dance when we got the OREF grant...

**David Bradford**...for believing in my research enough to support me through the year that we resubmitted the grant which eventually funded this dissertation project...

**Jeff Lotz**...for being the first person to introduce me to this idea of compressing a disc in the MR scanner...for being there so consistently and patiently through all the ups and downs of the project...

**Lucas Carvajal**...for asking me the hard questions and making me explain things to myself...for joining me at the Won Ton House for those late meals and discussions...for all the times swimming together...

**Debra Harris**...for guiding me through the bureaucracy and politics of the two campus Bioengineering group...for supporting me through my time as BEAST V.P., dealing with Stan and the Exec....for respecting and acknowledging my spiritual path...

**Bruce Hasegawa**...for being a mentor to me from my first rotation as a Bioengineering student through Qualls, Exec. meetings, Bioengineering politics, to the end of this process...for keeping me well fed at that Japanese restaurant Akagi in San Bruno...

**David Newitt**...for letting me bounce innumerable stupid questions off him about MR, IDL, computers, electronics, physics, the universe...for getting up early for those 8 AM scans... for helping me debug my primitive IDL code...for keeping me laughing with all those silly emails we keep forwarding to one another...  
for bringing me those dark chocolate Milky Way bars...

**Sharmila Majumdar**...for screaming at me to get things done...for regularly checking up on me to see how I was doing...for writing all those letters of recommendation that got me fellowships and, soon, my next job in life...for constantly challenging me to think about things... "You Guys!!!!" still echoes around the MRSC hallway and in my head...

**Janet Linder**...for being a friend, advisor and teacher on how to deal with life... for helping me learn to deal with the feelings, since they really don't go away if ignored...for helping me to figure out who I really am, and how not be afraid to be that person in the world...for teaching me to accept myself as I am...

**Tammy Gardner**...for strongly guiding me towards a spiritual path in life... for appearing in my life at the darkest, most difficult times, helping me to see what I often already knew...for telling me what to do at times when I needed that... for taking good care of J.C....

and, finally, to...

**Ellen Dayton**...for being there though so many ups and downs during graduate school, my life, and this dissertation...for supporting me in whatever decisions I thought were best for me...for being so patient with my social unconsciousness in the early years...for helping me to return to the path of clinical medicine...for being my life partner and sharing so much with me in the last four years...for believing in me through it all... may there be many more years to share together.

**Grant funding for this project was provided by the following:**

Orthopaedic Research and Education Foundation:

Serena S. Hu, M.D. and David C. Newitt, Ph.D.

Radiology Research and Education Foundation: Sharmila Majumdar, Ph.D. et al.  
Arbeitsgemeinschaft für Osteosynthesefragen/ Association for the Study of Internal Fixation (AO/ASIF): John Antoniou, M.D.

University of California, San Francisco, Student Research Awards: Elaine J. Chiu

**Graduate student support was provided by the following:**

National Institutes of Health, Bioengineering Student Training Grant  
University of California, San Francisco, Graduate Opportunity Fellowships  
University of California, San Francisco, Mentorship Fellowships  
Department of Orthopaedic Surgery, University of California, San Francisco  
University of California, San Francisco, Regents' Fellowships  
Orthopaedic Research and Education Foundation

Biochemical tissue analysis was performed in the laboratory of Mauro Alini, Ph.D. with John Antoniou, M.D. at the Orthopaedic Research Laboratory, Royal Victoria Hospital, McGill University, Montreal, Canada

## **ABSTRACT**

### **CHARACTERIZATION OF THE HUMAN INTERVERTEBRAL DISC WITH MAGNETIC RESONANCE IMAGING:**

- 1) MR Relaxation, Water Diffusion and Internal Displacements within the Disc with Compressive Loading;**
- 2) Relationship of Tissue Biochemistry to MR parameters: D, T1 and T2**

**by**

**Elaine Jannine Chiu**

Disorders of the intervertebral disc are an important cause of lost work and disability. Magnetic Resonance Imaging (MRI) has been used to visualize the disc for bulging and herniation.

The goal of this project was to use MRI to study the human intervertebral disc under compression, followed by mechanical testing. If possible, a model was to be developed to predict the creep behavior of the disc from the non-invasive MR parameters. Changes in the MR relaxation times, water diffusion and internal fiber displacements before and after compressive loading were measured. The effects of differences in the grade of disc degeneration and the anatomic region - peripheral annulus fibrosus or central nucleus pulposus - on the MR parameters were also studied.

The second goal of this project was to study the relationship between the MR parameters and the tissue biochemistry by using subspecimens of tissue from the intact discs.

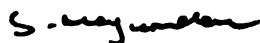
For the MR relaxation times, significant differences were found by region, by loading state and by grade of degeneration. For water diffusion, significant differences were found by region, loading state, diffusion direction and grade of degeneration. High resolution images were able to resolve the annular fiber deformation in some specimens.

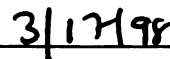
A water transport model was used to quantify the disc creep behavior. The creep parameters from the model correlated well with the degree of degeneration, and weak trends were found between MR derived water content and creep parameters.

For the biochemical analysis, tissue hydration was the most consistent predictor of the MR parameters. The collagen content was an additional factor for  $1/T_1$ , and the location of the tissue was an additional factor for  $1/T_2$ .

In summary, this project showed that MRI could be used to measure diffusion in the intervertebral disc *in vitro*, with significant differences found by location, direction, grade of degeneration and with compression. High resolution images could resolve annular fiber deformation before and after loading. For tissue biochemistry, hydration was the most predictive factor for the MR parameters. Finally, there was a weak correlation between the creep parameters and the MR derived water content of the disc tissue.

Approved by Sharmila Majumdar, Ph.D.





date

## TABLE OF CONTENTS

I. INTRODUCTION .....	1
II. GOALS OF THIS PROJECT .....	1
III. SPECIFIC AIMS .....	2
IV. SIGNIFICANCE .....	3
V. BACKGROUND .....	4
Anatomy .....	4
Biochemistry .....	7
Aging and Degeneration .....	10
Modeling the Creep Behavior of the Disc .....	11
Viscoelastic Models .....	12
Water Transport Model .....	14
Specimen Preparation; Temperature and Storage Effects .....	20
Magnetic Resonance Imaging .....	21
Diffusion Measurements with MRI .....	24
Diffusion Tensor Imaging .....	29
VI. MATERIALS/METHODS .....	30
Overview .....	30
Specimen Preparation .....	34
Specimen Testing .....	36
MR scanning .....	37
Subspecimen Preparation for Water Content Alteration .....	41
Hydration Assay .....	43
Biochemical Assay .....	43
VII. DATA ANALYSIS/MODELING .....	44
Analysis of T1, T2 Data .....	44
Analysis of Diffusion Data .....	46
Analysis of High Resolution Images .....	46
Analysis of Creep Data .....	48
Statistics .....	56
VIII. RESULTS .....	58
PRELIMINARY DATA .....	58
Reproducibility of T1, T2 Measurements in Liquids .....	58
Diffusion-Weighted Imaging of Liquids and IVD Specimens .....	59
Reproducibility of Diffusion Coefficient Estimation for Liquids .....	59
Measured Diffusion Under Stress Relaxation of Disc Specimens .....	60
High Resolution Midsagittal Images .....	61
Diffusion Tensor Imaging .....	62
Altering Tissue Hydration with PEG Solutions .....	64
A) MR Relaxation .....	67
B) Diffusion .....	68
C) High Resolution Midsagittal Images .....	70
D) Creep Models .....	71
E) Effect of Tissue Biochemistry on MR Parameters .....	74
F) Predicting Creep Parameters from MR Parameters .....	82
IX. DISCUSSION .....	82
A) MR Relaxation .....	82
B) Diffusion .....	84
C) High Resolution Midsagittal Images .....	85
D) Creep Models .....	86
E) Effect of Tissue Biochemistry on MR Parameters .....	89
F) Predicting Creep Parameters from MR Parameters .....	92
X. CONCLUSIONS .....	92
XI. FUTURE WORK .....	93
XIII. REFERENCES .....	94

## LIST OF TABLES

Table 1	Comparison of Creep Data from Published Studies	18-19
Table 2	Lumbar disc specimens used for this project.	31
Table 3	Thompson grading scheme for human intervertebral disc degeneration.	31
Table 4	Overview of the results to be presented. Lettered headings correspond to the results sections that discuss these findings in detail.	66
Table 5	Correlations between the creep parameters and Thompson grade, and the creep parameters and MR parameters, including specimens 3, 4 and 5, that had the LVDT problem.	67
Table 6	Mean T1 values (ms.) by loading state, region (NP or AF) and grade. T11 and T12 denote T1 before and after compression.	68
Table 7	Mean T2 values (ms.) by loading state, region and Thompson grade. T21 and T22 denote T2 before and after compression.	68
Table 8	Mean normalized diffusion coefficients by region and Thompson grade. DX1 and DX2 refer to before and after loading. The X, Y or Z refers to the diffusion direction measured.	69
Table 9	Water transport model parameters derived from the curve fits.	72
Table 10	3 parameter solid model parameters derived from the curve fits.	72
Table 11	4 parameter solid model parameters.	73
Table 12	Mean hydroxyproline and GAG ( $\mu\text{g}/\text{mg}$ dry weight), shown by location and Thompson grade.	75
Table 13	Summary of analysis of covariance results, showing which variables predicted the MR parameters, after adjusting for the effects of other covariates.	79
Table 14	MR parameters $\pm$ standard deviation, by Thompson grade.	80
Table 15	Univariate correlations of MR parameters with grade, location and biochemical factors.	81

## LIST OF FIGURES

Figure 1	Midsagittal diagram of a human intervertebral disc. Note the attachments of the annular lamellae to the vertebrae and the end-plates.	5
Figure 2	Peeled-away view of the disc. Note the alternating fiber directions in the adjacent annular lamellae.	6
Figure 3	Nucleus pulposus supporting an applied external load to the intervertebral disc.	7
Figure 4	Three parameter viscoelastic model with two springs and one dashpot.	13
Figure 5	Four parameter linear solid model with two springs and two dashpots, also defined as two Kelvin bodies in series.	13
Figure 6	Four parameter linear Burger's fluid model with two springs and two dashpots, also defined as one Kelvin body in series with a Maxwell unit (a spring and dashpot in series).	14
Figure 7	Schematic of the water transport model, showing the end-plate with permeability $K$ , the applied stress $\sigma$ , and the hydrostatic pressure within the disc $P_d$ .	15
Figure 8	Spin echo timing diagram in one dimension.	23
Figure 9	MR timing diagram with diffusion gradients added in the x, y and z directions, with amplitude of $G_i$ , duration of $\delta$ , and time between diffusion gradients of $\Delta$ , and including the imaging gradients in the three directions.	26
Figure 10	Thompson grade 1 disc	32
Figure 11	Thompson grade 3 disc	32
Figure 12	Intervertebral Disc Specimen Protocol.	33
Figure 13	Perspective view of the first nonmagnetic compression apparatus. Note the screw mechanism to the left and the force transducer to the right of the photograph.	35
Figure 14	Perspective view of the second compression device that was designed to apply step loads rather than step displacements. The non-magnetic stainless steel pneumatic cylinder (upper right) was pressurized with nitrogen gas to apply the loads.	35
Figure 15	Midsagittal image of an L4-L5 intervertebral disc for diffusion estimation with 10 x 10 pixel (2.5 mm. square) ROI's selected. The central three ROI's were considered nucleus pulposus and the peripheral four ROI's annulus fibrosus.	39
Figure 16	Normalized signal intensity versus the applied diffusion gradient. A gaussian curve fit was done, and the diffusion coefficient was calculated from this fit.	41
Figure 17	Six harvested nucleus pulposus specimens from one disc, prior to wrapping in dialysis membrane.	42

Figure 18	Sectioning map of the intact disc specimens, with a table showing PEG concentrations (gm./100cc 0.15M saline) used for the tissue subspecimens.	43
Figure 19	Graph of specimen temperature versus time from the beginning of the MR scan. An equation was fit to this graph to use for estimating the temperature at different points during the first seven specimens' scans.	45
Figure 20	Midsagittal image of an L4-L5 disc, age at death = 39 years, Thompson 2. Image on left is before compression, image on right is after compression.	47
Figure 21	Specimen 2 of the study, showing a tumor that had allowed the IVD to break through the inferior vertebral body. Inward annular bulging is seen for the annular fibers in the anterior disc (the right side of the image).	47
Figure 22	3 parameter solid model curve fit for specimen 10 (age = 37 years at time of death, Thompson grade 1), $r = 0.998$ , solid line is the curve fit.	49
Figure 23	4 parameter solid model curve fit for specimen 10 (age = 37 years at time of death, Thompson grade 1), $r = 0.998$ , solid line is the curve fit.	50
Figure 24	Water transport model curve fit for specimen 10 (age = 37 years at time of death, Thompson grade 1), $r = 0.999$ , solid line is the curve fit.	51
Figure 25	Water transport model curve fit for specimen 13 (age = 62 years at time of death, Thompson grade 3), $r = 0.999$ , solid line is the curve fit.	52
Figure 26	Water transport model curve fit for specimen 7 (age = 62 years at time of death, Thompson grade 4), $r = 0.997$ , solid line is the curve fit.	53
Figure 27	Normalized diffusion versus tissue hydration for the subspecimens of specimen 12. A graph like this was used to estimate nuclear tissue water from each of the intact specimens' images.	56
Figure 28	T1 and T2 relaxation measurements for a young and old IVD, shown by region, nucleus pulposus or annulus fibrosus.	59
Figure 29	Bar graph comparing the water diffusion coefficient, normalized to saline diffusion, measured with modified spin echo techniques for intact old and young intervertebral discs, by region - annulus fibrosus or nucleus pulposus, and before and after a step displacement	60
Figure 30	Midsagittal image of an L2-L3 intervertebral disc, before (left image) and after (right image) applying axial compression.	61
Figure 31	Example of water contents resulting from equilibrating tissue subspecimens from one disc in PEG solutions.	64
Figure 32	Plot of the percentage change in height or AP diameter of the disc, measured from the midsagittal FSE image, by Thompson grade.	71



Figure 33	K (m <sup>4</sup> /N.sec.), the permeability parameter from the water transport model, graphed versus Thompson grade. $r_s = 0.883, p = 0.003$	74
Figure 34	Normalized diffusion, x direction, all specimens $y = -1.06 + 1.98 x, r = 0.74, p < 0.001$	76
Figure 35	1/T1 versus collagen content $y = 0.000679 + 7.77 e^{-06}x, r = 0.37, (p = 0.0001)$	77
Figure 36	1/T2 vs. collagen content $y = 0.016 + 9.44 e^{-5} x, r = 0.27, p < 0.001$	78
Figure 37	1/T2 vs. GAG content $y = 0.0266 - 3.38 e^{-05}x, r = 0.30, p < 0.001$	79
Figure 38	Hydration vs. GAG content $y = 0.721 + 0.000320 x, r = 0.28, p < 0.001$	80
Figure 39	Hydration vs. collagen content, $y = 0.794 - 0.000377x, r = 0.11, p = 0.14$	81

# **CHARACTERIZATION OF THE HUMAN INTERVERTEBRAL DISC WITH MAGNETIC RESONANCE IMAGING:**

- 1) MR Relaxation, Water Diffusion and Internal Displacements within the Disc with Compressive Loading;**
- 2) Relationship of Tissue Biochemistry to MR parameters: D, T1 and T2**

## **I. INTRODUCTION**

In industrialized societies, disorders of the intervertebral disc (IVD) are an important cause of lost work and disability. Low back pain, which includes disorders of the disc, represents "the single greatest and most inefficient expenditure of health care resources in our society today" [1]. The lifetime prevalence of low back pain is thought to be between 60-90%, with the annual incidence about 5%.

In spite of the large number of affected individuals and years of spine research, there still exists an incomplete understanding of the mechanisms involved that lead to disc bulge and rupture. The behavior of the mechanically loaded disc is a complex function of disc age, its water content, and the degree of degeneration.

Magnetic Resonance Imaging (MRI) is currently used to clinically assess the intervertebral disc for bulging or herniation. The high water content of the IVD makes it an excellent region to assess with MRI. Additionally, the anatomic location of the IVD had made it difficult to assess noninvasively before MRI, requiring injection of contrast followed by fluoroscopy or a CT scan to visualize its structure.

## **II. GOALS OF THIS PROJECT**

The first goal of this project was to use MRI to collect data *in vitro* for use in modeling the behavior of the lumbar intervertebral disc. Long term this would allow work towards a model that could provide clinical predictive ability, noninvasively, for patients with possible disease of the IVD.

MRI was used before and after compressive loading to measure T1 and T2 relaxation within the disc tissue, to measure water diffusion within the disc, and to follow the movements of fibers within the IVD.

The second goal of this project was to study the relationship between the MR parameters and the tissue biochemistry: water, proteoglycan and collagen contents.

Using the disc specimens that had been imaged under compression, subspecimens were created and subjected to solutions to alter their hydration. These subspecimens of tissue were imaged to estimate diffusion, T1 and T2; then, biochemical assays were done on the dehydrated tissue.

### **III. SPECIFIC AIMS**

**A) By means of MRI spin-echo techniques, the characteristic relaxation times, T1 and T2, of different areas of the disc will be found. The values of T1 and T2 will be studied for differences related to region and grade of degeneration, followed by the changes in T1 and T2 with compression.**

**B) By modifying the spin-echo sequence with additional magnetic field gradients, one can use MRI to measure water diffusion. Diffusion MR sequences will be used to study water diffusion in three directions within the IVD, both before and after axial compression.**

**C) High resolution MR sequences will allow mapping fiber displacements within an intact IVD, with differences expected between the degenerated and normal discs.**

**D) The mechanical behavior of the IVD is highly dependent on the hydration level of the nucleus pulposus. Given an accurate measure of the**

**hydration level of the IVD, the mechanical properties of the disc may then be predicted.**

**E) The relative importance of tissue biochemistry, water content and grade of degeneration on the MR parameters will be investigated using a multivariate regression.**

#### **IV. SIGNIFICANCE**

In industrialized societies, disorders of the intervertebral disc have a tremendous impact because of the physical morbidity of affected patients as well as the financial effects of lost productivity and increased health care costs. Approximately 4.1 million Americans, or more than 1% of individuals between the ages of 17 to 64 years, report disorders of the intervertebral disc annually. In the United States, back pain is the second leading cause of work absenteeism (following upper respiratory complaints) and results in more lost productivity than any other medical condition [2]. Displacement of the intervertebral disc ranks third (after chronic ischemic heart disease and osteoarthritis) as the most frequent condition for which worker disability is approved. Furthermore, disc disorders resulted in an average of 334,000 hospitalizations annually from 1985 to 1988, with a total average of 2.3 million hospital days per year [3]. Estimates of direct costs of back pain in the year 1990 were 24.3 billion dollars, with more than 50 billion in indirect costs (lost wages, worker compensation) annually [4].

Studies have shown that certain repetitive environmental loading situations result in a higher incidence of disc disease [5]. Some of these situations involve heavy repetitive lifting, pushing, pulling [4, 6] or repetitive vibrations, like truck driving [6-8]. The unsupported sitting position has been found to have the highest measured intradiscal pressure of relaxed postures [9]. The time-dependent behavior of the intervertebral disc under a sustained load seems a reasonable experimental model for these exposures.

The goal of this project was to develop a model of mechanically loaded intervertebral disc behavior that would help clinical assessment of the disc. The use of diffusion MR sequences would allow noninvasive assessment of disc hydration beyond T1 and T2 estimates, while the characterization of fluid flow with these sequences would advance our understanding of disc physiology. For patients already undergoing MRI for suspected disc pathology, such MR sequences could be added to provide functional information about the individual's disc.

In particular, it was hoped that developing a disc model would allow improved assessment of those discs that may be at risk for disruption, permit better counseling of people with abnormal discs as to what behaviors may put their disc at risk, and better guide the treatment of intervertebral disc conditions. With better understanding of the dynamic behavior of the disc, physiologic disc repair or replacement techniques may also become feasible.

This project is also significant in that no researcher has thus far used high resolution MRI and diffusion sequences in dynamic studies of the intervertebral disc.

## **V. BACKGROUND**

### **Anatomy**

The intervertebral disc consists of three parts: the central gelatinous nucleus pulposus, the surrounding annulus fibrosus and the cartilaginous end-plates adjacent to the vertebral bodies above and below (Figure 1) [10-13]. The nucleus pulposus is about 85% water and the annulus fibrosus about 78% water, decreasing to about 70% with aging.

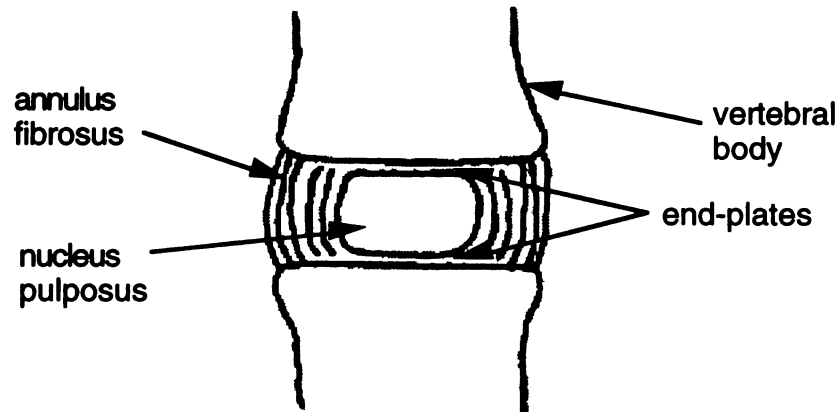


Figure 1: Midsagittal diagram of a human intervertebral disc. Note the attachments of the annular lamellae to the vertebrae and the end-plates.

The nucleus pulposus consists of a loose network of delicate fibrous strands with a water content that is highest at birth and decreases with age. The nucleus has a high concentration of proteoglycan (>50% of the dry weight) with a lower concentration of collagen, primarily type II [14].

The annulus fibrosus is that portion of the disc that becomes differentiated from the periphery of the nucleus and forms the outer boundaries of the disc. The transition between the nucleus and the annulus becomes progressively less discrete with age. The annulus is a laminated structure composed of lamellae of coarse collagen fibers, running obliquely between the adjacent vertebral bodies. The fibers run the same direction within a given lamellae and at approximately 60 degrees relative to those in adjacent lamellae (Figure 2) [14].

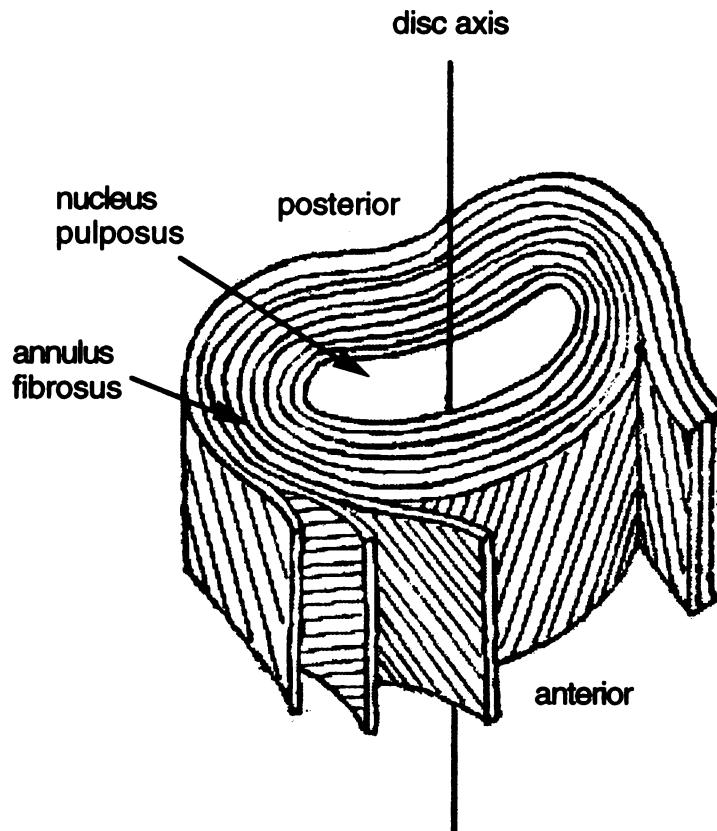


Figure 2: Peeled-away view of the disc. Note the alternating fiber directions in the adjacent annular lamellae.

The cartilaginous end-plates cover the end surfaces of the opposed vertebral bodies and serve as the cranial and caudal surfaces of the intervertebral disc. They are composed predominantly of hyaline cartilage. The inner lamellae of the annulus attach to the end-plates to form a closed vessel containing the nucleus, in contrast to the outer lamellae that are attached to the bone of the vertebral bodies. The outer lamellae may provide strength during twisting and bending while the inner lamellae provide strength and nuclear containment during compression [14].

With an increase in nuclear pressure due to axial compression, tension increases in the end-plates and inner lamellae, with possible bulging of the end-plates into the vertebral bodies (Figure 3) [14]. A roughly cylindrical sealed pressure vessel is created by the end-plates and the inner lamellae surrounding the nucleus. The contained hydrated gel within

the annular walls will then redistribute axial loads in all directions to the end-plates and annulus.

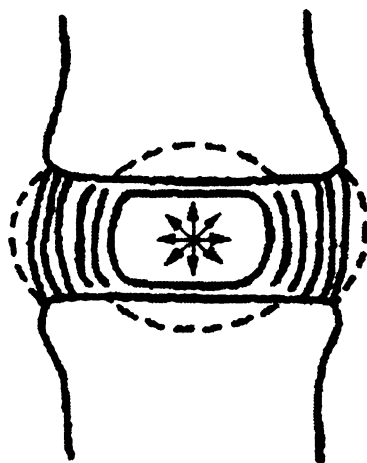


Figure 3: Nucleus pulposus supporting an applied external load to the intervertebral disc.

The intervertebral disc is the largest avascular structure in the human body. Transport by diffusion is the primary mechanism for transport of nutrients and cellular waste products, with the cyclic pumping of compression of tissues contributing relatively little to small solute transport [15]. Disc nutrition depends entirely on passive diffusion from vessels in the vertebral body near the endplate or circumferentially through the annulus fibers [16].

### **Biochemistry**

Given its acellular (about 4-5 cells/cc. [16]) and avascular structure, the intervertebral disc extracellular matrix is responsible for the tissue's biomechanical behavior. The extracellular matrix consists primarily of collagen and proteoglycan. The collagen lattice is believed to prevent unfolding of extended proteoglycan structures and to limit osmotic swelling. Collagen provides the tissue tensile properties, while the polyanionic proteoglycans imbibe water and give the tissue stiffness in compression [10].

Collagen content in the disc ranges from 60-70% of the dry mass in the outer annulus to 10-20% in the central nucleus pulposus. The predominant collagen in disc tissues is type II, although types I, III, V, VI, IX and XI are also present. Collagen



content is greatest in the outer lamellae of the annulus fibrosus and decreases toward the center of the disc. Type II predominates in the nucleus pulposus, gradually switching to type I in the outer most annulus. [10, 14]

Proteoglycans imbibe water through their fixed negative charge, which results in the swelling pressure responsible for extending tissues and maintaining disc height under load [14, 17]. Proteoglycan content increases toward the center of the nucleus pulposus. Each proteoglycan monomer is composed of polyanionic glycosaminoglycan chains covalently bonded to a protein core. Each glycosaminoglycan contains at least one sulfate ester, where the net negative charge of the monomer comes from the  $\text{SO}_4^{-2}$  and the  $\text{CO}_2^{-}$  groups. Chondroitin-6-sulfate and keratan sulfate II, in approximately equal amounts, are the two main glycosaminoglycans in the disc [10].

The noncollagenous proteins, which could constitute up to 45% of the dry weight of the nucleus and 25% of the annulus, include fibronectin, elastin, unnamed 58 kDa. and 59 kDa. proteins found in cartilage, degradative enzymes and other proteins in smaller quantities [10]. The small amounts of these proteins relative to other tissues in the human body have led to the belief that they have a small biomechanical role in the intervertebral disc, though there is little known about the composition or properties of these proteins [18].

The intervertebral disc is a complex structure, described as viscoelastic, heterogeneous, and anisotropic [13]. Its characteristic of viscoelasticity is particularly difficult for investigators attempting to characterize mechanical behavior. Part of this difficulty results from the dependence of the mechanical properties on tissue hydration [19, 20].

The disc derives its physical properties, in part, by its ability to retain water through the proteoglycans' fixed negative charge. The extracellular matrix tends to swell due to the increased osmotic gradient within the matrix exerting a "swelling pressure" that enables it to support an applied compressive load. The steady-state water content of the disc is therefore

determined by the balance between the osmotic pressure and the external load. Sustained application of external loads on the spine will cause fluid shifts into or out of the disc [21, 22], resulting in a change in the steady-state balance between the swelling pressure and the external force on the disc. Diurnal changes in disc height are a physiologic example of this phenomenon, where one loses disc height during the day and regains disc height over night while laying horizontally [19, 23].

Due to differences between the extracellular matrix and structure of the nucleus pulposus and annulus fibrosus, one would expect that compressive loading would have different effects in these regions. Ohshima et al. [24] demonstrated that although the swelling pressure rises in proportion to the applied compressive load in the nucleus pulposus and the inner layer of the annulus fibrosus, few changes occur in the outer layer of the annulus fibrosus. As a result, changes in steady-state load on the disc can result in dramatic changes in the stress distribution within the disc. McNally and Adams found that when the spine is loaded in compression, there is a shift in the load distribution between that carried by the nucleus and that carried by the annulus [25]. Normally, the majority of the compressive load transmitted to the spine is supported by the nucleus; however, with fluid movement out of the disc and loss of nuclear water, large compressive loads can be transmitted to the annulus, which may result in potential structural injury to the annulus [26].

Abnormal bulging of the inner annular fibers radially inward has been hypothesized to be part of the development of weakening of the annular ring that leads to herniation of the nucleus pulposus or fibrotic annulus fibrosus [27, 28]. Yasuma et al. [29] documented pathologic evidence to support this theory.

Fluid movements result in significant changes in the mechanical behavior of disc. Andersson and Schultz investigated the effect of changes in nuclear pressure produced by fluid injection on the mechanical response of the spine [30]. They noted increased stiffness after fluid injection into the nucleus and concluded that the nuclear state of hydration is an

important determinant of mechanical behavior. In a review article on the diurnal changes in spinal mechanics, Adams and coworkers [19] reported that changes in disc height, compressive stiffness, disc bulging, apophyseal joint loading, forward bending properties, backward bending properties and potential for traumatic prolapse were all attributable to changes in disc hydration.

### **Aging and Degeneration**

By the third decade of life, the distinction between the nucleus and the annulus is gradually lost as the nucleus becomes replaced by fibrocartilaginous tissue. Meanwhile, there is a decrease in proteoglycan, water and noncollagenous protein content with an increase in collagen content. Collagen fibers increase in number and in diameter in all parts of the disc with aging [10]. Collagen fibers increase in the posterior compared with the anterior quadrants of the disc, with more type I collagen found posteriorly. Proteoglycan monomers decrease in size and exhibit less aggregation with aging. The decrease in proteoglycan content with age parallels the decrease in water content.

The process of degeneration of the intervertebral disc may not be the same as the normal aging process. Attempts to differentiate the aging process from that of degeneration have been difficult [10]. Similarities between degenerated and aged discs include decreased water content, decreased proteoglycan content and increased collagen. However, Pearce et al. [31] found similar biochemical contents in discs from the same spine for degenerated and normal discs. Other contrasts between degenerated and aged discs are found in differences in the collagenolytic and elastinolytic enzymes, where changes in these enzymes correlated with degeneration, but not age. Significant morphologic degeneration is rare if normal proteoglycan content is present, but whether a decrease in proteoglycan is a cause or effect of degeneration is not known [10]. From a mechanical standpoint, many elderly joints are just as strong in torsion or compression as the younger ones. Also, degenerative joints appear stiffer than normal, but fail before healthier ones. This is a typical mechanical

characteristic of scar tissue, and scar tissue implies that there was previous injury to the area [32].

### **Modeling the Creep Behavior of the Disc**

Previous research on the intervertebral disc has shown it to have a complex response to mechanical loads. This response is time-dependent and includes fluid shifts between the disc and the surrounding environment [24, 25] as well as creep of the collagen fibers in the annulus [33, 34]. This mechanical response is critically dependent on the fluid content of the disc. A study by Wilder et al. [35] found an increase in the instability of discs after exposure to one hour of sustained loading, and this gave experimental evidence to support a mechanism for the epidemiologic observation of an association between the seated environment and both low back pain and acute herniated discs.

Creep is defined as the slow deformation of a body after the application of a sudden stress (force per unit area) that is maintained over time (i.e. a step load). In contrast, stress relaxation is the decrease in stress in a body after the application of a sudden strain (change in length divided by the initial length) that is maintained over time (i.e. a step displacement). [36]

For vertebral spinal units, Kazarian [28] found that, compared to healthy discs, degenerated discs crept at a faster rate, equilibrated in less time and deflected more distance. In general, the higher the grade of degeneration, the less time to equilibration. Additionally, the effect of creep was to reduce the compliance of the spinal unit, by increasing the modulus of elasticity with time.

Methods for characterizing or predicting the creep behavior of the intervertebral disc have included both closed-form analytic and finite element analysis techniques. Using an analytic approach, Broberg [37, 38] developed a model for the disc under creep loading and estimated that one fourth of the disc height change was due to viscoelastic deformations of the annular fibers as compared to loss in height due to fluid movement.

Burns et al. [39] demonstrated that for 47 human intervertebral discs *in vitro*, the compressive creep behavior was well characterized using either a three-parameter or four-parameter viscoelastic solid model (mean errors between experiment and theory were 2.31 and 4.45 percent, respectively). Similar success in characterizing the creep behavior of discs using a three-parameter viscoelastic model was reported by Keller et al. [40], with older and more degenerated discs having faster creep rates and lower material constants than younger, less degenerated discs. Li et al. [41] found a decrease in the creep time constant, in  $E_1$  (elastic element constant) and in  $\mu$  (viscous element constant) with increasing disc degeneration.

Cassidy et al. [42] developed a model for the creep response based upon water transport across the cartilage endplates due to the pressure gradient from the applied external stress. Good agreement was found between the model and canine experimental data, and a disc system permeability was derived. This model was shown to be equivalent to the four-parameter viscoelastic fluid model [43].

More recently, the use of finite element analysis that includes poroelastic-swelling behavior has demonstrated the potential to characterize the time-dependent state of stress present within the disc in addition to predicting the time-dependent mechanical response [44].

### **Viscoelastic Models**

The three-parameter standard linear model consists of two springs and a dash-pot (Figure 4). After the application of a step load, the strain as a function of time can be written as follows:

$$\frac{\varepsilon(t)}{\sigma_o} = \frac{1}{E_1}(1 - e^{-t/\tau}) + \frac{1}{E_2}$$

where  $\varepsilon(t)$  = strain as a function of time  $t$

$\sigma_o$  = applied constant stress (MPa.)

Equation 1 [45]

$E$  = elastic modulus (MPa.)

$\tau$  = relaxation time constant

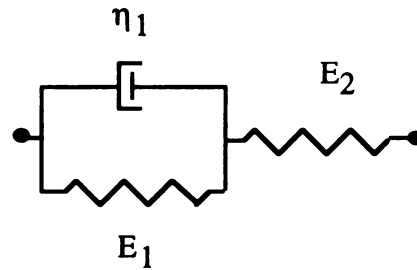


Figure 4: Three-parameter viscoelastic model with two springs and one dashpot.

The second term on the right-hand side of equation 1 is associated with the initial elastic deformation, while the first term on the right-hand side is the primary creep term, which is associated with a delayed elastic deformation. The viscous damping constant,  $\eta$ , (GPa. s.) can be calculated from the elastic modulus and the time constant:  $\eta = E\tau$ . The three-parameter viscoelastic model is considered a solid model and will show finite deformation at finite loads: strain will approach a constant as time approaches infinity.

The four-parameter linear solid model considers two Kelvin units (a spring and a dashpot in parallel) connected in series (Figure 5). The strain as a function of time is given by the following:

$$\frac{\varepsilon(t)}{\sigma_o} = \frac{1}{E_1}(1 - e^{-t/\tau_1}) + \frac{1}{E_2}(1 - e^{-t/\tau_2})$$

Equation 2 [39]

where  $\eta_i = E_i \tau_i$

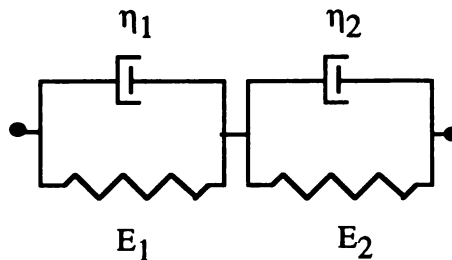


Figure 5: Four-parameter linear solid model with two springs and two dashpots, also defined as two Kelvin bodies in series.

This model is again a solid model, and it will approach a constant value of strain as time approaches infinity.

The four-parameter Burger's fluid model has two springs and two dashpots, as shown in Figure 6. This model is described by the following equation:

$$\frac{\varepsilon(t)}{\sigma_o} = \frac{1}{E_1} (1 - e^{-t/\tau_1}) + \frac{1}{E_2} + \frac{t}{\eta_2} \quad \text{Equation 3 [45]}$$

where  $\eta_1 = E_1 \tau_1$

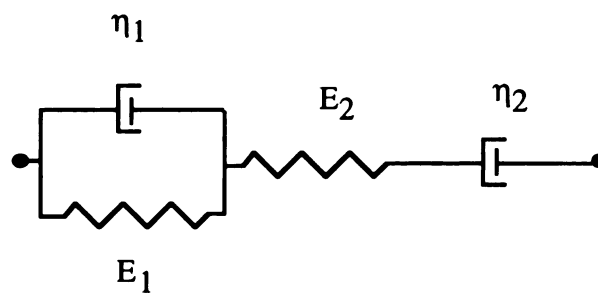


Figure 6: Four-parameter linear Burger's fluid model with two springs and two dashpots, also defined as one Kelvin body in series with a Maxwell unit (a spring and dashpot in series).

The last term on the right side of Equation 3 is the secondary creep term, associated with the stationary viscous deformation. The damping constant,  $\eta_2$  (GPa. s.), represents a form of normalized linearly increasing displacement. The Burger's model is a fluid model, and it will therefore show infinite deformation at finite loads as time approaches infinity.

### Water Transport Model

The water transport model derived by Cassidy et al. [42] models the intervertebral disc as a system that consists of the disc together with the cartilage end-plates attached to the vertebral bodies. On compressing the system, pressure is created within the disc, which is the driving force for water to flow through the cartilage end-plates and into the vertebral bodies.

The schematic for this model is shown in Figure 7.

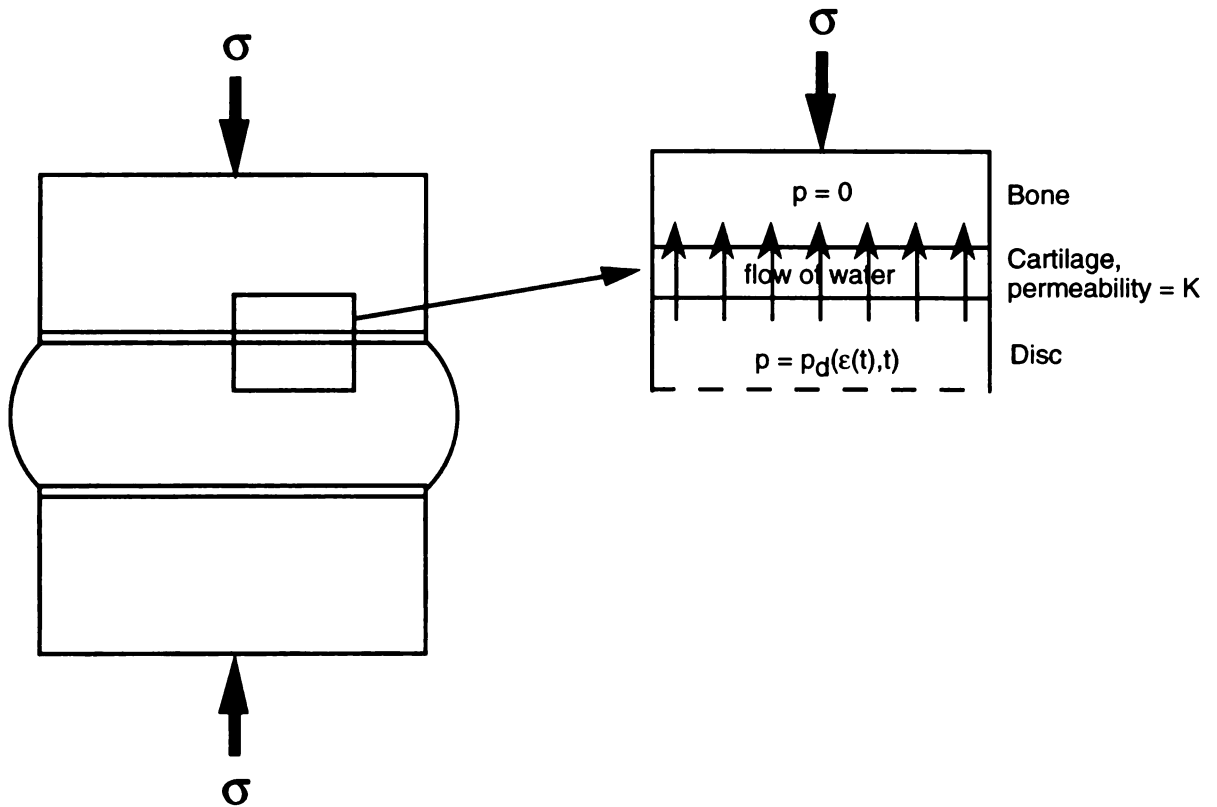


Figure 7: Schematic of the water transport model, showing the end-plate with permeability  $K$ , the applied stress  $\sigma$ , and the hydrostatic pressure within the disc  $p_D$ .

The assumptions made for this model are 1) the cartilage permeability controls the rate at which water is expressed from the compressed disc, 2) the compressive creep is due to the flow of water out of the disc as the result of the pressure gradient across the cartilage end-plates caused by an externally applied stress and 3) the hydrostatic pressure within the disc is homogeneous.

The Darcy equation is used to describe the relationship between the volumetric flux across two end-plates with a permeability coefficient  $K$  and the pressure gradient. Laminar flow and a linear pressure gradient across the end-plates are assumed. The relationship between the hydrostatic pressure,  $P_D$ , and the strain,  $\epsilon(t)$ , is given by the following:



$$q = h_i \frac{d[\varepsilon(t) - \varepsilon_o]}{dt} = \frac{2K}{L} P_d \quad \text{Equation 4}$$

$h_i$  is the initial disc height

$\varepsilon(t)$  is the strain

$q$  is the volume flux ( $\text{m}^3 \text{m}^{-2} \text{sec}^{-1}$ )

$t$  is the time

$\varepsilon_o$  is the strain at  $t = 0$

$P_d$  is the pressure in the disc ( $\text{Nm}^{-2}$ )

$L$  is the thickness of the barrier layer, the cartilage

$K$  is the permeability constant ( $\text{m}^4 \text{N}^{-1} \text{sec}^{-1}$ )

From this basic model, Cassidy considers that there would be an increase in osmotic pressure as the amount of water decreases. Assuming that the increase in osmotic pressure is linear with strain, he gives the following equation for the hydrostatic pressure:

$$P_d = \sigma_o - \{P_o + D[\varepsilon(t) - \varepsilon_o]\} \quad \text{Equation 5}$$

where  $D$  ( $\text{Nm}^{-2}$ ) represents the magnitude of the strain - dependence

Substitution of Equation 5 into Equation 4 and integrating yields the following:

$$\varepsilon(t) = \varepsilon_o + \frac{\sigma_o - P_o}{D} \left[ 1 - \exp\left(-\frac{2KDt}{h_i L}\right) \right] \quad \text{Equation 6}$$

The last modification to the strain equation is to add a linear, time-dependent term to the equation for the hydrostatic pressure to accommodate the fact that the disc often does not approach an asymptotic value, possibly due to non-recoverable strain when unloaded. The hydrostatic pressure equation becomes the following:

$$P_d = \sigma_o - \{P_o + D[\varepsilon(t) - \varepsilon_o] - Gt\} \quad \text{Equation 7}$$

where  $G$  ( $\text{Nm}^{-2} \text{sec}^{-1}$ ) represents the magnitude of the time - dependence

Substitution into Equation 4 and integrating gives the following equation that has both an exponential and a linear dependence of strain on time:

$$\varepsilon(t) = \varepsilon_o + \left( \frac{\sigma_o - P_o}{D} - \frac{h_i LG}{2KD^2} \right) \times \left[ 1 - \exp\left( -\frac{2KDt}{h_i L} \right) \right] + \frac{G}{D} t \quad \text{Equation 8}$$

Cassidy shows that this equation for the creep response is equivalent to the equation that describes the four-parameter viscoelastic fluid model (Burger's model), Equation 3 above. Comparing the equations, he finds the combination of terms K, D and G that are equivalent to the E,  $\tau$  and  $\eta$ .

A summary of published studies using the 3 or 4 parameter viscoelastic models and the water transport model to describe the creep of intervertebral discs is given in Table 1. Included are differences in the experimental setup, tissue type, loading conditions and creep periods. Reference will be made to this table in the Materials/Methods section of this paper, when discussing the loads and creep periods applied to the specimens of this project.

paper	reference #	tissue	vivo	levels	posterior elements?	grades (range of the scale)	n	sampling	preload?	load (N.)	stress (MPa.)	loading period	creep period (min.)	dynamic?	prevent drying	
Li, 1995	41	human	in vitro	T5-6; T9-10; L1-2; L3-4	no	2-4 Nachemson= (1-4)	16	10 hz.	no	200-450		7.6-23 sec.	60	no, but done later as separate test	wrapped in saline soaked gauze	
Keller, 1987	40	human	in vitro	from T11-12 to L3-4	yes	1-3 Nachemson= (1-4)	18	not given	no	235.5-309.7	0.096-0.189 with mean of 0.145	not given	30	no	sealed plastic bag	
Ekström, 1996	45	porcine	in vivo	L2-3	yes	young pigs	7	25 hz.	yes, in vivo	50		not given	13.3	yes, 5 hz.	in vivo	
Burns, 1984	39	human	in vitro	from T1-2 to L5-S1	yes	not given, though donors aged 27 to 46 yrs.	7	not given	no	100 177.9		30 lb. weight placed on tray	480 plus/minus 60	no	humidifier	
Kazarian, 1975	28	human	in vitro	from T3-4 to L3-4	yes	0-3 Friberg and Hirsch = (0-3)	32	analog	no	93.6		weight placed on tray	110-190	no	humidified box	
Koeller, 1986	48	human	in vitro	from T9-10 to L5-S1	no	0-3 Nachemson	178	not given	10 N.	950		not given	5	yes, plus/minus 540 N. at 1 hz.	no, in air	
Cassidy, 1990	42	canine	in vitro	from T11-12 to L6-7	no	young dogs	3	not given	0.1 MPa.		2.70	70 kN./sec.	60	no	sealed in plastic	
							3		0.1 MPa.		5					
							2		0.1 MPa.		7					
							1		0.1 MPa.		10					

Table 1: Comparison of Creep Data from Published Studies

paper	E1 (MPa.) lumber	E2 (MPa.) lumber	mu or eta (GPa-sec.)	tau (min.)	E1	E2	eta 1	eta 2	eta 3	K (m4 N-1 sec-1)	D (MN m-2)	G (x 10-6 MN m-2 sec-1)
Li, 1995	7.62	5.06	19.6	42.1								
Keller, 1987	6.264	1.607	5.409	9.87								
Elstiröm, 1996	87.2	12.5	1.9		31.1	10.7		1.7	124			
				0.363								
Burns, 1984	.015 to 200.7	2.9 to 160	2.5 to 29.6	3.3	8.87	7.5	17.3	1.7	22.3			
					1.2 to 98	4.1 to 24	1.5 to 2020	1.2 to 270				
Kazanian, 1975												
Koeller, 1986	creep measure was delta h by end of 5 min.											
Cassidy, 1980										0.85 e-17	18.2	421
										0.39 e-17	34.5	795
										0.27 e-17	51.5	853
										0.26 e-17	52.2	1609

## **Specimen Preparation; Temperature and Storage Effects**

Any *in vitro* experiment using human tissue must, of course, consider the effects of temperature and storage on the results. All testing for this project was done at room temperature, about 20 to 22°C. Hasberry and Percy [46] have shown that this will not affect the mechanical characteristics of interspinous ligaments, though thermal expansion of ligaments was measured. Discs and tendons at 37°C (body temperature) creep faster than those at room temperature [20], estimated by some researchers at a rate that is 10-15% greater [47, 48].

In considering the effects of freezing on disc tissue, a study by Smeathers et al. [49] found no difference between fresh and frozen human intervertebral disc specimens for compressive stiffness. Panjabi et al. [50] tested fresh versus frozen intervertebral disc specimens for biomechanical properties between the groups, as well as the effect of repeated testing over time on each of the specimens. They found that no significant difference existed between the fresh and frozen groups. Additionally, the change in mechanical properties after times of up to 14 days was small and not considered significant.

Bass et al. [51] found that the disc creep behavior in pigs was significantly affected by frozen storage. Their testing protocol tested the creep in repeated cycles on specimens immediately postmortem and after six weeks of frozen storage. The frozen specimens showed larger displacements during creep loading than the fresh specimens and diverged even further with repeated cycles of creep loading. They also note, however, that the swelling pressure of the human disc is much higher than in pigs and that the fluid content of the porcine disc is much higher than in humans; so it is unclear if the same magnitude of change would be seen in human specimens.

In summary, since it is necessary to remove spine specimens in order to test their mechanical properties, the experiments must be done *in vitro*. Researchers to date have done experiments at room temperature, so for comparison purposes it is valid to compare testing across a group of specimens at room temperature and with published studies under

the same conditions. The lack of significant differences between frozen and fresh human tissue is reassuring, because due to the testing and MR imager scheduling constraints, all tissue studied in this project was frozen the day of autopsy and thawed prior to imaging and mechanical testing.

In regards to the possible effects that freezing may have on the MR signal, Yu et al. [52] found the appearance of annular tears in MR images before and after freezing to correlate well. Terti et al. [53] found that the signal intensities from disc images on T2-weighted images were unaffected by changes in temperature at 10, 22 and 37°C. Gunzburg et al. [54] found few histologic artifacts after freezing and felt that the MR scans of previously frozen tissue were representative of the *in vivo* state.

Specimen preparation included removal of the posterior elements from the vertebral bodies. After cutting transversely through each vertebral body, one half a vertebral body remained on either side of an intact disc for each test specimen. Isolation of the intervertebral disc in this manner allowed studying only the disc-vertebral body system. Tencer et al. [55] have shown the disc to be the primary load bearing component in axial compression, and Kasra et al. [56] showed that removing the posterior elements did not significantly affect the dynamic stiffness and hysteresis of spinal segments.

### **Magnetic Resonance Imaging**

Magnetic resonance imaging has been used to estimate water content and degeneration of the intervertebral disc. Biologic tissues have been shown to have a decreasing linear relationship between increasing water content and  $1/T_1$  and  $1/T_2$  [57, 58]. MRI provides structural information on disc herniation, as well as qualitative comparisons between adjacent discs of T1 and T2-weighted signal intensity [53, 54, 59-63].

Beyond the anatomic structural information of MR imaging, estimations of MR relaxation constants, T1 and T2, have been measured in an attempt to better quantify changes in the disc with aging and degeneration [64-66]. In MRI, the tissue contrast is a function of several factors, including water content, the chemical environment of the tissue

water that governs the tissue characteristic relaxation times, T1 and T2, the flow and diffusion of water and other factors.

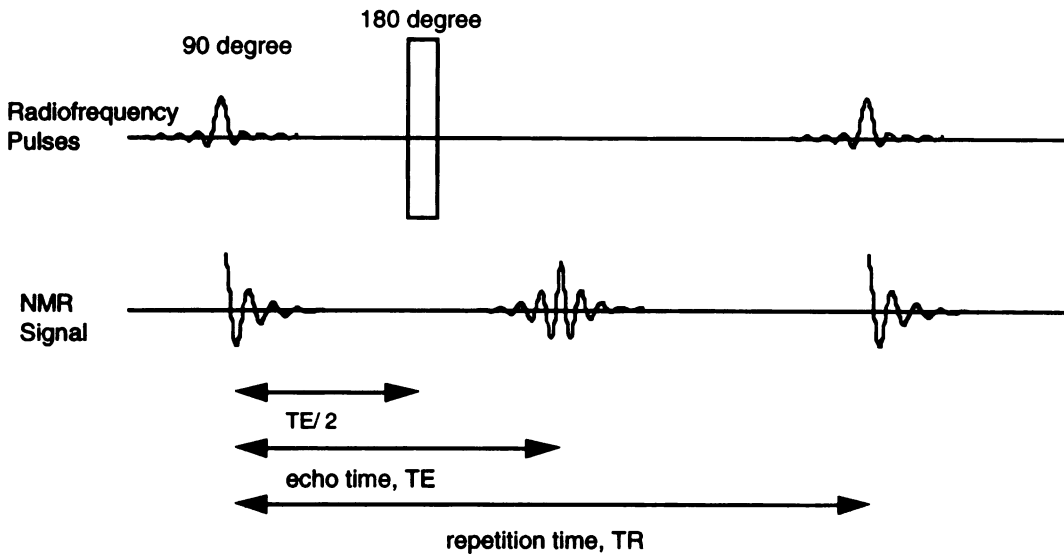
Different MR imaging sequences with varying timing parameters have been developed to quantify each of these factors. MR estimation of tissue water diffusion, D, has also been used in cartilage and disc [67-69]. These MR signals depend not only on the amount of water, but also on the biochemical environment that surrounds the water [65, 70-72]. Principal biochemical constituents of the disc, collagen and proteoglycan, vary with the region and degree of degeneration [31, 53, 73-75].

Several different imaging sequences are in existence in MR, the most common being spin-echo and gradient-echo sequences. These sequences will not be reviewed in detail here, however, a good description may be found in Wehrli et al. [76]. A brief summary of the relevant concepts will be presented here.

In MRI, the specimen is first placed within a large static magnetic field to align a slight majority of the tissue protons, the most abundant nuclei with a magnetic moment, with the field. These protons will precess about the axis of the field with a frequency that is proportional to the field strength and characteristic for that nucleus, here protons. Next, the tissue water is perturbed using radiofrequency (RF) pulses with an energy at the resonance frequency of the protons in the magnetic field, after which the tissue water tends to reorganize itself, or relax, at characteristic rates T1 and T2, inducing an RF signal in a surrounding receiver coil. The image is formed by applying a sequence of magnetic field gradients which, by altering the phase and frequency of the spins, encode the position of the protons in space.

In a spin-echo experiment, the precessing spins are subjected to a 90° RF pulse that knocks the spins to a transverse plane relative to the static field. As these spins relax, they will tend to lose phase coherence after the RF pulse is applied due to inhomogeneity of the magnetic field. A 180° RF pulse can then be applied, which leads to refocusing of the

spins and an "echo". The following diagram reviews the relevant radiofrequency pulses and NMR signals during a spin-echo sequence:



E. Chiu 3/95

Figure 8: Spin echo timing diagram in one dimension.

Using a spin-echo experiment in magnetic resonance, one can estimate tissue relaxation times, T1 and T2, as well as tissue water content. The signal intensity in such images is approximated by

$$SI(TR, TE) = N(H)e^{-\frac{TE}{T_2}} \left(1 - e^{-\frac{TR}{T_1}}\right) \quad \text{Equation 9}$$

where  $N(H)$  reflects the water content and machine dependent factors [76]. The relaxation times T1 and T2 may be quantified by obtaining images at different TR and TE values and using non-linear optimization techniques. These techniques have been used by Boos et al. [23, 77] to obtain relaxation times in intervertebral discs presumed to relate to tissue water content. Jenkins et al. [64] found decreases in both T1 and T2 with age, a lower T1 in degenerate compared to normal discs, and a lower T2 in young degenerated discs than in normals. In another study, Ke et al. [78] found that calibration of disc hydration to relaxation rate  $1/T_2$  in animals could be used to predict *in vivo* changes in disc hydration in human subjects. The results of these *in vitro* calibration studies were used to predict age-related variations in disc hydration.



Weidenbaum and coworkers [79] demonstrated a moderate negative correlation between  $1/T_2$  and water content for disc tissue samples. In addition, collagen content was shown to be negatively correlated with water content. It was suggested that a weakened collagen network could permit a greater degree of swelling, i.e. a higher water content in the disc. Chatani et al. [80] found a linear relationship between  $T_1$  and water content in bovine discs, with variation in  $T_1$  and  $T_2$  by region, annulus or nucleus, of the disc. Furo et al. mapped  $T_1$  of disc samples and found  $1/T_1$  had a linear relationship to both dry matter content and bound water content [81].

In muscle tissue, Scholz et al. [82, 83] found that  $T_1$  and  $T_2$  had linear relationships to tissue water content, and that curvilinear relationships existed between both  $T_1$  and  $T_2$  versus hydroxyproline content (a measure of collagen content). For myocardium, they concluded that water content was a major determinant of  $T_1$ , while both water content and collagen content contributed to variability in  $T_2$ .

### **Diffusion Measurements with MRI**

Molecular water diffusion is caused by thermally induced random Brownian motion [84]. The mean path length was derived by Einstein as follows [84]:

$$L = \sqrt{2Dt} \quad \text{Equation 10}$$

where  $D$  is the diffusion coefficient  
and  $t$  is the observation time.

For free water the diffusion coefficient,  $D$ , is about  $2.5 \times 10^{-5}$  cm.<sup>2</sup>/sec. For solid biologic tissues such as liver and muscle tissue,  $D$  ranges from about 25 to 40% of free water diffusion [72].

In addition to the chemical environment of tissue water, the mobility and diffusion of tissue water affects the spin-echo signal. Molecular diffusion decreases the spin-echo signal and has been used to develop MR methods to measure the self-diffusion coefficient,  $D$ , of liquids [85, 86]. To estimate diffusion using nuclear magnetic resonance, one adds symmetric magnetic field gradients before and after the  $180^\circ$  RF pulse. The first gradient

causes a phase shift in the spins dependent on their position in the field. After the 180° RF pulse, the phase shifts are reversed, and application of the second diffusion gradient will cause a phase shift equal and opposite to the first. In the absence of diffusion, the second gradient will exactly undo the first. With diffusion present, however, there will be a loss of phase coherence and lower signal. Stejskal and Tanner derived the loss in signal intensity due to diffusion with these gradients applied [85]. Beginning from Abragam [87]

$$\frac{\partial \psi}{\partial t} = -i\gamma(\mathbf{r} \cdot \mathbf{G})\psi + D\nabla^2 \psi \quad \text{Equation 11}$$

$$\psi(\mathbf{r}, t) = M_x + iM_y = \psi \exp\left[-(i\omega_o + 1/T_2)t\right] \quad \text{Equation 12}$$

where the applied magnetic field =  $H_o$ ,

$\psi$  is the transverse magnetization in a rotating coordinate frame with angular velocity  $\omega_o = \gamma H_o$  = Larmor frequency,

$\gamma$  is the gyromagnetic ratio, characteristic for the nuclear species,

$M_x + iM_y$  represents the behavior of the components

of the nuclear magnetization in the plane perpendicular to  $H_o$ ,

the z axis is chosen parallel to  $H_o$ ,

and the gradient  $\mathbf{G}(t)$  is defined as  $H_z = H_o + (\mathbf{r} \cdot \mathbf{G})$ .

$D$  is the diffusion coefficient.

They derived that the loss in signal intensity with diffusion gradients present, compared to the signal intensity without gradients, was given by Equation 13:

$$\ln\left[\frac{A(TE)}{A(0)}\right] = -\gamma^2 \int_0^{TE} \left( \mathbf{F}(t') - 2H(t' - \frac{TE}{2})\mathbf{f} \right)^T \cdot \mathbf{D} \left( \mathbf{F}(t') - 2H(t' - \frac{TE}{2})\mathbf{f} \right) dt'$$

where

$$\mathbf{G}(t) = (G_x(t), G_y(t), G_z(t))^T \quad \text{Eq. 14}$$

$$\mathbf{F}(t) = \int_0^t \mathbf{G}(t') dt' \quad \text{Eq. 15}$$

$$\mathbf{f} = \mathbf{F}\left(\frac{TE}{2}\right) \quad \text{Eq. 16}$$

$\mathbf{G}(t)$  is the applied magnetic field gradient

$TE$  is the echo time

If one assumes that the diffusion sensitizing magnetic field gradients of amplitude  $G_i$  will be applied for a duration of  $\delta$  and are separated by a time  $\Delta$  (Figure 9), the derivation reduces to the following:

$$\ln\left[\frac{A(TE)}{A(0)}\right] = -\gamma^2 \delta^2 G_i^2 \left(\Delta - \frac{1}{3}\delta\right) D \quad \text{Equation 17}$$

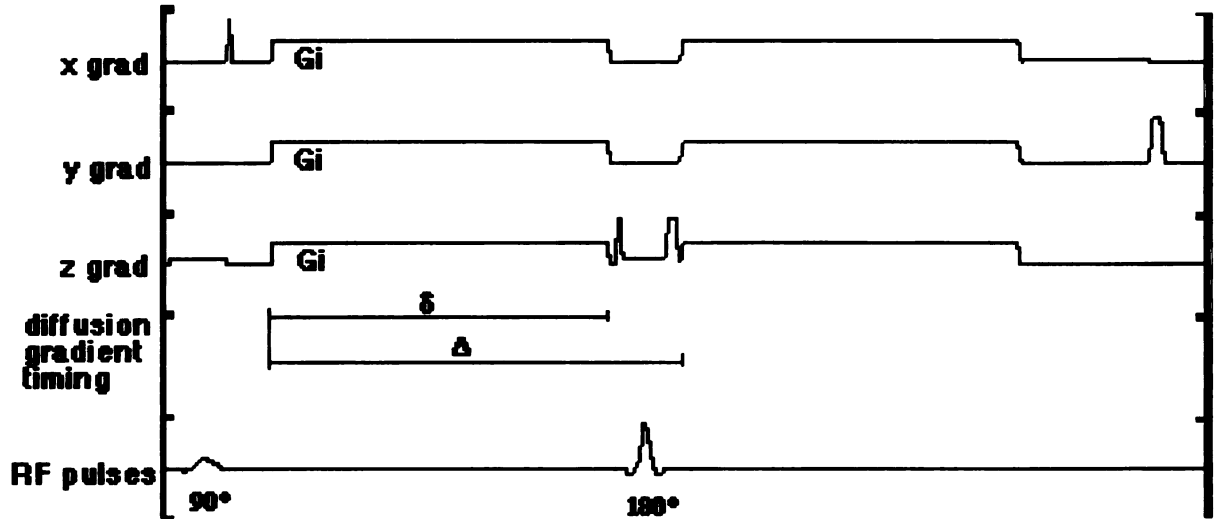


Figure 9: MR timing diagram with diffusion gradients added in the x, y and z directions, with amplitude of  $G_i$ , duration of  $\delta$ , and time between diffusion gradients of  $\Delta$ , and including the imaging gradients in the three directions.

Alternatively, one can say that the observed signal intensity with diffusion gradients is

$$SI \sim e^{(-\gamma^2 \delta^2 G_i^2 (\Delta - \frac{\delta}{3}) D)} \quad \text{Equation 18}$$

where  $\gamma$  is the gyromagnetic ratio that is a characteristic of the nuclear species under study.

In the case where tissue water is being studied, this nucleus is  $^1\text{H}$ , and  $\gamma = 4.26 \times 10^3$

Hz/Gauss. This decay is in addition to the T1 and T2 effects in Equation 9. Thus, by varying the magnitude and the direction of  $G_i$  and obtaining a series of diffusion-weighted images, not only can the diffusion coefficient be measured, but by applying the gradients along different orthogonal axes, the directionality or the preferred diffusion direction may be derived.

To account for the effects of temperature on diffusion, the Stokes-Einstein equation is used to correct diffusion results for temperature differences [88]:

$$D_{298K} = \frac{D_m}{T_m} \frac{\mu_{T_m}}{\mu_{298K}} 298K \quad \text{Equation 19}$$

where  $D_m$  is the diffusivity measured at room temperature,  $T_m$ , and published values for the viscosity,  $\mu$ , at 298K and  $T_m$  are used.

Another method used to correct for the effect of temperature is to calculate the tissue diffusion relative to the free water diffusion of a sample in the same image, at the same temperature. If one uses the Stokes-Einstein equation on each region (tissue and saline), the correction factors for temperature cancel out.

The second reason that normalization to free saline diffusion is done is that this will correct for the imaging gradients' effects on diffusion. The gradients applied to create the image will themselves cause losses in signal intensity. These effects of the imaging gradients are usually assumed to be small relative to the diffusion gradients (one can calculate the relative areas under the gradient curves). In Equation 13 from Stejkal and Tanner, one can see that the diffusion term is actually a factor separate from the quantities within the brackets, such that the choice of TE and applied gradient,  $G$ , are what determines the signal intensity. Even if the exact applied magnetic field gradient is not known, one can estimate diffusion relative to a known substance [85]. The two substances will be exposed to the same gradients and will therefore have the same combined effects of imaging and diffusion gradients on them.

Burstein et al. [67] used nuclear magnetic resonance spectroscopy and magnetic resonance imaging to measure a self-diffusion coefficient ( $D$ ) for small solutes in samples of explanted cartilage. With compression of the cartilage, they found the diffusivity of water decreased by 19% relative to uncompressed values. After treatment with trypsin to remove proteoglycans and noncollagenous proteins, the diffusivity of water increased by 20%. They felt that these data and the lack of an effect of charge on diffusivity were consistent with a dependence of  $D$  on the composition and density of the solid tissue matrix in cartilage. After the matrix was compressed, its density increased; therefore, the ability of water to diffuse decreased. When some of the proteoglycans and proteins were removed, the water was able to diffuse more freely, reflected in an increase in  $D$ .

Koh et al. [68, 69] used a spin-echo NMR system to find a diffusion coefficient for pieces of human and bovine discs. Differences were seen by region of the discs as well as by the degree of degeneration of the human specimens. Anisotropy was seen in the diffusion coefficient in various regions of the annulus fibrosus.

Recently proposed and implemented fast spin-echo techniques in MRI permit the acquisition of high resolution, T2-weighted images (MR timing parameters chosen to emphasize tissue T2 differences) in relatively short scan times [89-91]. In these sequences multiple echoes are phase encoded in the same repetition time, TR. So, by generating a sequence of 8 echoes, and phase encoding each echo, an image matrix of 512 x 512 can be acquired in 1/8 the scan time that would be required to obtain a standard T2-weighted MR image. Using these techniques researchers have obtained images with resolutions of 156-300  $\mu\text{m}$ . in-plane in less than 10 minutes.

Examples of such images with a resolution of 156  $\mu\text{m}$ . through the intervertebral disc are shown in the preliminary data section. These images clearly resolve the structure of the annular fibers and their movement with loading and have tremendous potential for studying the internal deformation of the intervertebral disc with loading.

## Diffusion Tensor Imaging

As part of the preliminary work for this study, an attempt was made to use the method of diffusion tensor imaging to collect data and estimate tissue anisotropy. Originally proposed by Bassler et al. [92], this method applies steps of gradients in combinations of the gradient directions to obtain data with information about the diffusion in multiple directions within the tissue.

Basser et al. [92, 93] extended the concepts of Stejskal and Tanner [85] for the change in signal intensity due to diffusion to include all gradients present in MR imaging: slice select, readout, crushers. They define a diffusion tensor that is a 3 x 3 matrix of diffusion coefficients as follows:

$$\mathbf{J} = \begin{bmatrix} J_x \\ J_y \\ J_z \end{bmatrix} = -\mathbf{D}\nabla C = - \begin{bmatrix} D_{xx} & D_{xy} & D_{xz} \\ D_{yx} & D_{yy} & D_{yz} \\ D_{zx} & D_{zy} & D_{zz} \end{bmatrix} \begin{bmatrix} \frac{\partial C}{\partial x} \\ \frac{\partial C}{\partial y} \\ \frac{\partial C}{\partial z} \end{bmatrix} \quad \text{Eq. 20}$$

where  $\mathbf{J}$  is the flux, or rate of mass transport across a unit surface area, and  $C$  is the concentration of solute.

The diagonal elements of the diffusion tensor scale fluxes and concentration gradients in the same direction. The off-diagonal elements couple fluxes and concentration gradients in orthogonal directions. In anisotropic media, the concentration gradient is not necessarily parallel to the diffusive flux. [92]

For each imaging step, one compares the image with diffusion gradients applied to the image with no gradients, where the equation for the loss in signal intensity becomes

$$\ln \left[ \frac{A(TE)}{A(0)} \right] = - \sum_{i=1}^3 \sum_{j=1}^3 b_{ij} D_{ij} \quad \text{Eq. 21}$$

Each image requires the calculation of nine "b" values that multiply the nine elements of the diffusion tensor. Due to symmetry of the diffusion tensor matrix above and below the diagonal, this reduces to six unique elements of the b matrix and diffusion tensor matrix.

If one ignores the imaging gradients applied in MRI and calculates the diffusion coefficient,  $D$ , assuming only diffusion gradients, there will tend to be an overestimation of the diffusion [94]. Also, knowledge of the off-diagonal elements of the diffusion tensor gives insight to anisotropic organization of the tissue or sample being studied [92].

## **VI. MATERIALS/METHODS**

### **Overview**

Thirteen vertebral specimens consisting of an intervertebral disc with adjacent vertebral bodies were used in this study. Specimens were harvested from spine necropsy material obtained from the Pathology Department at UCSF. Table 2 summarizes the data on the specimen donors, including age at time of death, cause of death, known concurrent medical conditions and gender.

Each specimen was imaged with MRI - unloaded and loaded - for high resolution images, MR relaxation constants, and diffusion coefficients. Mechanical testing was done with an electrohydraulic test system immediately after the MR scanning was completed. Each specimen was then cut midsagittally for Thompson grading [95] (Table 3). Figures 10 and 11 show examples of Thompson grade 1 and grade 3 discs.

From each of the specimens, 3 mm. cubes of nucleus and annulus were then subjected to dehydration in polyethylene glycol (PEG) to develop a calibration curve for  $T_1$ ,  $T_2$  and  $D$  versus water content for each specimen.

<b>OREF</b>	<b>level used</b>	<b>age</b>	<b>sex</b>	<b>cause of death</b>	<b>other known medical conditions</b>
1	L3-L4	61	M	lung abscess	
2	L4-L5	25	M	rhabdomyosarcoma	
3	L4-L5	16	F	disseminated candidiasis	systemic lupus erythematosus
4	L4-L5	39	F	cystic fibrosis	
5	L4-L5	54	M	myocardial infarction	cardiomyopathy, chronic obstructive pulmonary disease
6	L2-L3	56	M	brain embolis	postop. esophageal cancer, prev. aortic valve
7	L4-L5	62	F	gram negative sepsis	endstage renal disease, diabetes mellitus
8	L4-L5	68	M	myocardial infarction	
9	L4-L5	69	F	intracerebral hemmorage	
10	L4-L5	37	M	myelodysplastic syndrome	
11	L4-L5	66	F	intravascular lymphoma	osteoporosis (no lymphoma in spine)
12	L4-L5	32	M	sepsis	
13	L4-L5	62	M	coronary artery bypass graft x 2	hypertension

Table 2: Lumbar disc specimens used for this project.

<b>grade</b>	<b>nucleus</b>	<b>annulus</b>	<b>end-plate</b>	<b>vertebral body</b>
1	bulging gel	discrete fibrous lamellas	hyaline, uniformly thick	margins rounded
2	white fibrous tissue peripherally	mucinous material between lamella	thickness irregular	margins pointed
3	consolidated fibrous tissue	extensive mucinous infiltration; loss of annular-nuclear demarcation	focal defects in cartilage	early chodrophytes or osteophytes at margins
4	horizontal clefts parallel to end-plate	focal disruptions	fibrocartilage extending from subchondral bone; irregularity and focal sclerosis in subchondral bone	osteophytes less than 2 mm.
5	clefts extend through nucleus and annulus		diffuse sclerosis	osteophytes greater than 2 mm.

Table 3: Thompson grading scheme for human intervertebral disc degeneration.





Figure 10: Thompson grade 1 disc



Figure 11: Thompson grade 3 disc

The following flowchart (Figure 12) summarizes the overall test procedure.

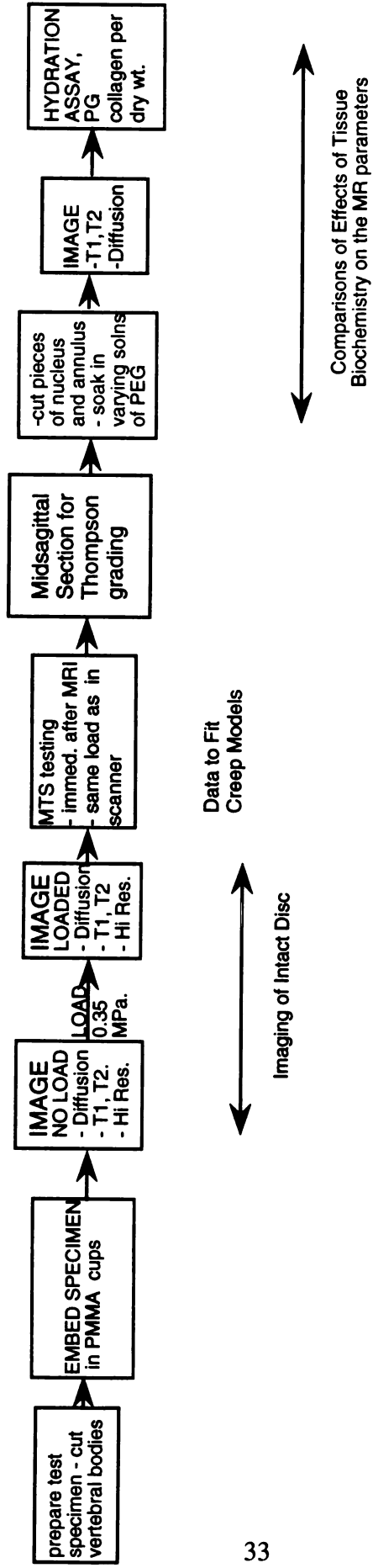


Figure 12: INTERVERTEBRAL DISC SPECIMEN PROTOCOL

## **Specimen Preparation**

Frozen spine specimens were cut transversely through adjacent vertebral bodies to produce test specimens consisting of one intervertebral disc with a vertebral endplate and half a vertebral body on each side. The vertebral bodies were embedded in acrylic cups using polymethylmethacrylate (PMMA) cement to prevent specimen slippage with compression. Specimens were thawed for four to six hours at room temperature, preloaded to a peak of 250 N/20 sq.cm. (0.125 MPa.) and held immersed in saline under refrigeration at slightly above 0 °C.

Prior to imaging, the specimens were placed in a compression frame made of nonmagnetic materials that was constructed for this study. The first compression device (Figure 13) was a rigid frame made of acrylic with a nonmagnetic force transducer (West Coast Research, Santa Monica, CA, model 31-5.2-2.5F) at its base to measure the applied load while imaging was performed. A screw mechanism allowed loading of up to 1,500N. (about 350 pounds) while the specimen was enclosed in an acrylic tube to surround the specimen with physiologic saline and prevent dehydration. This device would therefore apply a step in displacement, and the measured decrease in load would show stress relaxation.

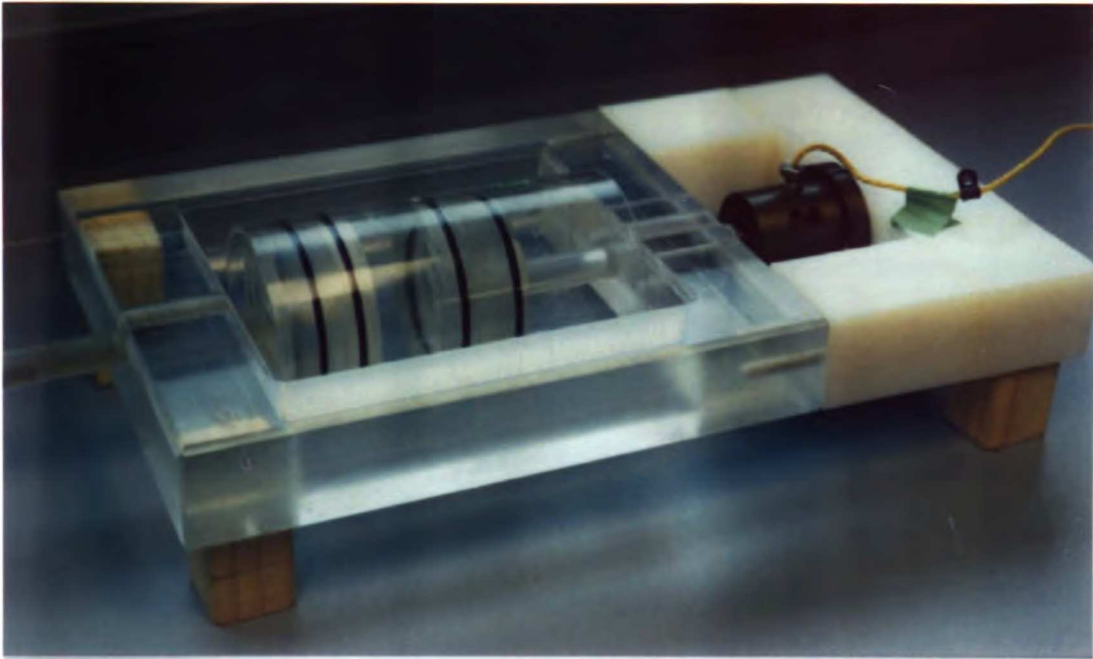


Figure 13: Perspective view of the first nonmagnetic compression apparatus. Note the screw mechanism to the left and the force transducer to the right of the photograph.

The second compression device was designed to apply a constant load by utilizing a pneumatic cylinder (Clippard Minimatic, Cincinnati, OH, 2" bore stainless steel cylinder) as the actuator (Figure 14).



Figure 14: Perspective view of the second compression device that was designed to apply step loads rather than step displacements. The non-magnetic stainless steel pneumatic cylinder (upper right) was pressurized with nitrogen gas to apply the loads. The force transducer (lower left) allowed recording the actual loads applied while scanning.

A non-magnetic, aluminum nitrogen cylinder (size E) with non-magnetic, one-stage pressure regulator (Puritan-Bennett, Lanexa, KS, model 30) was used to apply step loads of 700 N./20 sq.cm. (0.35 MPa). This load was chosen as a physiologic load experienced *in vivo* by lumbar discs while an individual is in the sitting position [9], with 20 sq.cm. used as an average area of L3-L4 discs [96]. The anterior/posterior dimension multiplied by the left/right dimension, then scaled by a factor of 0.84 was used to estimate specimen cross-sectional areas [96]:

$$Area = D_{A/P} \times D_{L/R} \times 0.84 \quad \text{Equation 22}$$

### **Specimen Testing**

Each specimen was placed in the compression frame and loaded to 0.35 MPa. while being imaged by a 1.5 Tesla General Electrics SIGNA scanner (General Electric Medical Systems, Waukesha, WI) with a knee or wrist coil. MR scanning was used to measure disc deformation with compression, and relaxation constants and water diffusion before and after compression (details in MR scanning section).

It must be noted that specimen 10 was preloaded in the MR scanner, while none of the other specimens were subjected to this load. Because of this difference in protocol, this specimen's data was not included in the analysis of the MR parameter changes with compression.

Mechanical testing was done with a MTS Bionix, Model 858 (MTS Corp., Eden Prairie, Minnesota) mechanical testing system that allowed computer control of force or displacement inputs with simultaneous measurement and recording of displacement or force outputs.

With the test specimens still embedded in the PMMA cups, the specimens were placed in a saline tank on the MTS test platform and loads applied through the same test configuration that was present in the MR scanner (acrylic cups with the specimen embedded in PMMA above and below). To precondition the specimen, specimens were first preloaded for 30 minutes [47] with 0.10 MPa., a physiologic preload consistent with

published values of intradiscal pressure while supine [97]. Then, to emulate the physiologic load while in the sitting position, a step load of 0.35 MPa. was applied, and the creep displacement was measured. Loads were applied in a time period of one second. Data acquisition on the MTS system was set at one sample every 10 seconds during the preload period, increased to 10 samples per second during the first minute after application of the step load and completed at one sample every 10 seconds for the remainder of the four hours of creep testing.

The creep time period was chosen to be four hours to simulate the maximal sitting load that a desk worker would ordinarily subject the disc to *in vivo*. Other researchers have used times ranging from five minutes to eight hours with loads varying from 0.025 MPa. to 10 MPa. Table 1 summarized these differences in the background section of this paper (pages 18-19). The preload was applied to overcome the extra swelling of the disc that is seen *in vitro*. This supraphysiologic swelling is due to removal of the ligaments and posterior elements that normally limit swelling *in vivo* [47].

### **MR scanning**

All imaging was done using a 1.5 Tesla General Electrics SIGNA (General Electric Medical Systems, Waukesha, WI) scanner. Each specimen was placed with the same orientation in the magnet bore: prone, with superior disc first into the bore. The first four specimens were imaged in an extremity coil (G.E. Medical Systems); the next nine were imaged with a linear wrist coil (Medical Advances, Inc., Milwaukee, WI) to increase the signal to noise ratio of the images. After obtaining low resolution localizers in the axial, sagittal, and coronal planes to choose the locations for the higher resolution images, spin-echo sequences were used to quantify T1 and T2 in regions of the disc. The signal intensity in such images is given by Equation 9, repeated here for convenience:

$$SI(TR,TE) = N(H) e^{-TE/T2} (1 - e^{-TR/T1}), \quad \text{Equation 9}$$

The signal intensity was measured from a mid-sagittal slice of intact IVD using spin-echo experiments with the following values of TE and TR:

T1 data	
TE (ms)	TR (ms)
20	60
20	125
20	250
20	500
20	1000
20	2000

T2 data	
TE (ms)	TR (ms)
20	4000
40	4000
60	4000
80	4000

Image acquisition took about 20 minutes for this set of 10 images.

The relaxation times, T1 and T2, were calculated using these images, Equation 9 and non-linear optimization techniques (Levinberg-Marquadt algorithm), with IDL (Interactive Data Language, Research Systems, Boulder, CO), running on a Sun Sparc 10 or Ultra workstation. A set of vials containing different amounts of Gadolinium DTPA (Magnevist, Berlex) doped distilled water were included as calibration standards. Regional values of T1 and T2 were extracted for comparison with disc hydration and biochemistry.

IDL (Interactive Data Language, Research Systems, Boulder, CO) was used to select regions of interest (ROI's) 2.5 mm. square on each specimen in the image. For the midsagittal slice in the intact intervertebral disc, four annulus fibrosus ROI's and three nucleus pulposus ROI's were selected, with equal spacing between the ROI's from anterior to posterior. Figure 15 shows a midsagittal image with seven ROI's selected.

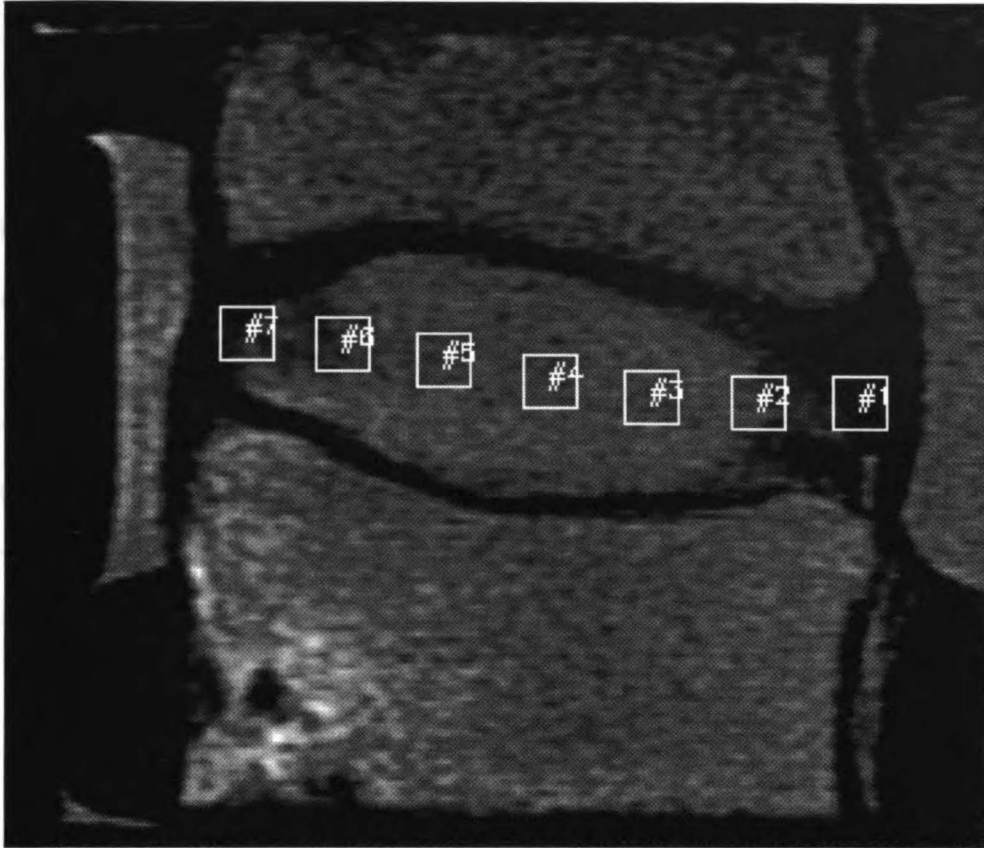


Figure 15: Midsagittal image of an L4-L5 intervertebral disc for diffusion estimation with 10 x 10 pixel (2.5 mm. square) ROI's selected. The central three ROI's were considered nucleus pulposus and the peripheral four ROI's annulus fibrosus.

After compression, the seven ROI's were shifted inferiorly on the post compression images. Mean signal intensities were extracted from each ROI, and from the series of images with varied TE and TR, exponential curve fits were used to estimate T1 and T2 for each region.

To measure tissue diffusion, a modified spin-echo sequence with pulsed gradients was developed. The spin-echo sequence was modified by applying additional pairs of magnetic field gradients,  $G_i$  (values ranging from 0-2.2 Gauss/cm). The signal intensity of such sequences is given by

$$SI(TR,TE) = N(H) e^{-TE/T2} (1 - e^{-TR/T1}) \exp(-\gamma^2 \delta^2 G_i^2 (\Delta - \delta/3) D). \quad \text{Eq. 23}$$



Thus, by using different values of the pulsed gradient, a series of diffusion-weighted images were generated, at constant values of TE and TR. The simplified equation is given by

$$SI = K e^{-bD} \quad \text{Equation 24}$$

where K is a constant.  $b = \gamma^2 \delta^2 G_i^2 (\Delta - \delta/3)$ . b is a function of the gradients that are pulsed on, their duration and separation, and b can be calculated for each image. Gradients were applied in the three orthogonal directions, x = tissue anterior/posterior, y = left/right and z = superior/inferior, and used to derive D along the x, y, and z axes to map the regional characteristics of water diffusion within the disc before and after compressive loads were applied. For each gradient step the image acquisition time was about 75 seconds.

To estimate diffusion, gaussian curve fits were done to plots of signal intensity vs. applied gradient (Figure 16) for the same ROI's used for T1 and T2.

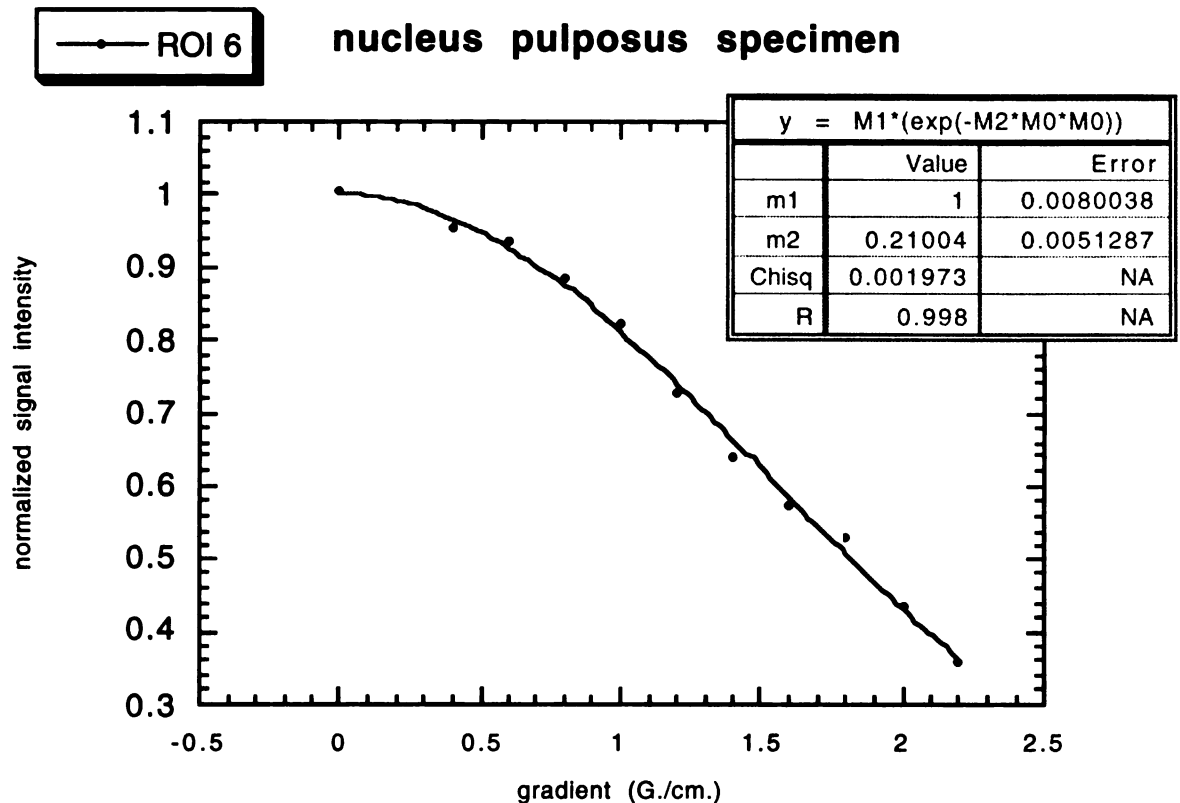


Figure 16: Normalized signal intensity versus the applied diffusion gradient. A gaussian curve fit was done, and the diffusion coefficient was calculated from this fit.

High resolution images of the disc before and after compressive loading conditions were generated using a fast spin-echo imaging sequence [89-91]. Images were obtained in the sagittal plane with the following parameters: TR = 4000, TE = 124, FOV = 8cm, matrix = 512 x 512 and slice thickness = 3.0 mm. The acquisition time for each image was about 30 minutes.

### Subspecimen Preparation for Water Content Alteration

To examine the relationship between water content and T1, T2 and D, while controlling for variations between specimens in proteoglycan structure and content, individual disc specimens were sampled and these pieces of disc soaked in polyethylene glycol (PEG) to alter their hydration. Slices were cut from superior to inferior to create 3

mm. square strips with disc in the center and endplate and vertebral body on the top and bottom, shown below (Figure 17).

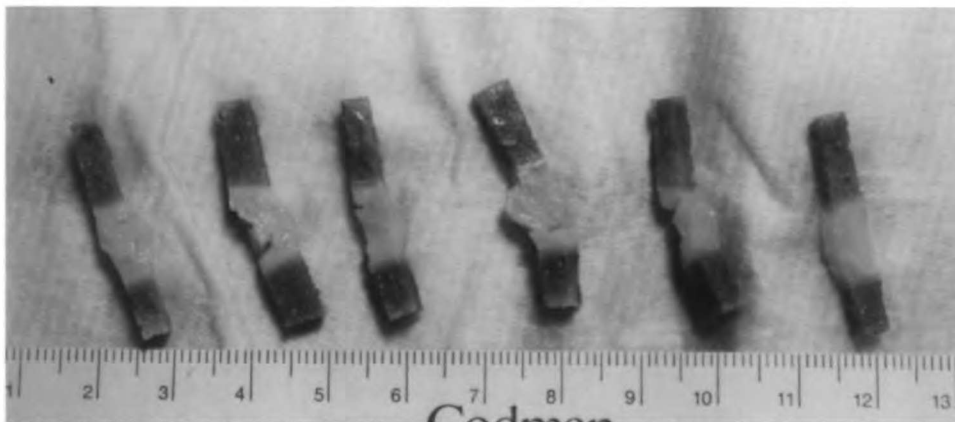
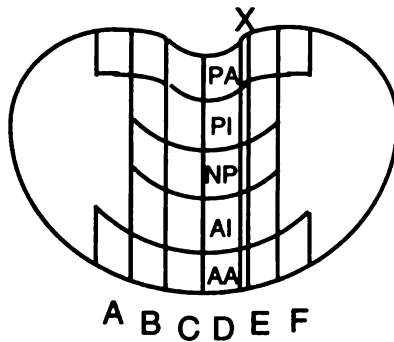


Figure 17: Six harvested nucleus pulposus specimens from one disc, prior to wrapping in dialysis membrane.

Six nuclear and ten annular specimens were cut out with an Exakt saw (a diamond-edged bandsaw for biologic tissues) to include the endplates and part of the vertebral body at each end. These specimens were enclosed in dialysis tubing (MWCO 1100 Daltons, Spectra/Por, Spectrum Medical Industries, Houston, TX) to prevent leakage of the proteoglycan matrix from the cut surfaces and placed in solutions of PEG, MW 20000 (Spectrum Chemical, Gardena, CA), in 0.15M NaCl (physiologic saline) at concentrations ranging from 0g/100cc to 30g/100cc saline for 48 hours with slow stirring while refrigerated. This technique has been shown by Urban et al. [17] to produce a physiologic range of tissue hydrations. Figure 18 shows the mapping of the specimens to the concentrations of PEG solutions. The T1, T2 and D of these specimens were remeasured as described above.



PA = post. annulus  
 PI = post. intermediate  
 NP = nucleus pulposus  
 AI = ant. intermediate  
 AA = ant. annulus

tissue X was used to measure hydration

<b>APA</b>	<b>BPA</b>	<b>CPA</b>	<b>DPA</b>	<b>EPA</b>	<b>FPA</b>
0	5	10	biochem.	20	30
	<b>BPI</b>	<b>CPI</b>	<b>DPI</b>		
	0	30	biochem.		
	<b>BNP</b>	<b>CNP</b>	<b>DNP</b>		
	10	20	biochem.		
	<b>BAI</b>	<b>CAI</b>	<b>DAI</b>		
	5	10	biochem.		
<b>AAA</b>	<b>BAA</b>	<b>CAA</b>	<b>DAA</b>	<b>EAA</b>	<b>FAA</b>
0	5	10	biochem.	20	30

Figure 18: Sectioning map of the intact disc specimens, with a table showing PEG concentrations (gm./100cc 0.15M saline) used for the tissue subspecimens.

### Hydration Assay

The samples cut for calibration of T1 and T2 to the water content of a particular disc had the endplates and vertebral bodies removed, leaving the central 3 mm. cube of disc tissue. This piece of tissue was weighed and dehydrated at 65° C to equilibrium (approximately 24 to 48 hrs). The percent water content was calculated as the difference in wet versus dry weight divided by the initial wet weight.

### Biochemical Assay

For the biochemical assays, the dried samples were digested with proteinase K to quantify glycosaminoglycan (GAG) content (µg/mg) using the DMMB (dimethylmethylene blue) dye binding colorimetric assay [98]. Aliquots of the proteinase K digest were also hydrolyzed overnight with 6N HCl at 110 deg. C prior to performing a colorimetric assay to evaluate the hydroxyproline content for collagen estimation [99, 100]. Total collagen is

calculated as ten times the hydroxyproline content, considering hydroxyproline as 10% of the weight of each collagen alpha chain [101].

## **VII. DATA ANALYSIS/MODELING**

### **Analysis of T1, T2 Data**

For the intact disc specimens, the T1 and T2 values from the ROI's in the nucleus and annulus were compared using an analysis of variance (ANOVA) with the following factors: location - annulus or nucleus, loading state - compressed or not and the Thompson grade.

For the subspecimens of nucleus and annulus (from within the same specimen), an analysis of covariance, a multivariate linear regression, was used to examine the relationship of T1, T2 and D to the biochemical parameters of water, proteoglycan and collagen content.

### **Correction for Temperature Effects**

The first seven specimens were imaged before they had completely come to room temperature. A sample specimen was run through the whole preparation and thawing procedure to estimate the amount of temperature change during the three hours of MR scanning. Figure 19 shows the temperature vs. time graph for this specimen, with a curve fit to describe this relationship. For the worst case of the first seven specimens, the temperature at the first T1, T2 measurements was about 12°C, rising to about 16°C by the end of the scanning.

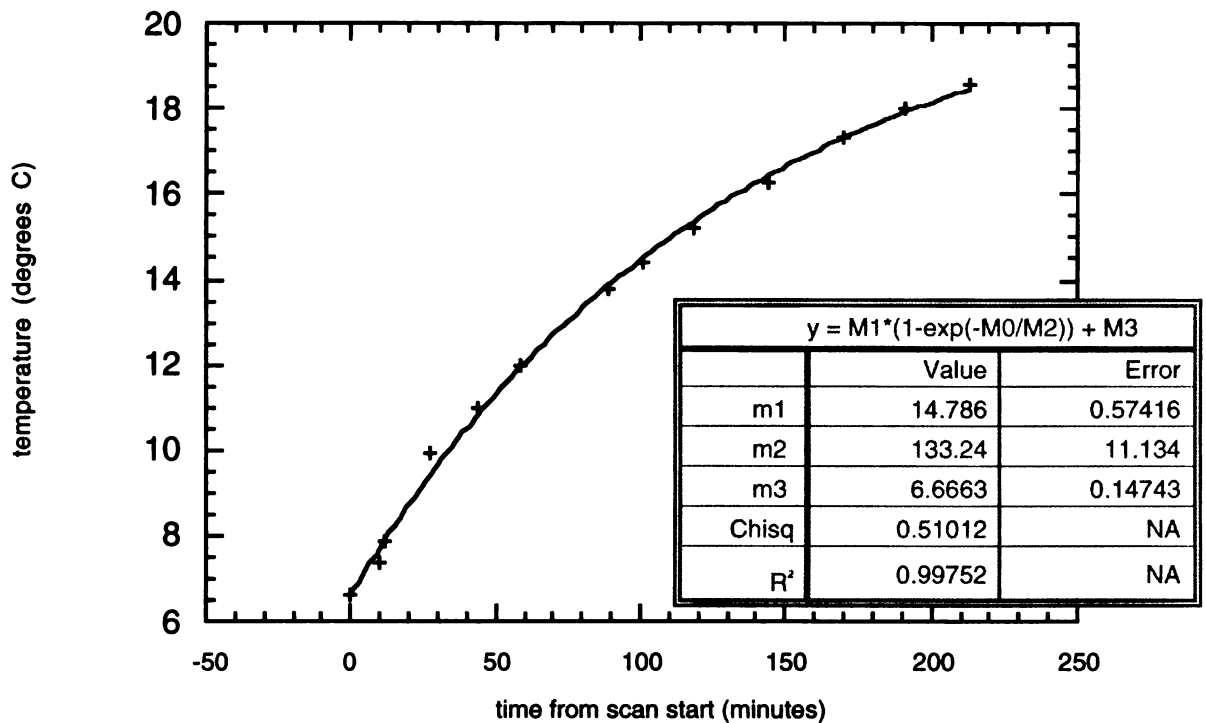


Figure 19: Graph of specimen temperature versus time from the beginning of the MR scan. An equation was fit to this graph to use for estimating the temperature at different points during the first seven specimens' scans.

By the proportional relationship between the temperature and the T1 relaxation time [102], a change in temperature from 12 to 16°C could amount to an increase in T1 of about 2%. Effects of temperature on T2 are even less significant [87].

The effect that the change in T1 could have had on the diffusion coefficient measurement is that the signal intensity could change by Equation 9 over the course of acquiring a set of diffusion images. For the 11 steps of diffusion gradient applied, the time period of acquisition would be about 15 minutes. From Figure 19 this would result in a temperature change of 1°C, which would not significantly affect T1 during the diffusion measurements.

## **Analysis of Diffusion Data**

In calculating the diffusion coefficients for the intact disc specimens, the same regions of interest were considered as for the T1 and T2 measurements. After extracting the mean signal intensities for the ROI's and using a Gaussian curve fit to estimate the diffusion coefficients, normalized to saline in the same image, an analysis of variance was used to look for significant differences in D according to diffusion direction, degree of degeneration, location (annulus or nucleus) and compressive loading state.

As for the T1 and T2 data, the subspecimens of the disc tissue were analyzed with a multivariate regression model to see which parameters: water content, proteoglycan content, collagen content, Thompson grade or location - annulus or nucleus - predicted the diffusion coefficients.

## **Analysis of High Resolution Images**

High resolution FSE MR images of the disc before and after compression were examined for the internal deformation of the annular fibers and degree of compression of the entire disc height. NIH Image 1.55 (NIH, Bethesda, MD) software was used to measure distances before and after loading at the central disc height, the anterior-posterior diameter, and the inner annular fiber distance anterior to posterior, where possible.

Figure 20 shows typical high resolution images before and after compression. Abnormal patterns of deformation of the inner annular fibers were to be quantified by direction and magnitude of displacement in the sagittal images before and after loading. A correlation of displacements with water content and degree of degeneration of the specimen was to be examined with multivariate regression; however, measurements of disc height before and after compression, and disc anterior/posterior diameter before and after did not show any correlation to Thompson grade, as will be shown in the Results section.

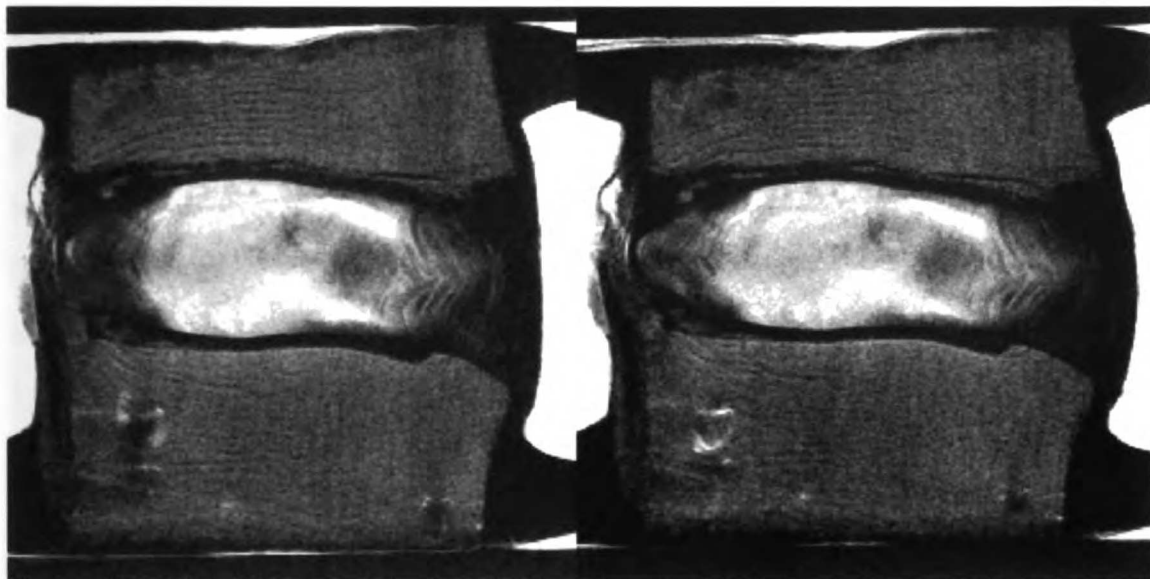


Figure 20: Midsagittal image of an L4-L5 disc, age at death = 39 years, Thompson 2. Image on left is before compression, image on right is after compression.

Assessment of inner annular fibers was not possible in discs 1, 2, 11 and 12 due to the lack of clear nuclear/annular boundaries due to the degenerative state of the disc. Disc 2 had a tumor within the inferior vertebral body, and given the lack of constraint of the nucleus pulposus, inferior protrusion of disc material and inward anterior annular bulging was seen (Figure 21).



Figure 21: Specimen 2 of the study, showing a tumor that had allowed the IVD to break through the inferior vertebral body. Inward annular bulging is seen for the annular fibers in the anterior disc (the right side of the image).



## **Analysis of Creep Data**

To analyze the time-dependent behavior of the disc, the change in height with time after applying a step load to the disc/vertebral body system was measured. It was expected that the creep displacement would converge towards an equilibrium value where the applied load is balanced by the swelling pressure of the nucleus. This experimental approach allowed quantification of the transient behavior of the disc system. The 3 and 4 parameter viscoelastic solid models [39, 40] were used, as well as the water transport model by Cassidy et al. [42].

For the initial height of the disc, the height was measured from the high resolution midsagittal image acquired prior to loading the disc, using NIH Image software. This initial height was used to calculate the strain (change in length/initial height) for the disc creep data.

Given the large number of data points (on the order of 2,500), the data set was subsampled, taking every tenth sample for the curve fitting. KaleidaGraph 3.0.4 (Abelbeck Software, Synergy Software, Reading, PA) run on a Macintosh Powerbook 540c (Apple Computer, Cupertino, CA) was used to fit the data, using the Levinburg-Marquadt algorithm. Sample curve fits for the 3 parameter solid, 4 parameter solid and the water transport model are shown in Figures 22-26.

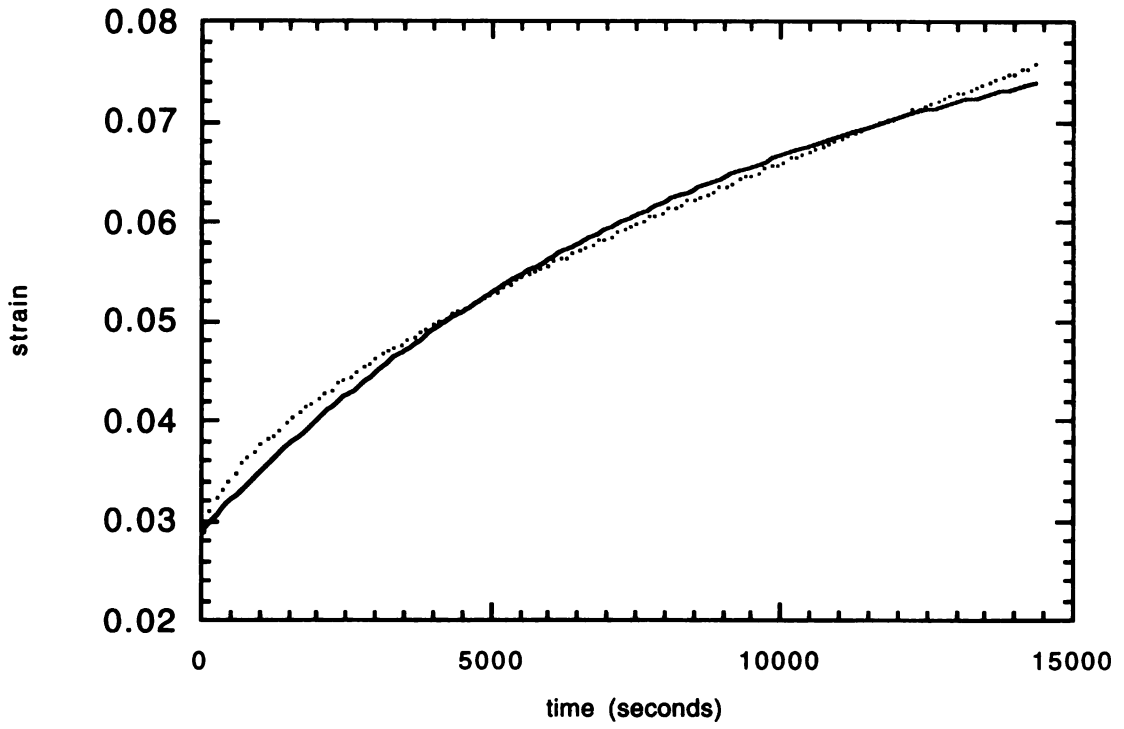


Figure 22: 3 parameter solid model curve fit for specimen 10 (age = 37 years at time of death, Thompson grade 1),  $r = 0.998$ , solid line is the curve fit.

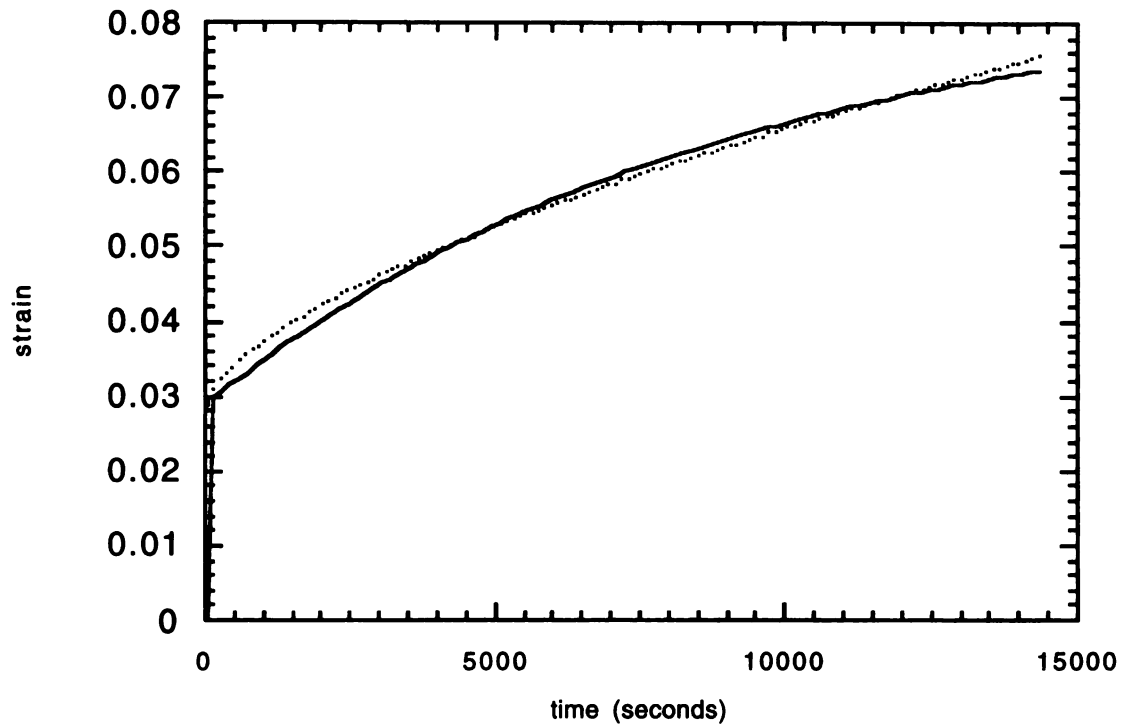


Figure 23: 4 parameter solid model curve fit for specimen 10 (age = 37 years at time of death, Thompson grade 1),  $r = 0.998$ , solid line is the curve fit.

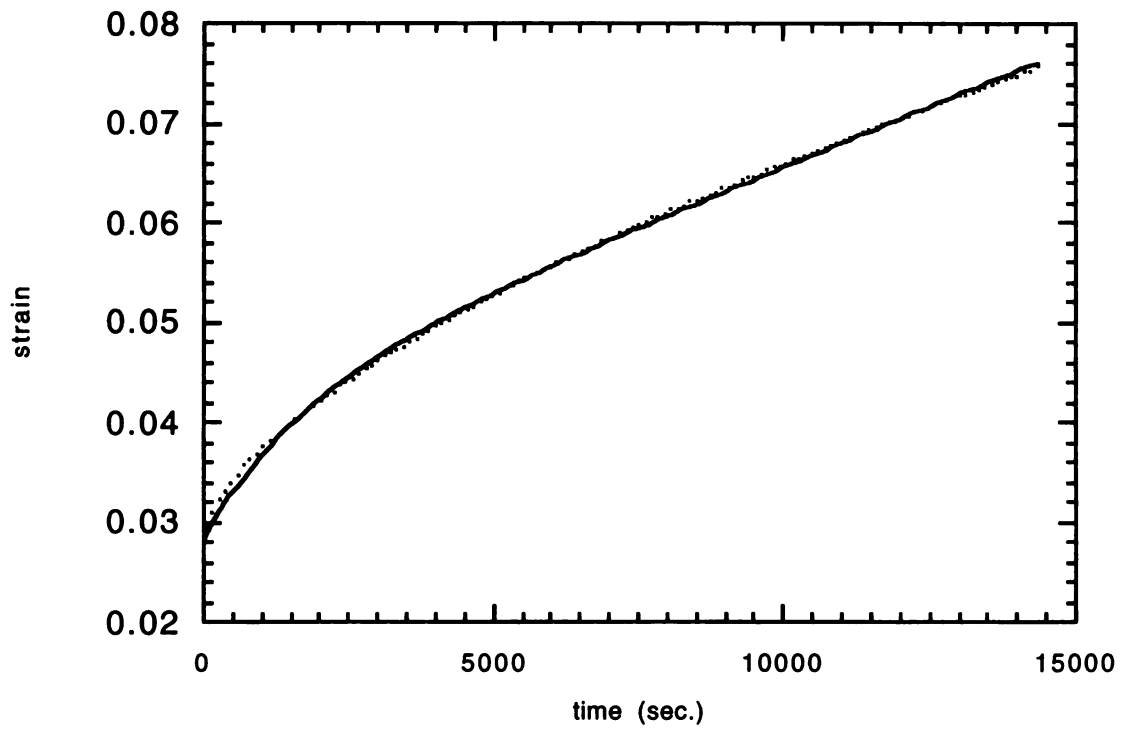


Figure 24: Water transport model curve fit for specimen 10 (age = 37 years at time of death, Thompson grade 1),  $r = 0.999$ , solid line is the curve fit.

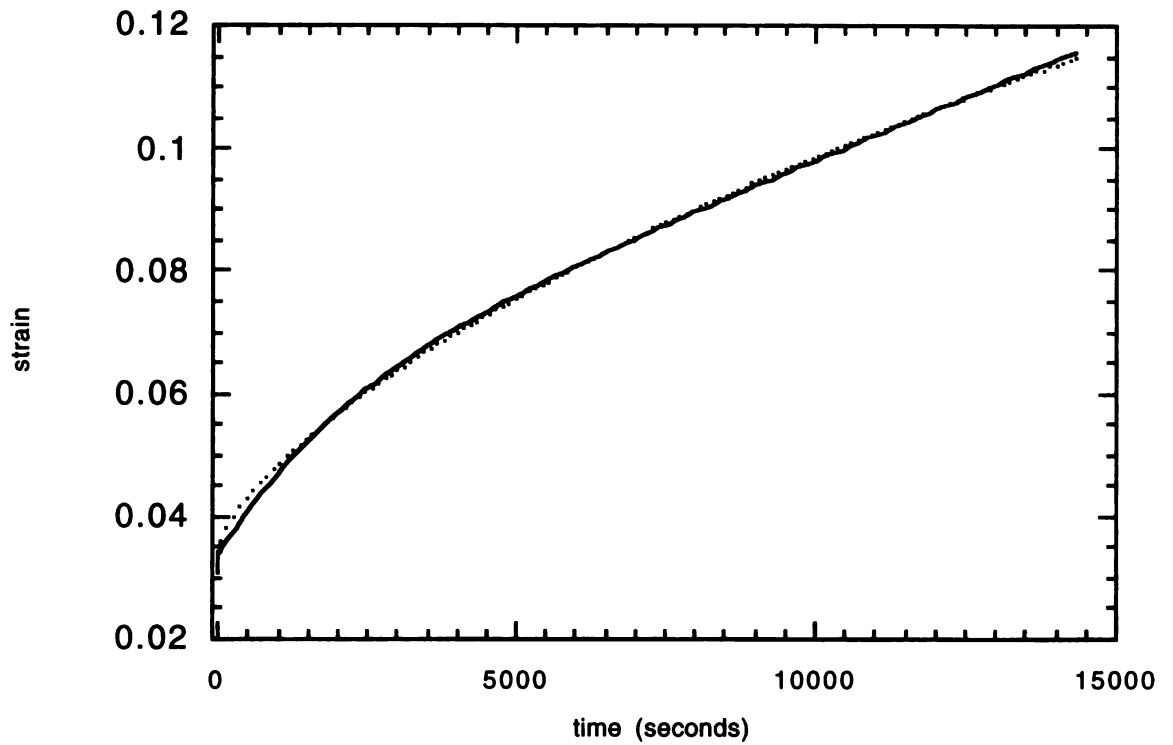


Figure 25: Water transport model curve fit for specimen 13 (age = 62 years at time of death, Thompson grade 3),  $r = 0.999$ , solid line is the curve fit.

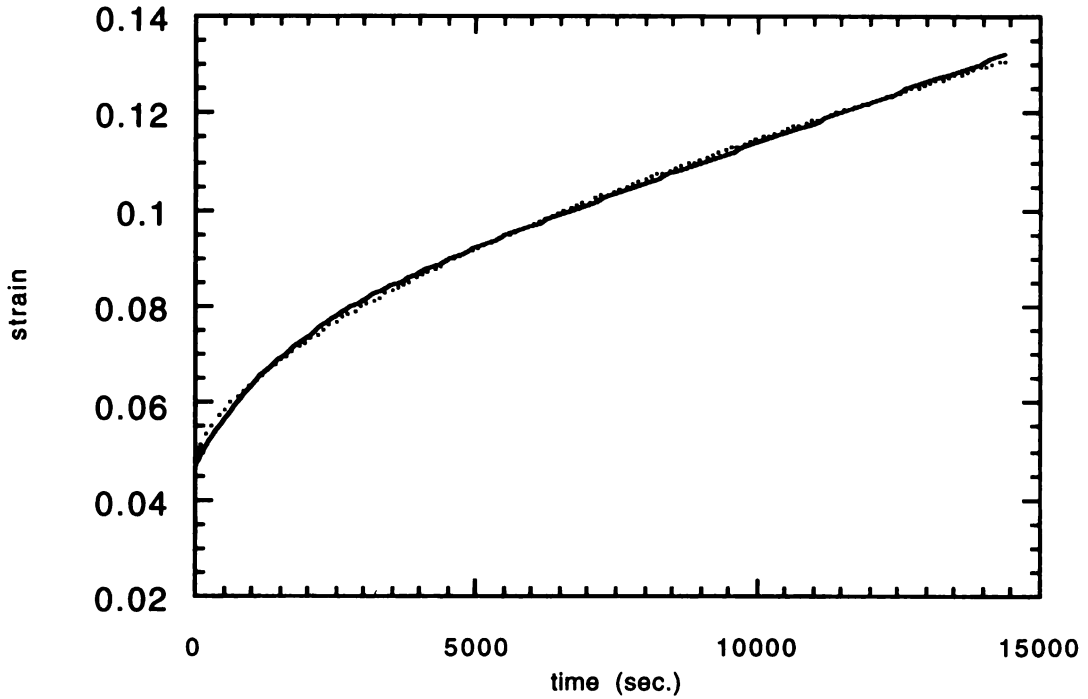


Figure 26: Water transport model curve fit for specimen 7 (age = 62 years at time of death, Thompson grade 4),  $r = 0.997$ , solid line is the curve fit.

For the 3 and 4 parameter solid models, the stiffness and creep rate(s) were calculated from the elastic and viscous parameters as follows:

$$\text{stiffness ratio} = \frac{E_2}{E_1} \quad \text{Equation 25}$$

$$\text{creep rate} = \frac{E_i}{\eta_i} \quad \text{Equation 26}$$

The water transport model assumes certain values for the disc-endplate-vertebral body system. The thickness of cartilage,  $L$ , was assumed to be 0.5 mm. and the initial osmotic pressure,  $P_0$ , was assumed to be 0.2 MPa. The initial disc height,  $h_0$ , was measured from the high resolution MR images and taken as the average of the central nucleus height and the peripheral annulus height.

For the water transport model, an overall system parameter, the time constant,  $\tau$ , for the creep curve, was also calculated:

$$\tau = \frac{h_i L}{2KD} \quad \text{Equation 27}$$

One difficulty found in the analysis of early specimens (numbers 1 through 7) was that the MTS computer did not correctly sample immediately after the application of the step load. A delay in sampling the data (with a gap in the data) at the point in time when the load was actually being applied led to uncertainty as to where to designate  $t = 0$ . This may have introduced a small error in the first four specimens; however, the time interval ranged from 0.43 to 0.50 second, and this was quite small relative to the total time of four hours that the creep experiment was performed. The last data point before the step load was assumed to be  $t = 0$ . Specimen 7 had a delay of 10 seconds before the first loaded point was recorded. For this one specimen, the first loaded point was taken as  $t = 0.5$  seconds.

Because there was some uncertainty as to the actual  $t = 0$  point, the initial strain point, which could be subtracted off before fitting the water transport model (see Equation 8), was fit as a fourth parameter of the curve.

Another technical problem found with the MTS machine was that the LVDT (linear variable differential transformer) developed a partially broken wire leading to it. While some tests were prematurely terminating during this period of time, it was not realized that an intermittent loss of continuity of one of the LVDT wires was the cause, until gross inaccuracies of displacement were noted. The accuracy of the measurements for specimens 3 through 5 is, therefore, questionable. The initial strain on these specimens is, in fact, nearly an order of magnitude larger than the remaining nine specimens. Because of the uncertainty of this displacement data, these three specimens were excluded from the final analysis of creep parameters vs. Thompson grade or MR parameters.

Considering the mechanism of action of an LVDT, that is, a primary transformer winding that is energized while a ferromagnetic core that induces current in the secondary

windings moves, it could be argued that a partially broken wire leading to the sensor could result in an increased resistance in series with the LVDT. One might expect an offset of the voltage from the expected, but there would be no way to predict the magnitude of the offset or its consistency from test to test.

Interestingly, the data from specimens 3-5 could be fit with the water transport model, showing an initial strain that was about 10 times larger than the remaining 8 specimens. The parameters derived for the model were also within the range of the other specimens. A table presenting the results of the comparisons including these specimens will be included in the Results section; however, the validity of this data is in question.

After noting that the water transport model had the best fit to the experimental data, each of the parameters from the water transport model was plotted versus the Thompson grade, the MR parameters and the calculated water content to look for trends between these. The individual disc's subspecimens that had been subjected to alteration in hydration were used to calibrate the diffusion coefficients to the tissue water. Figure 27 shows a sample plot of the nuclear subspecimens from one disc. This graph was used to estimate water content before compression of the disc.



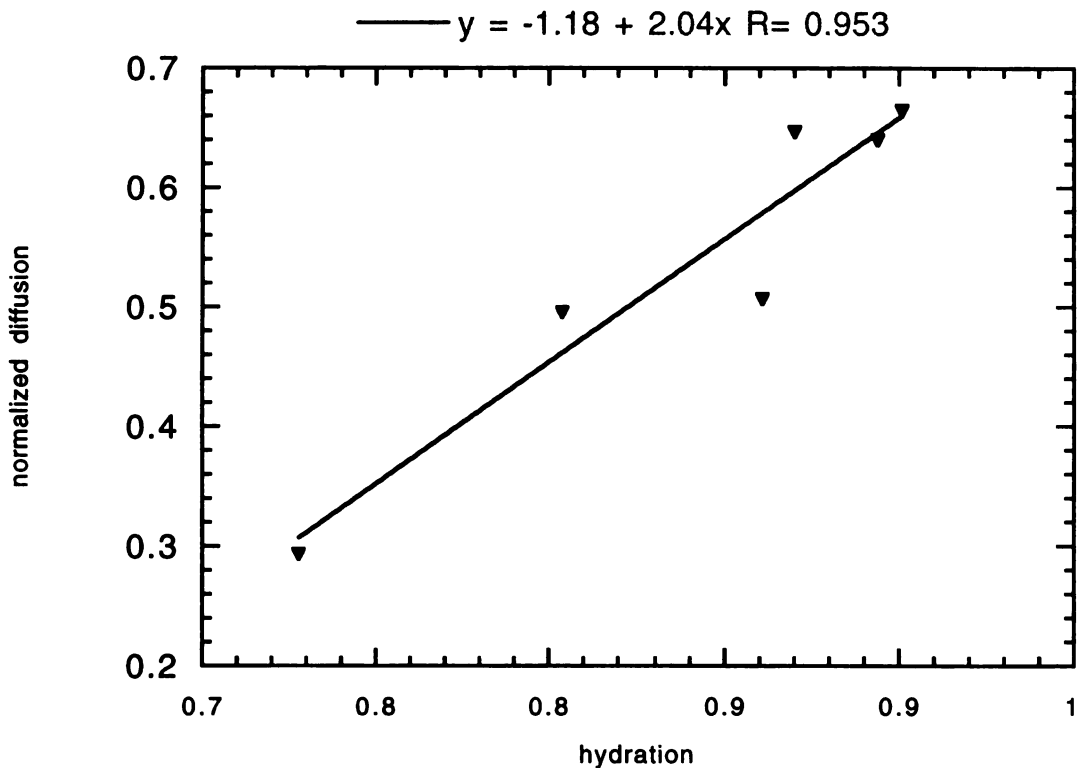


Figure 27: Normalized diffusion versus tissue hydration for the subspecimens of specimen 12. A graph like this was used to estimate nuclear tissue water from each of the intact specimen's images.

### Statistics

Statistical analyses were computed with SAS, version 6.12 (SAS Institute, Cary, NC), run on a Sun workstation. For the intact disc data, a repeated measures analysis of variance was used to compare MR parameters before and after compression, by location and grade. For the subspecimens' data, an analysis of covariance, a multivariate regression, was used to account for all the variables that would affect each of the MR parameters, thus adjusting for several covariates (predictors) simultaneously.

In order not to overestimate the significance of differences between MR parameters, the three nuclear ROI's were combined to one mean value for the nucleus of each specimen, and the same was done for the annular ROI's for each specimen. This resulted

in two values for each of the specimens, or 24 values (13 specimens minus one specimen loaded incorrectly in the scanner) measured before and after compression (T1, T2 and D) and also the x, y and z directions for the diffusion data.

The analysis of data for trends in the creep parameters to the MR parameters used linear regression implemented in Kaleidagraph 3.0.4. Pearson's product-moment correlation coefficient,  $r$ , was reported to describe the degree of scatter about the best-fit line, and the  $p$  value was calculated using the  $t$  statistic (Equation 28) to estimate the probability that one could have observed the trend in the data by chance alone [103].

$$t = \frac{r}{\sqrt{(1-r^2)/(n-2)}} \quad \text{t statistic} \quad \text{Equation 28}$$
$$v = n - 2 \quad \text{degrees of freedom}$$

To analyze the trends between the creep parameters and the Thompson grade, the Spearman rank order statistic was used [103]. This is the analogous test to the Pearson's correlation coefficient, used for data that is grouped and ranked (the Thompson grade).

## **VIII. RESULTS**

### **PRELIMINARY DATA**

#### **Reproducibility of T1, T2 Measurements in Liquids**

To test for T1 reproducibility, five vials of liquids with varying concentrations of gelatin and gadolinium (a paramagnetic T1 contrast agent) were imaged with the spin-echo sequences described in the methods section, using the knee coil. The average change in T1 on a repeat scan was 6.6%, with a range from 1.7 to 14%. The 14% difference was on the vial at the end of the knee coil, near the opening. The estimated T2 for the water and saline vials, repeated 5 times, had a coefficient of variation (mean/st. dev.) of 2.3%.

To test the consistency of relaxation measurements at different spatial locations within the wrist coil, twelve four-milliliter Wheaton vials (Fisher Scientific, Pittsburg, PA) were filled with gadolinium-doped saline (0.075 mM., Magnevist, Berlex Laboratories, Wayne, N.J.) to result in a T1 of approximately 2500 ms. and a T2 of approximately 200 ms. The spin-echo parameters were the same as described for the tissue imaging. On earlier images, it was noted that the signal intensity of phantoms near the openings of the coil was much smaller, so that any specimens imaged were placed beyond the first 2 cm. of the coil opening.

The mean T1 over the twelve vials was 2480 ms. with a standard deviation of 351 ms., giving a coefficient of variation (mean/st. dev.) of 14.1%. A repeat image of three vials centrally in the wrist coil gave T1 values within 6% of the initial values. The mean T2 of the vials was 207 ms. with a standard deviation of 12.9 ms, giving a coefficient of variation of 6.2%. The repeat image of three central vials gave T2 values within 8.7% of the initial values.

The relaxation time constants, T1 and T2, for regions within the disc were estimated using spin-echo sequences to image a central 3 mm. slice of disc in an old and young specimen. TR and TE were varied as described in the methods section. The following data were found (Figure 28):

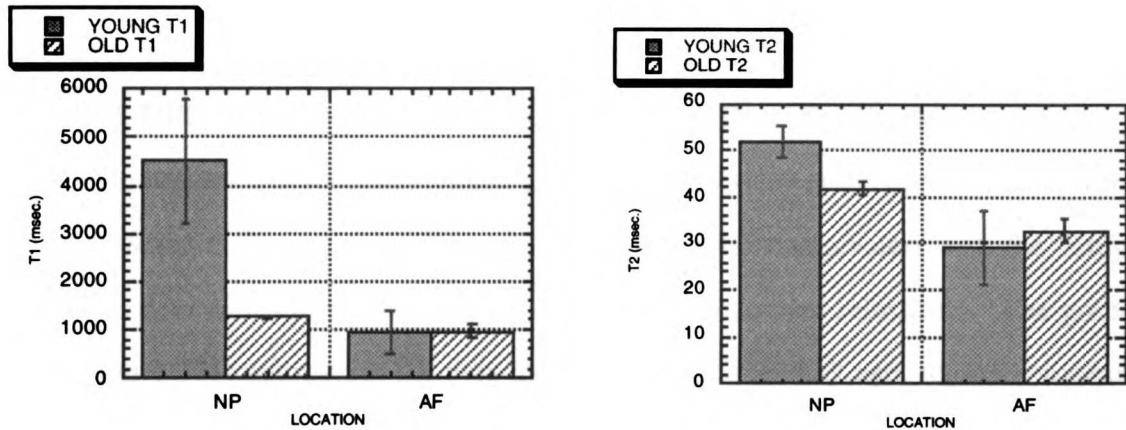


Figure 28: T1 and T2 relaxation measurements for a young and old IVD, shown by region, nucleus pulposus or annulus fibrosus.

By an analysis of variance with post hoc comparisons, the T1 for the young NP was significantly greater than the other regions. T2 was significantly greater for the young NP compared with the young AF or the old AF.

### Diffusion-Weighted Imaging of Liquids and IVD Specimens

The modified spin-echo diffusion sequences were tested on vials of water, saline, acetone, glycerol, and different concentrations of gelatin. Diffusion gradients were applied for a duration of 25 ms. separated by 29 ms. Initially, gradients were applied in the readout direction, physically from left to right in the magnet bore, and a 5 mm. axial slice of liquid was imaged at steps of gradient varying from 0 to 2.2 Gauss/cm.

The measured  $D(\text{water})$  was  $2.2 \times 10^{-5} \text{ cm}^2/\text{sec.}$ , which is within 5% of published values for the diffusion coefficient of water [104, 105].  $D$  for acetone was  $5.2 \times 10^{-5} \text{ cm}^2/\text{sec.}$ , which is within 10% of published values. Varying dilutions of glycerol/water and gelatin/water produced slower diffusion coefficients than that of free water, and these values decreased, as expected, with increasing amounts of glycerol or gelatin.

### Reproducibility of Diffusion Coefficient Estimation for Liquids

The ability of this technique to reproducibly estimate the diffusion coefficient of liquids was tested by repeating the diffusion-weighted imaging of the same set of vials of

liquids on another day. Repeated diffusion coefficients for saline and water were within 5%, and repeated measures for acetone varied about 10%.

### Measured Diffusion Under Stress Relaxation of Disc Specimens

Two preliminary specimens, aged 25 years and 60 years at the time of death, were tested for water diffusion measurements before and after compression with the screw mechanism device, resulting in a step of displacement or stress relaxation. The graph below (Figure 29) summarizes the data for the two specimens by age, region - nucleus pulposus or annulus fibrosus - and before or after loading.

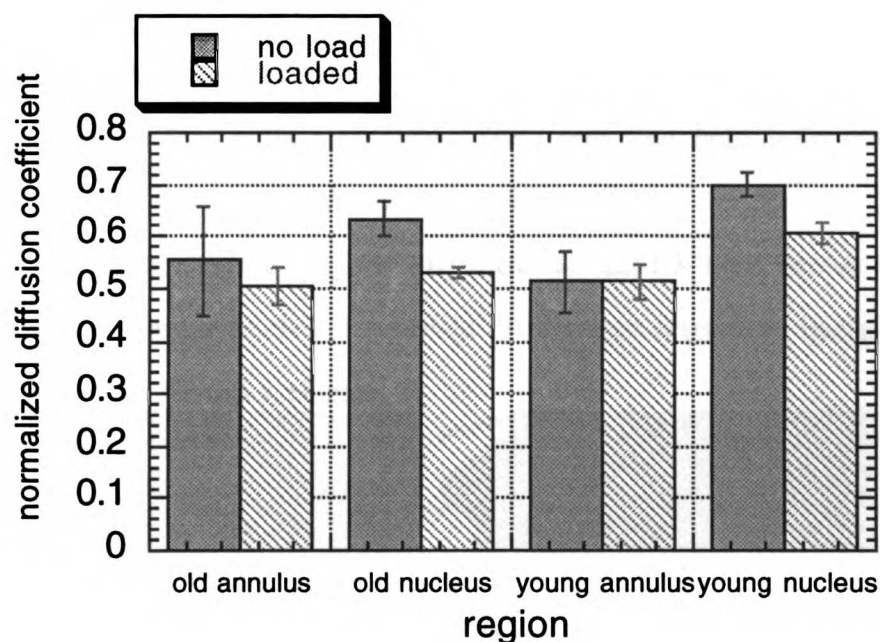


Figure 29: Bar graph comparing the water diffusion coefficient, normalized to saline diffusion, measured with modified spin-echo techniques for intact old and young intervertebral discs, by region - annulus fibrosus or nucleus pulposus, and before and after a step displacement.

The diffusion coefficient within the disc tissue was 40 to 70% of free water diffusion. This is consistent with the values that other researchers have obtained for tissue [67]. Significant differences ( $p < 0.05$ ) were found in the diffusion coefficients for young nucleus > young annulus, but not for the old nucleus versus annulus. Diffusion in the young nucleus was significantly greater than the old nucleus, but there was not a significant

difference by age for the annular regions. The diffusion in the nucleus unloaded was greater than the loaded diffusion coefficient for both specimens.

### **High Resolution Midsagittal Images**

A nonmagnetic compression apparatus with integral load cell was designed and manufactured for use in the MRI scanner. High resolution imaging was performed with a 1.5 Tesla MRI scanner (Signa, General Electric) using a wrist coil. The imaging sequence was optimized to be a fast spin-echo (FSE) sequence with TR = 4000, TE = 124, FOV = 8cm, matrix = 512 x 512 and slice thickness = 3.0 mm. Sagittal images were obtained that resolved annular fibers before and after compression.

Images were taken in the axial and midsagittal planes before and after applying 250 pounds of compressive load to the specimens. Specimens were held in the nonmagnetic apparatus shown in the Materials/Methods section (Figure 13).

The following images (Figure 30) show an L2-L3 disc before and after compression. The annular fibers are resolved in this high resolution image and seen bulging radially outward in this specimen.

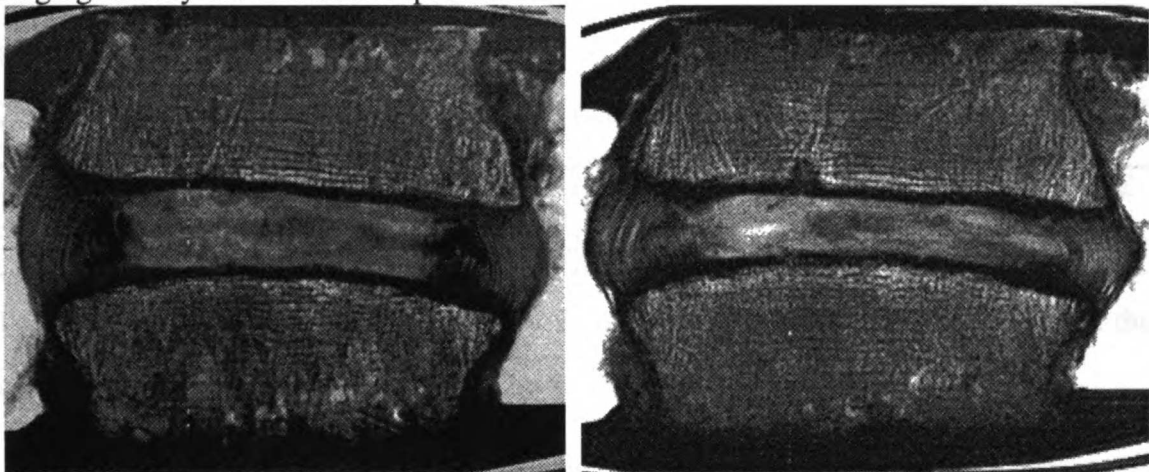


Figure 30: Midsagittal image of an L2-L3 intervertebral disc, before (left image) and after (right image) applying axial compression.

Thus, the feasibility of using MRI to follow intradiscal fiber deformation during compression in the scanner was established with preliminary images such as these.

## Diffusion Tensor Imaging

Preliminary data was collected for a uniform saline phantom that had been doped with gadolinium. The standard spin-echo sequence was modified to include trapezoidal diffusion gradients from 0 to 2.2 Gauss/cm. Combinations of x (readout), y (phase encode) and z (slice select) were applied at 0, 1.0, and 2.2 G/cm. in the following seven directions: (1,0,0), (0,1,0), (0,0,1), (1,1,0), (1,0,1), (0,0,1), and (1,1,1). A total of 15 points were sampled. TE = 70 ms., TR = 500 ms., field of view = 8 cm., slice thickness = 10 mm., matrix size = 256 x 128.

After determining the b matrix values for each of the 14 steps of applied diffusion gradients, multiple linear regression was used to determine the best values for the diffusion tensor matrix.

A comparison of the diffusion tensor with and without taking into account imaging gradients was simulated by zeroing the imaging gradients in the b matrix values prior to numerical integration and multiple linear regression.

The diffusion tensor values for the saline phantom at 22°C with and without imaging gradients were as follows:

with imaging gradients (mm.sq./sec.)	without imaging gradients (mm.sq./sec.)
1.97E-03   -4.24E-04   -8.35E-05	2.30E-03   -4.07E-04   -6.43E-05
-4.24E-04   2.16E-03   -1.32E-04	-4.07E-04   2.02E-03   -1.15E-04
-8.35E-05   -1.32E-04   2.22E-03	-6.43E-05   -1.15E-04   2.20E-03

To adjust for the temperature difference to allow comparison with published values for the water diffusion coefficient, the Stokes-Einstein equation was used:

$$D_{298K} = \frac{D_m \mu_{T_m}}{T_m \mu_{298K}} 298K \quad D_m \text{ is measured at temp.} = T_m \quad \text{Eq. 19}$$

The diffusion tensors then become

<b>with imaging gradients (mm.<sup>2</sup>/sec.)</b>			<b>without imaging gradients (mm.<sup>2</sup>/sec.)</b>		
2.19E-03	-4.70E-04	-9.26E-05	2.55E-03	-4.52E-04	-7.13E-05
-4.70E-04	2.40E-03	-1.46E-04	-4.52E-04	2.24E-03	-1.28E-04
-9.26E-05	-1.46E-04	2.46E-03	-7.13E-05	-1.28E-04	2.44E-03

The values for diffusion in the x, y and z directions are close to the published values for water of 2.34E-3 mm<sup>2</sup>/sec. at 25.5° C [85]. The diffusion coefficient in the x direction is overestimated when the imaging gradients are assumed to be zero. The x direction is the readout direction, or, the direction in which a gradient is applied while acquiring the echo. It includes the read dephaser, the gradient applied to dephase the spins in the opposite direction to the readout gradient, early in the sequence and the readout gradient at the end. The long time between these gradients would allow some diffusion to occur between them and add to the loss in signal intensity due to the diffusion gradients.

The diffusion coefficient in the y direction was actually smaller when the imaging gradients were not included. This is probably due to the fact that the phase encode direction's gradients were assumed to be zero in both cases while it actually changes for each phase encode step, and the diffusion coefficient calculated then varied due to the multiple linear regression fit weighted by the nonzero b values for the x and z directions.

The z direction diffusion coefficient was very similar. This maybe due to the small size of the slice select gradient (the gradient applied to select the spins in the appropriate slice for imaging) and the fact that the crusher gradients (gradients placed to remove unwanted transverse magnetization) were placed very close on either side of the 180 degree pulse, with little diffusion time between them.

When these techniques of data collection with multiple gradient applications were attempted on actual human disc specimens, the signal intensity remaining after adding two directions of gradients at amplitudes of 2 Gauss/cm. was too low to visualize the disc: the image became lost in the noise. The amount of tissue water, and therefore protons, was too low to use this technique on the disc specimens.



Instead of using the diffusion tensor method to account for the imaging gradients, normalization of the specimen diffusion to saline diffusion in the same image at the same temperature was used for the diffusion results, as mentioned in the Diffusion Measurements with MRI in the Background section (page 27). This method corrects for the effects of imaging gradients on the specimens' observed diffusion coefficients. Estimates are made of diffusion along the direction of the applied gradients.

### Altering Tissue Hydration with PEG Solutions

As discussed in the Materials/Methods section, the subspecimens of each intact disc were equilibrated in PEG solutions to alter the disc tissue hydration. An example of the range of hydrations that resulted from the different PEG concentrations used is shown in Figure 31 below.

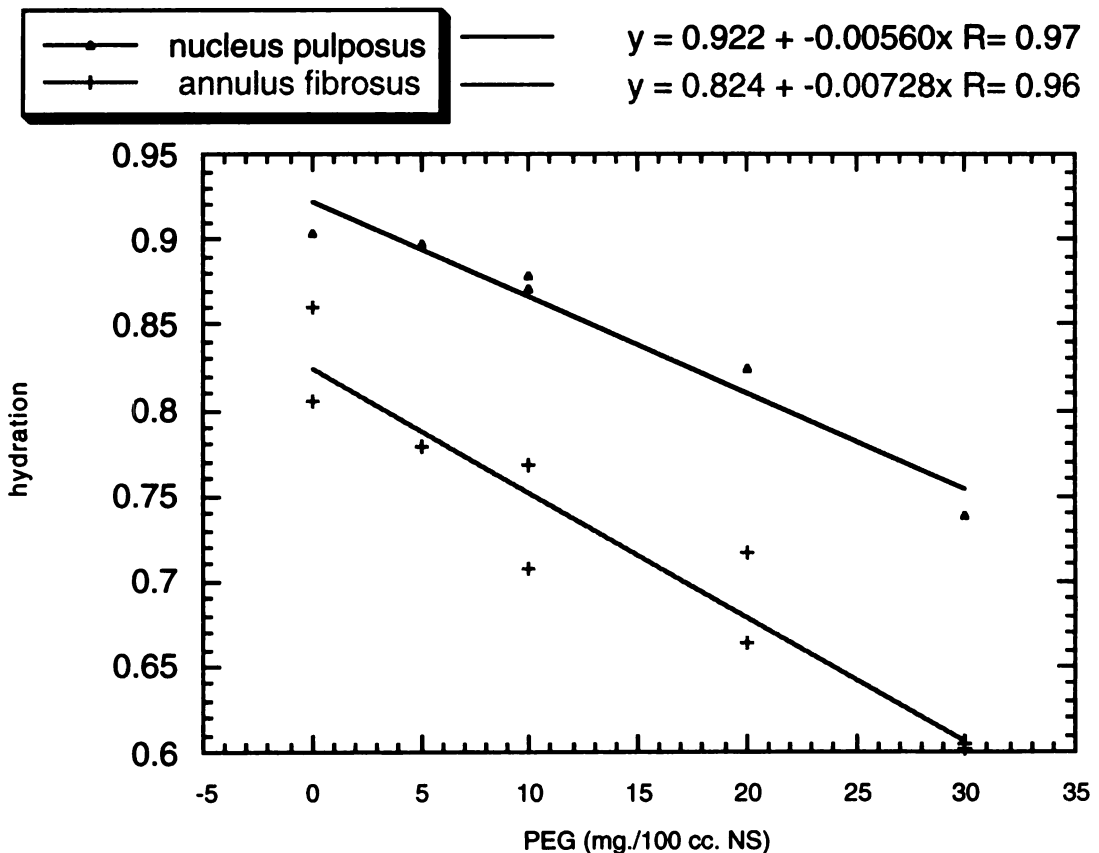


Figure 31: Example of water contents resulting from equilibrating tissue subspecimens from one disc in PEG solutions.

To give an overview of all the data to be presented in this section, Table 4 shows the comparisons that will be studied. The letters A, B, C, D, E and F refer to the corresponding section that follows and describes in detail the findings. Section D will also consider the fit of the different creep models to the mechanical test data.

As discussed in the data analysis section, specimen 2, which had a tumor in the inferior vertebral body, was excluded from both the MR data and the creep data ( $n = 12$ ). For the MR of the intact discs, specimen 10 was excluded due to preloading in the scanner ( $n = 11$ ). For the creep data, specimens 3 through 5 were excluded due to the malfunctioning LVDT ( $n = 9$ ). For comparisons between the MR data and the creep parameters,  $n = 8$ .

	A) MR relaxation		B) Diffusion Coefficients		
	T1	T2	Dx	Dy	Dz
<b>INTACT</b> n = 13	comparisons by grade, location and loading state	comparisons by grade, location and loading state	comparisons by grade, location, loading state and diffusion direction	comparisons by grade, location, loading state and diffusion direction	comparisons by grade, location, loading state and diffusion direction

C) High Resolution Images

High Res n = 13	before loading	parameters measured: A/P diam., height and presence of inward bulge
	after loading	

E) Effects of Tissue Biochemistry on MR Parameters

Subspecimens	T1	T2	Dx	Dy	Dz
NP n = 78	Comparisons by hydration, collagen content, proteoglycan content and Thompson grade				
AF n = 130					

D) Creep Parameters vs. Thompson grade F) Creep Parameters vs. MR Parameters

	K	D	G	$\epsilon_0$	$\tau$
1/T1	no correlation	no correlation	no correlation	r = 0.53 p ~ 0.20 n = 8	no correlation
1/T2	no correlation	no correlation	no correlation	no correlation	no correlation
D	no correlation	no correlation	no correlation	r = 0.29 p ~ 0.50 n = 8	r = 0.28 p ~ 0.50 n = 8
grade	$r_s = 0.88$ p = 0.003 n = 9	$r_s = -0.80$ p = 0.013 n = 9	$r_s = -0.80$ p = 0.013 n = 9	$r_s = 0.125$ p = 0.742 n = 9	$r_s = 0.65$ p = 0.058 n = 9
% H2O	r = 0.54 p = 0.18 n = 8	r = -0.45 p = 0.29 n = 8	r = -0.55 p = 0.17 n = 8	no correlation	r = 0.43 p = 0.31 n = 8

Table 4: Overview of the results to be presented. Lettered headings correspond to the results sections that discuss these findings in detail.

As mentioned in the analysis section, the calculated parameters for the water transport model for specimens 3, 4 and 5 fell within the range of the other specimens, except for the initial strain. If these specimens are included in the analysis, the following correlations result (Table 5).

	K	D	G	$\epsilon_o$	$\tau$
1/T1	no correlation	no correlation	no correlation	r = 0.53 p ~ 0.20 n = 8	r = 0.18 n = 11
1/T2	no correlation	no correlation	no correlation	no correlation	r = 0.31 p = 0.40 n = 11
D	no correlation	no correlation	no correlation	r = 0.29 p ~ 0.50 n = 8	r = 0.42 p = 0.20 n = 11
grade	$r_s = 0.787$ p = 0.003 n = 12	$r_s = -0.745$ p = 0.007 n = 12	$r_s = -0.612$ p = 0.037 n = 12	$r_s = 0.125$ p = 0.742 n = 9	$r_s = 0.353$ p = 0.256 n = 12
% H2O	r = 0.30 p = 0.39 n = 11	r = -0.38 p = 0.27 n = 11	r = -0.49 p = 0.13 n = 11	no correlation	r = 0.59 p = 0.19 n = 11

Table 5: Correlations between the creep parameters and Thompson grade, and the creep parameters and MR parameters, including specimens 3, 4 and 5 that had the LVDT problem.

#### A) MR Relaxation

An analysis of variance with repeated measure for loading state (loaded or not, same ROI) was used to compare the T1 and T2 measured from the images. For the T1 data, a significant difference was found by region, nucleus (mean = 1191 ms.) > annulus (mean = 902 ms.), p = 0.0014; and loading state, loaded > unloaded (p = 0.038). Table 6 summarizes the values for T1. The Thompson grade did not significantly affect the measured T1.

Level of region	Unloaded			Loaded	
	N	Mean	SD	Mean	SD
A	12	887	126	917	113
N	12	1179	233	1202	226

Level of Thompson	Unloaded			Loaded	
	N	Mean	SD	Mean	SD
1	2	1068	440	1197	511
2	6	940	195	1048	254
3	8	1107	249	1077	178
4	4	1007	161	1022	112
5	4	1032	310	1011	312

Table 6: Mean T1 values (ms.) by loading state, region (NP or AF) and grade. T11 and T12 denote T1 before and after compression.

For the T2 values, there was a significant difference by region, nucleus > annulus ( $p = 0.003$ ) and Thompson grade ( $p = 0.0129$ ). Table 7 summarizes these results. The loading state did not significantly affect the measured T2 ( $p = 0.120$ ).

Level of region	Unloaded			Loaded	
	N	Mean	SD	Mean	SD
A	12	38.6	6.13	41.4	5.60
N	12	56.2	22.0	57.8	20.8

Level of Thompson	Unloaded			Loaded	
	N	Mean	SD	Mean	SD
1	2	75.2	49.2	78.1	44.1
2	6	49.9	11.5	52.5	10.9
3	8	45.0	13.6	49.8	13.5
4	4	30.7	1.31	36.1	8.28
5	4	51.3	12.0	44.2	7.81

Table 7: Mean T2 values (ms.) by loading state, region and Thompson grade. T21 and T22 denote T2 before and after compression.

## B) Diffusion

By the method of analysis of variance with the repeated measures of diffusion direction (x, y or z) and compressive state (loaded or not), there were found to be

significant differences in the measured diffusion coefficients for region, nucleus > annulus (p = 0.04), Thompson grade (0.006), direction (p = 0.017) and state of compression (p = 0.018). Table 8 summarizes these results.

Level of region	-----DX1-----			-----DX2-----	
	N	Mean	SD	Mean	SD
A	12	0.377	0.0866	0.431	0.0715
N	12	0.462	0.123	0.497	0.104
Level of region	-----DY1-----			-----DY2-----	
	N	Mean	SD	Mean	SD
A	12	0.367	0.0657	0.434	0.0534
N	12	0.445	0.130	0.502	0.105
Level of region	-----DZ1-----			-----DZ2-----	
	N	Mean	SD	Mean	SD
A	12	0.439	0.0695	0.453	0.0708
N	12	0.465	0.132	0.475	0.101
Level of thompson	-----DX1-----			-----DX2-----	
	N	Mean	SD	Mean	SD
1	2	0.553	0.154	0.581	0.189
2	6	0.426	0.132	0.484	0.0520
3	8	0.422	0.0786	0.474	0.0661
4	4	0.312	0.0594	0.371	0.0526
5	4	0.446	0.121	0.449	0.124
Level of thompson	-----DY1-----			-----DY2-----	
	N	Mean	SD	Mean	SD
1	2	0.560	0.163	0.549	0.158
2	6	0.433	0.109	0.459	0.0707
3	8	0.392	0.0755	0.495	0.0442
4	4	0.282	0.0332	0.341	0.0491
5	4	0.442	0.0798	0.516	0.0756
Level of thompson	-----DZ1-----			-----DZ2-----	
	N	Mean	SD	Mean	SD
1	2	0.580	0.178	0.615	0.0835
2	6	0.477	0.0717	0.443	0.0802
3	8	0.446	0.0897	0.441	0.0580
4	4	0.327	0.0460	0.396	0.0663
5	4	0.486	0.0897	0.533	0.0416

Table 8: Mean normalized diffusion coefficients by region and Thompson grade. DX1 and DX2 refer to before and after loading. The X, Y or Z refers to the diffusion direction measured.

For post-hoc comparisons, the Student-Newman-Keuls test was used to look for differences between the directions and the Thompson grades. By diffusion direction,  $z > x$  and  $y$ , while the increase in diffusion was greater in the  $x$  and  $y$  directions than the  $z$  direction ( $p = 0.074$ ). Thompson grade 1 had the fastest diffusion and grade 4 the slowest, with 2, 3 and 5 intermediate in diffusion.

### **C) High Resolution Midsagittal Images**

The data acquired for this study included the high resolution FSE midsagittal image of each disc specimen before and after loading. Figure 32 summarizes the percentage change in heights and A/P diameters, as measured from the midsagittal images. Except for the most degenerated discs (grade 5), which decreased in height twice as much as the other discs, the specimens all had very similar increases in AP diameter and decreases in height.

As mentioned in the analysis section, for the specimens where a distinction could be made between the nuclear and annular regions on the image, the discs were all found to have outward bulging of the inner annular fibers, except for the disc with a tumor in the inferior vertebral body.

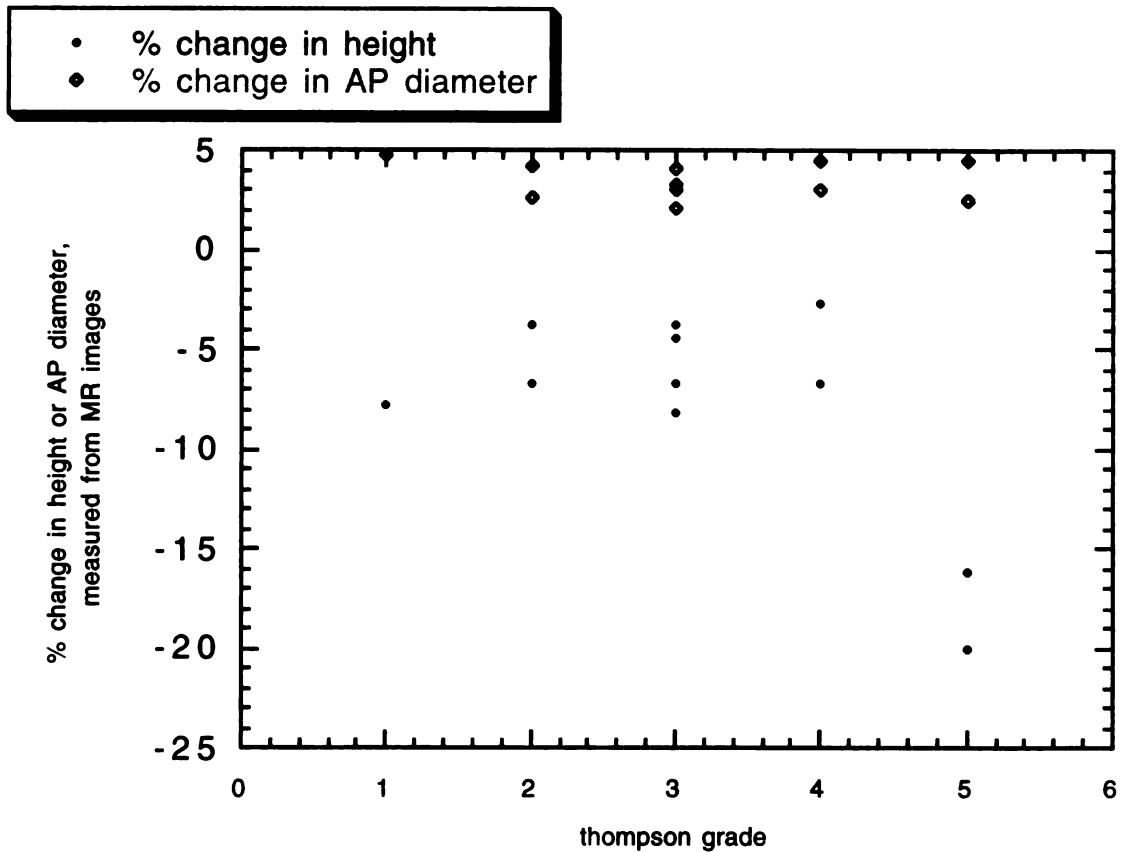


Figure 32: Plot of the percentage change in height or AP diameter of the disc, measured from the midsagittal FSE image, by Thompson grade.

#### D) Creep Models

The 3 and 4 parameter solid and the water transport models were used to fit the experimental data. The curve fits had high correlation coefficients; however, qualitatively one sees that the 3 parameter solid model does not match the early data well (the equation itself does not, in fact, begin from the origin). The 4 parameter solid model fits the early data better; however one sees a systematic steep linear portion of the curve leading to a sharp corner, followed by an overshoot and then a progressive under estimation of the strain with time, plateauing lower than the experimental data.

The water transport model, equivalent to the 4 parameter fluid model, had the best overall fit to the data. Because of the linear term in the equation, the increasing strain at the end of the four hour test period could be well-approximated.



Tables 9 to 11 summarize the creep model parameters derived from the curve fits.

<b>water transport model</b>							
<b>specimen</b>	<b>K</b>	<b>D</b>	<b>G</b>	<b>Eo</b>	<b>tau</b>	<b>thompson</b>	<b>calc. water</b>
1	3.12E-16	1.34E+06	9.34	0.0648	2628.6	5	0.738
2	2.91E-16	3.51E+06	20.34	0.1088	2164.3	2	0.832
3	2.57E-16	5.17E+06	18.60	0.1975	2249.9	1	0.866
4	2.43E-16	5.74E+06	21.18	0.1678	2013.4	2	0.756
5	3.33E-16	5.69E+06	21.54	0.1867	1327.7	3	0.692
6	1.42E-16	7.73E+06	23.35	0.0341	1740.7	2	0.747
7	3.54E-16	4.70E+06	19.32	0.0476	1623.8	4	0.652
8	2.74E-16	6.49E+06	20.57	0.0297	1729.8	3	0.794
9	2.96E-16	3.95E+06	17.86	0.0269	2164.1	4	0.687
10	1.83E-16	8.79E+06	21.24	0.0286	1709.3	1	0.752
11	4.88E-16	1.51E+06	7.52	0.0284	2621.1	5	0.808
12	3.09E-16	3.86E+06	20.19	0.0369	1752	3	0.764
13	2.10E-16	4.66E+06	18.86	0.0341	2079.5	3	0.710

<b>units</b>	<b>m<sup>4</sup>/ (N sec.)</b>	<b>N/m<sup>2</sup></b>	<b>N/ (m<sup>2</sup>s.)</b>	<b>unitless</b>	<b>sec.</b>		
--------------	------------------------------------	------------------------	---------------------------------	-----------------	-------------	--	--

Table 9: Water transport model parameters derived from the curve fits.

<b>3 parameter solid model</b>					
<b>specimen</b>	<b>E1</b>	<b>E2</b>	<b>eta 1</b>	<b>stiffness</b>	<b>creep rate</b>
1	1.71E+06	4.86E+06	1.16E+10	0.353	1.48E-04
2	2.35E+06	3.12E+06	2.69E+10	0.756	8.74E-05
3	3.81E+06	1.75E+06	4.08E+10	2.175	9.35E-05
4	3.74E+06	2.06E+06	4.29E+10	1.819	8.72E-05
5	4.26E+06	1.83E+06	3.54E+10	2.333	1.20E-04
6	4.65E+06	9.61E+06	5.44E+10	0.483	8.54E-05
7	3.63E+06	6.79E+06	3.29E+10	0.534	1.10E-04
8	4.18E+06	9.87E+06	5.50E+10	0.423	7.59E-05
9	2.88E+06	1.04E+07	3.54E+10	0.278	8.15E-05
10	5.46E+06	1.07E+07	7.34E+10	0.511	7.44E-05
11	2.24E+06	8.40E+06	1.45E+10	0.267	1.55E-04
12	2.55E+06	7.56E+06	3.26E+10	0.337	7.81E-05
13	3.20E+06	8.65E+06	4.13E+10	0.370	7.75E-05

<b>units</b>	<b>N./m<sup>2</sup></b>	<b>N./m<sup>2</sup></b>	<b>kg./ (m-sec.)</b>	<b>unitless</b>	<b>1/sec.</b>
--------------	-------------------------	-------------------------	--------------------------	-----------------	---------------

Table 10: 3 parameter solid model parameters derived from the curve fits.

<b>4 parameter solid model</b>							
<b>spec.</b>	<b>E 1</b>	<b>E 2</b>	<b>eta 1</b>	<b>eta 2</b>	<b>stiffness</b>	<b>creep 1</b>	<b>creep 2</b>
1	1.70E+06	5.27E+06	1.08E+10	2.62E+06	0.323	1.57E-04	2.008
2	2.42E+06	3.20E+06	2.52E+10	5.67E+05	0.757	9.59E-05	5.632
3	3.86E+06	1.76E+06	3.90E+10	5.59E+05	2.186	9.90E-05	3.157
4	3.85E+06	2.08E+06	4.00E+10	4.46E+05	1.850	9.62E-05	4.658
5	4.33E+06	1.86E+06	3.08E+10	4.31E+05	2.325	1.41E-04	4.315
6	4.82E+06	1.01E+07	5.00E+10	3.16E+06	0.478	9.64E-05	3.195
7	3.68E+06	7.17E+06	3.01E+10	3.07E+06	0.514	1.23E-04	2.335
8	4.73E+06	1.16E+07	4.16E+10	8.38E+05	0.407	1.14E-04	13.88
9	3.15E+06	1.27E+07	2.85E+10	1.01E+06	0.247	1.11E-04	12.62
10	6.21E+06	1.21E+07	5.61E+10	7.27E+05	0.513	1.11E-04	16.64
11	2.19E+06	1.20E+07	1.16E+10	1.46E+06	0.182	1.89E-04	8.198
12	2.86E+06	9.27E+06	2.50E+10	7.21E+05	0.308	1.14E-04	12.86
13	3.55E+06	1.01E+07	3.28E+10	7.14E+05	0.351	1.09E-04	14.18

<b>units</b>	<b>N./m<sup>2</sup></b>	<b>N./m<sup>2</sup></b>	<b>kg./ (m-sec.)</b>	<b>kg./ (m-sec.)</b>	<b>unitless</b>	<b>1/sec.</b>	<b>1/sec.</b>

Table 11: 4 parameter solid model parameters.

The water transport model parameters (K, D and G) correlated well with the Thompson grade of degeneration. The Spearman rank order correlation was used to study the graph of K, D or G versus Thompson grade, with  $n = 9$  (excluding the specimen with the tumor and the 3 specimens with the LVDT problem). The coefficients were  $r_s = 0.88$  with  $p = 0.003$ ,  $r_s = -0.80$  with  $p = 0.013$  and  $r_s = -0.80$  with  $p = 0.013$ , respectively.

Figure 33 shows the data for K, the permeability coefficient.

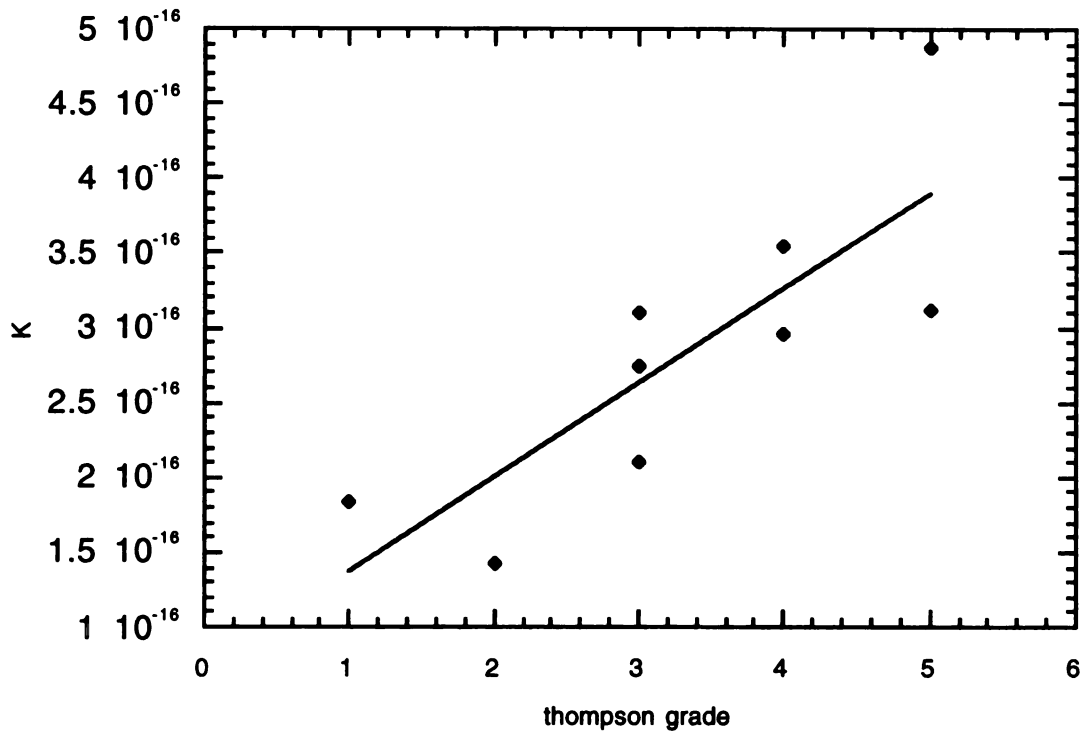


Figure 33: K (m<sup>4</sup>/N.sec.), the permeability parameter from the water transport model, graphed versus Thompson grade.  $r_s = 0.883$ ,  $p = 0.003$

The initial strain parameter from the water transport model had a minimal correlation to Thompson grade,  $r_s = 0.125$ ,  $p = 0.742$ , while the system parameter,  $\tau$ , showed a good correlation with grade:  $r_s = 0.65$ ,  $p = 0.058$

If specimens 3, 4 and 5 are included (Table 4), the relationships between K, D and G and Thompson grade remain about the same; and the system parameter,  $\tau$ , shows a lower correlation:  $r_s = 0.35$ ,  $p = 0.26$ .

#### E) Effect of Tissue Biochemistry on MR Parameters

For the disc tissue subspecimens that had been equilibrated in PEG solutions, examining both hydroxyproline (equivalent to collagen content) and GAG (equivalent to proteoglycan content) per dry weight, an analysis of variance of within specimen to between specimen variations showed highly significant differences,  $p = 0.0001$ , with the

variation between specimens being much greater than within specimens. This can be stated as the interspecimen variation in tissue biochemistry was greater than the intraspecimen variation.

Mean hydroxyproline ( $\mu\text{g}/\text{mg}$ ) was 61.9 for annulus specimens and 37.5 for nucleus specimens, with annular being significantly greater than nuclear specimens,  $p = 0.0001$ . Mean GAG ( $\mu\text{g}/\text{mg}$ ) for annulus was 145, and for nucleus was 199, with nucleus significantly greater than annulus,  $p = 0.0001$ .

Mean hydroxyproline and GAG ( $\mu\text{g}/\text{mg}$  dry weight), shown by location and Thompson grade, are given in Table 12. GAG tended to decrease with increasing Thompson grade for both NP and AF; while collagen decreased in the annulus, but had no trend in the nucleus pulposus.

Thompson grade	location	hydroxyproline			GAG	
		n	mean	s.d.	mean	s.d.
1	A	52	80.7	20.0	164.8	61.2
1	N	36	34.9	13.5	264.3	84.9
2	A	80	70.4	21.8	157.5	45.3
2	N	54	46.9	25.6	251.6	113.0
3	A	117	58.0	13.9	142.9	48.0
3	N	72	30.3	14.8	194.7	48.8
4	A	57	43.8	8.8	169.4	53.4
4	N	36	25.4	6.9	165.8	36.9
5	A	58	54.6	17.6	95.9	24.3
5	N	35	52.6	12.2	99.0	19.6

Table 12: Mean hydroxyproline and GAG ( $\mu\text{g}/\text{mg}$  dry weight), shown by location and Thompson grade.

The normalized diffusion results for the specimens were studied with an analysis of covariance considering Thompson grade (as a continuous measure), location (annulus or nucleus), diffusion direction (x, y or z), and biochemical measures: hydration, collagen and GAG. Hydration accounted for most of the variation in diffusion values ( $p = 0.0001$ ), with diffusion showing an increasing linear relationship to hydration (Figure 34).

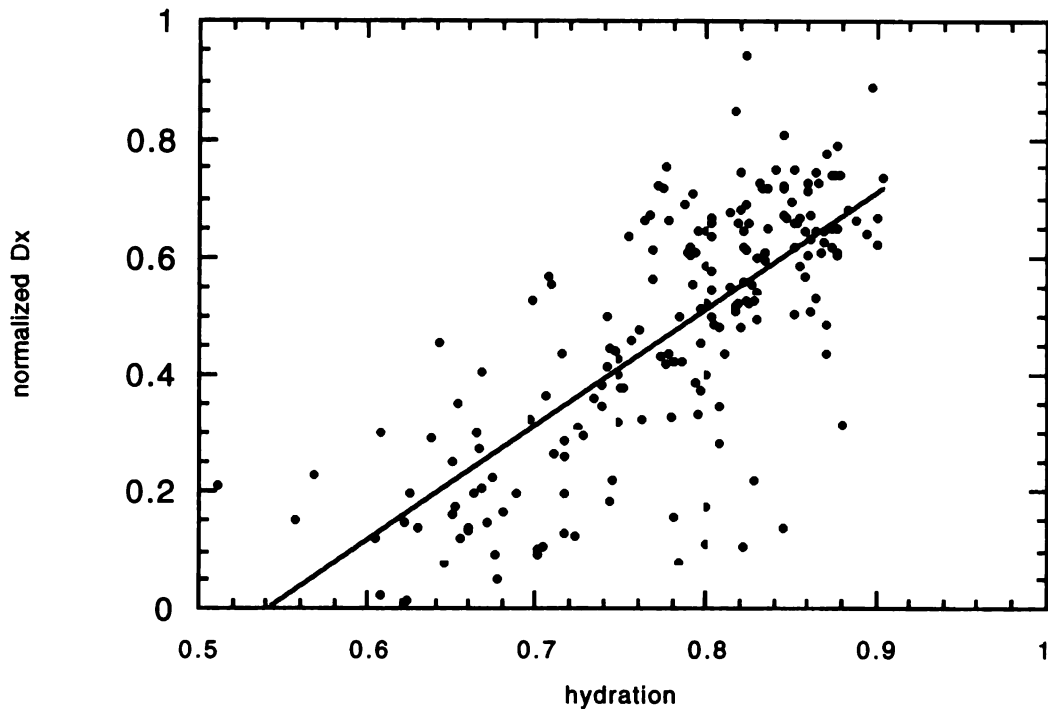


Figure 34: Normalized diffusion, x direction, all specimens:  $y = -1.06 + 1.98 x$ ,  $r = 0.74$ ,  $p < 0.001$

The relaxation rate,  $1/T1$ , studied with an analysis of covariance as for diffusion, without a direction category, showed significant effects of hydration ( $p = 0.0001$ ) and collagen content ( $p = 0.0001$ ).  $1/T1$  decreased with increasing hydration (slope=  $-0.003$   $1/\text{msec} \cdot \text{fraction hydration}$ ), and  $1/T1$  increased with collagen content (Figure 35).

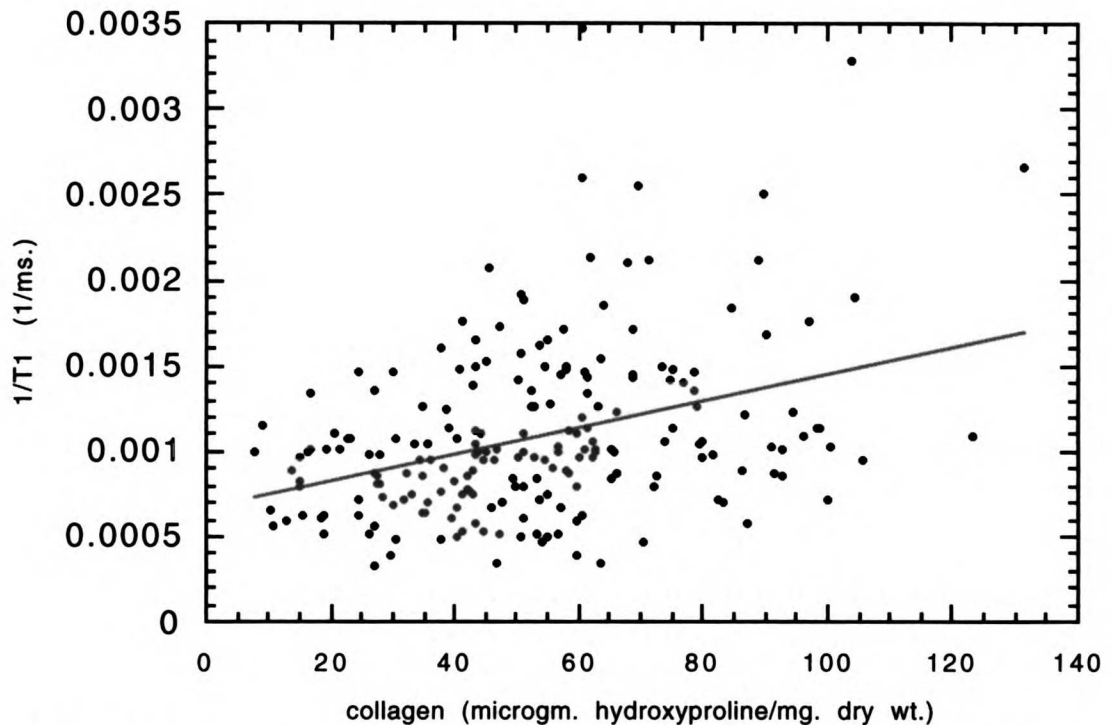


Figure 35: 1/T1 versus collagen content:  $y = 0.000679 + 7.77 e^{-06}x$ ,  $r = 0.37$ , ( $p = 0.0001$ )

1/T2, studied with the same categories and biochemical variables as for 1/T1, showed significant effects of hydration ( $p = 0.0002$ ) and location, with 1/T2 greater in the annulus than in the nucleus ( $p = 0.0004$ ).

For the purpose of comparison to published data on 1/T2 vs. collagen or 1/T2 vs. GAG, Figures 36 and 37 show these relationships. It should be noted, however, that in an analysis of covariance, neither collagen nor GAG was a significant predictor of 1/T2 after accounting for hydration and location. Values for  $p$ , the probability of observing the linear trend by chance, are calculated for the univariate case.

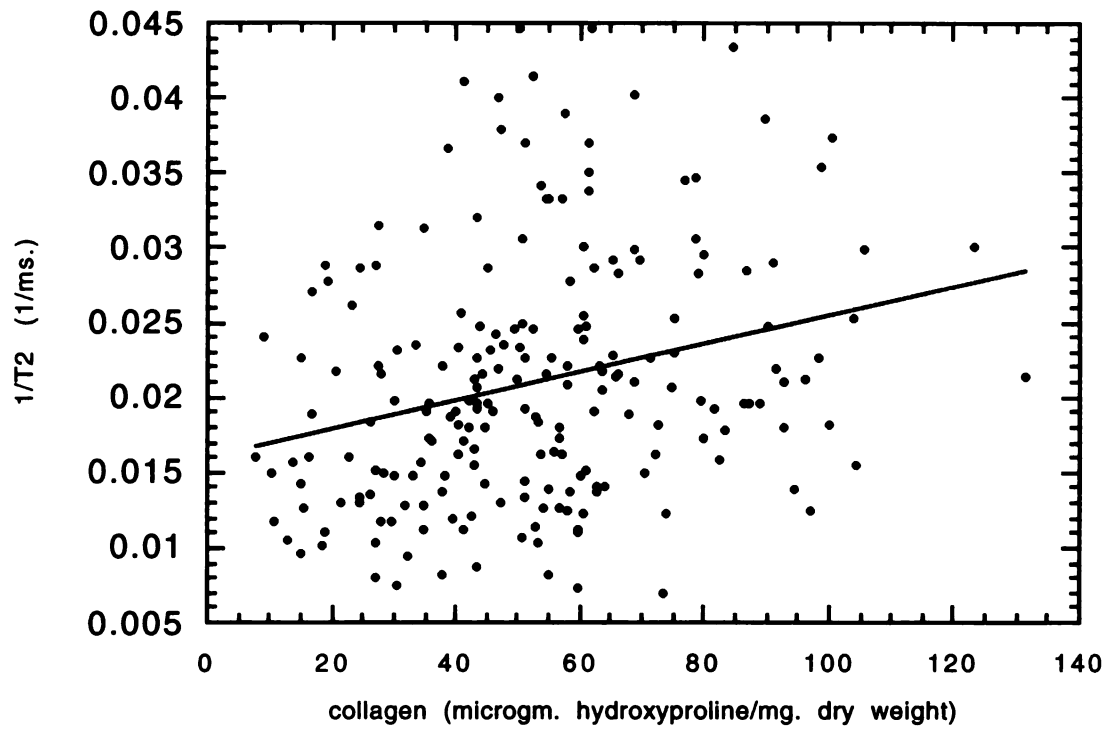


Figure 36: 1/T2 vs. collagen content:  $y = 0.016 + 9.44 \times 10^{-5} x$ ,  $r = 0.27$ ,  $p < 0.001$

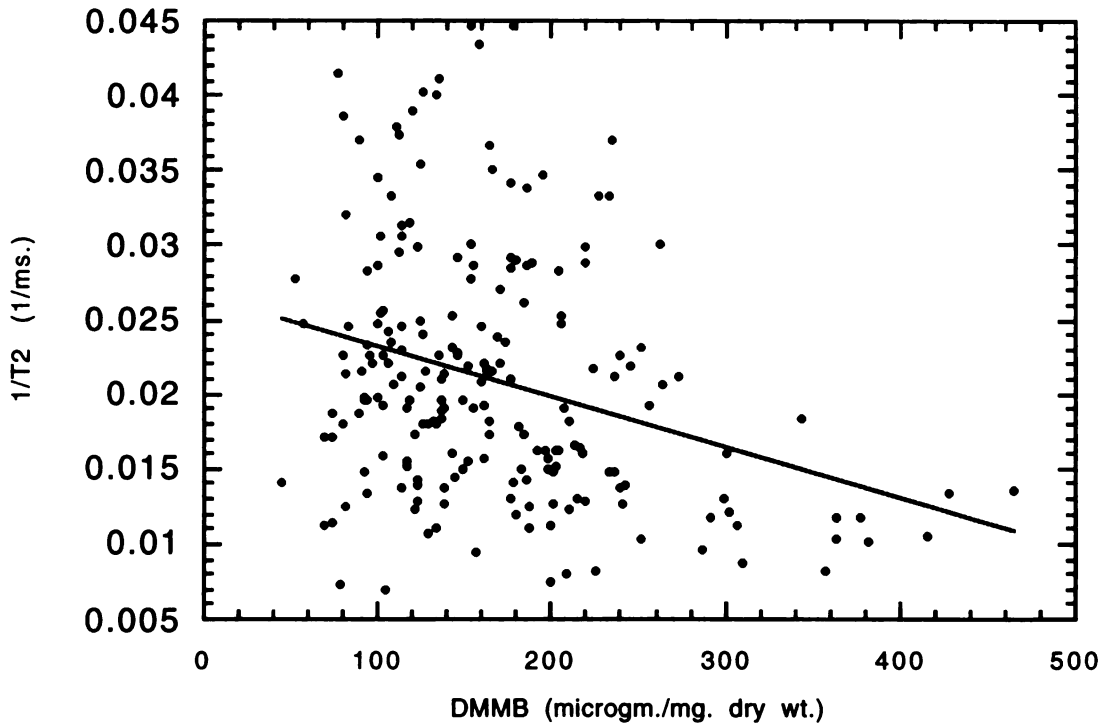


Figure 37:  $1/T2$  vs. GAG content:  $y = 0.0266 - 3.38 e^{-05}x$ ,  $r = 0.30$ ,  $p < 0.001$

Table 13 summarizes the results of the analysis of covariance, showing which variables predicted the MR parameters. Table 14 summarizes the MR data by Thompson grade. The grade 1 specimens had faster diffusion and longer T1 and T2 than the other grades, but the MR parameters did not tend to decrease as the degree of degeneration increased.

MR measured	direction x, y or z	hydration	GAG	hydroxy-proline	location - annulus/nucleus	Thompson grade
D	ns	p = .0001	ns	ns	ns	ns
1/T1	NA	p = .0001	ns	p = .0001	ns	ns
1/T2	NA	p = .0002	ns	ns	p = .0004	ns

Table 13: Summary of analysis of covariance results, showing which variables predicted the MR parameters, after adjusting for the effects of other covariates.



Thompson grade	normalized diffusion	T1 (ms.)	T2 (ms.)
1	$0.559 \pm 0.215$	$1348 \pm 618$	$70 \pm 32$
2	$0.466 \pm 0.234$	$951 \pm 436$	$52 \pm 23$
3	$0.472 \pm 0.195$	$1139 \pm 455$	$55 \pm 23$
4	$0.509 \pm 0.189$	$1089 \pm 312$	$49 \pm 14$
5	$0.458 \pm 0.242$	$1026 \pm 536$	$55 \pm 16$

Table 14: MR parameters  $\pm$  standard deviation, by Thompson grade.

The relationship between hydration and GAG for all samples is shown in Figure 38, while the relationship between hydration and collagen content is shown in Figure 39. Again,  $p$  is calculated for the univariate case.

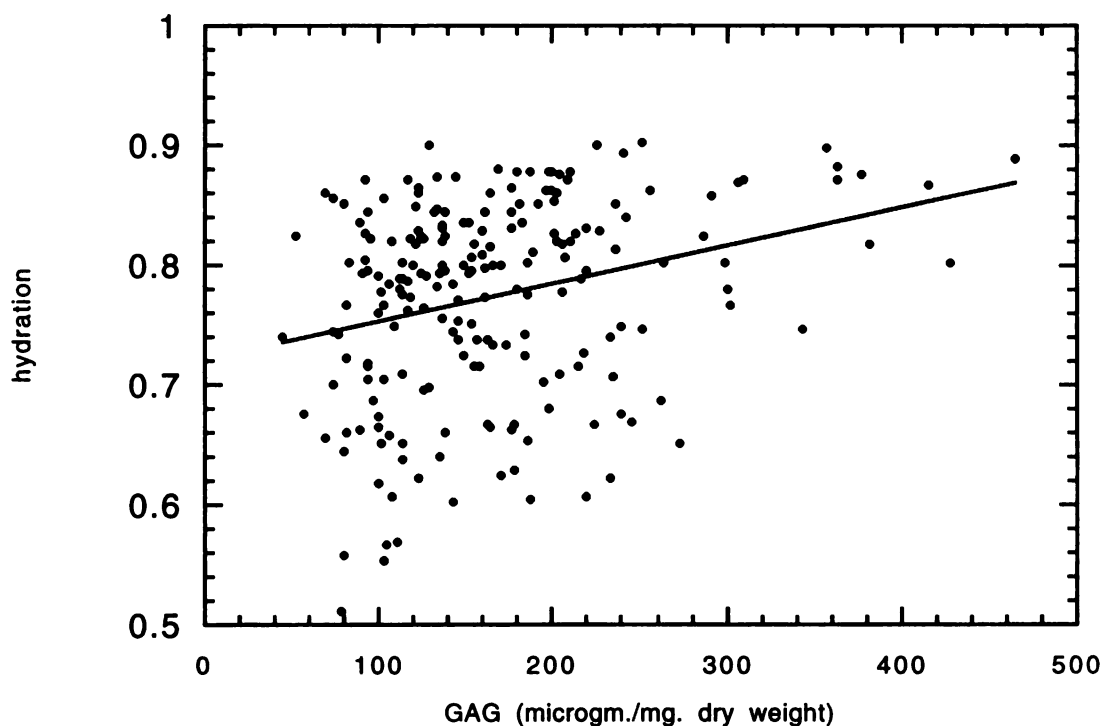


Figure 38: Hydration vs. GAG content:  $y = 0.721 + 0.000320x$ ,  $r = 0.28$ ,  $p < 0.001$

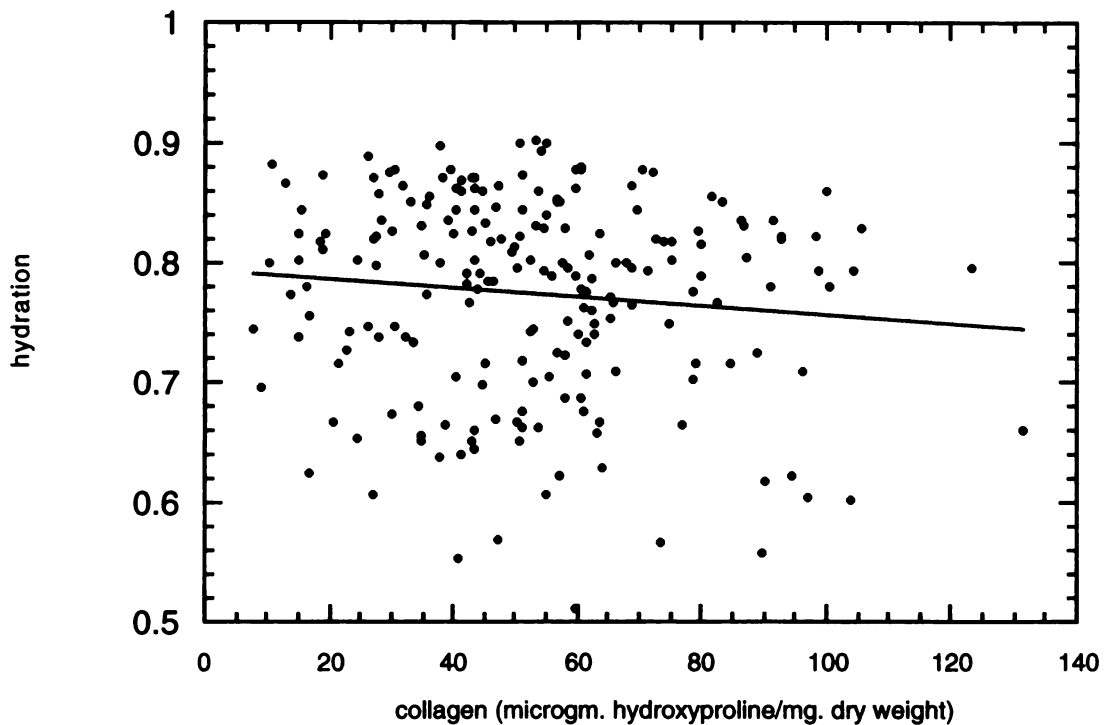


Figure 39: Hydration vs. collagen content,  $y = 0.794 - 0.000377x$ ,  $r = 0.11$ ,  $p = 0.14$

Table 15 summarizes the univariate correlations between MR parameters and the factors Thompson grade, annulus or nucleus location, hydration, GAG and hydroxyproline contents.

MR measured	hydration	GAG ( $\mu\text{g./mg.}$ )	hydroxyproline ( $\mu\text{g./mg.}$ )	Thompson grade
D	x: $r = 0.74$ ( $p < .001$ ) y: $r = 0.73$ ( $p < .001$ ) z: $r = 0.76$ ( $p < .001$ )	$r = 0.22$ ( $p = .002$ )	$r = -0.13$ ( $p = .07$ )	$r = 0.04$ NS
1/T1	$r = -0.56$ ( $p < .001$ )	$r = -0.26$ ( $p < .001$ )	$r = 0.37$ ( $p < .001$ )	$r = 0.002$ NS
1/T2	$r = -0.38$ ( $p < .001$ )	$r = -0.30$ ( $p < .001$ )	$r = 0.27$ ( $p < .001$ )	$r = 0.03$ NS
hydration		$r = 0.28$ ( $p < .001$ )	$r = 0.11$ ( $p = 0.14$ )	

Table 15: Univariate correlations of MR parameters with grade, location and biochemical factors.

The most consistent predictor of the MR parameters was tissue hydration. Collagen content was an additional factor for  $1/T_1$ , while the annulus or nucleus location was a factor for  $1/T_2$ .

#### **F) Predicting Creep Parameters from MR Parameters**

When the creep parameters from the water transport model ( $K$ ,  $D$ ,  $G$ ,  $\epsilon_0$  and  $\tau$ ) were examined for their possible correlation directly to the MR parameters ( $T_1$ ,  $T_2$  and  $D$ ), no correlations were found for  $K$ ,  $D$  and  $G$  ( $n = 8$ ). The system parameter,  $\tau$ , did not correlate with  $1/T_1$  or  $1/T_2$ , and it had a low correlation with  $D$  ( $r = 0.28$ ,  $p \sim .50$ ).

Moderate correlations were found between  $\epsilon_0$  versus  $1/T_1$  ( $r = 0.53$ ,  $p \sim 0.20$ ) and  $\epsilon_0$  versus  $D$  ( $r = 0.29$ ,  $p \sim 0.50$ ). No correlation was found for  $\epsilon_0$  versus  $1/T_2$ .

When the diffusion versus hydration curves for each of the intact disc's subspecimens were used to estimate hydration before compression from the MR images, there were moderate correlations found between the water transport model parameters and the calculated water content: for  $K$ ,  $r = 0.54$  ( $p = 0.18$ ); for  $D$ ,  $r = -0.45$  ( $p = 0.29$ ); for  $G$ ,  $r = -0.55$  ( $p = 0.17$ ) and for  $\tau$ ,  $r = 0.43$  ( $p = 0.31$ ).

After including specimens 3, 4 and 5, the correlations between the MR parameters and the individual creep parameters still showed no relationships; the correlations between the MR parameters and the system parameter,  $\tau$ , showed weak correlations for  $1/T_1$ ,  $1/T_2$  and  $D$ :  $r = 0.18$ ,  $r = 0.31$  and  $r = 0.42$ , respectively.  $D$  and  $G$  versus the calculated water content from MR images had about the same correlations, and  $K$  and  $\tau$  showed a small increase in the correlations with calculated water content (Table 5).

## **X. DISCUSSION**

### **A) MR Relaxation**

The higher value of  $T_1$  in the nucleus compared to the annulus is consistent with the higher water content in the nucleus than the annulus. More hydrated tissue is known to have a longer  $T_1$ . It is also known that shortening of the  $T_1$  within the disc is found with degeneration, and presumably due to tissue water loss.

The increase in T1 with loading has also been observed by other researchers [106, 107]. Both bovine and human discs were loaded with a pneumatic apparatus in the MR scanner, and the T1 values were followed. Uemura et al. [106] concluded that because they had previously found a linear relationship of T1 to water content, that the increase in T1 in the nucleus meant the water increased in the disc. This does not actually make logical sense. It is known that water is incompressible and leaves the disc with loading. There is no pressure gradient or osmotic gradient that would cause water to enter the central disc with loading.

The phenomenon that is more likely causing the increase in T1 is a shift of the water from a bound state within the proteoglycan matrix (where there are shorter relaxation times) to a more free state within pockets in the tissue, thereby lengthening T1.

The lack of correlation of T1 with grade of degeneration was somewhat unexpected; however, the T2 relaxation time is more sensitive to changes in water content than the T1 relaxation time. In studies in human intervertebral discs *in vivo*, the percent change in T2 was greater than the change in T1 for degenerated versus normal discs [66]. Also, T2 weighted images are used to visualize disc degeneration clinically [61, 62].

The significant differences in T2 by region and by Thompson grade are best explained by the differences in the tissue biochemistry. Compared to the nucleus pulposus, the annulus fibrosus has much more collagen, and therefore much more tissue matrix that will tend to dephase the protons on the water molecules. Similarly, the more degenerated discs will have increased tissue organization and collagen that will increase the matrix density and shorten the T2 of the tissue.

The loaded state did show an increase in T2 over the unloaded state; however, this was less statistically significant ( $p = 0.12$ ) than for the T1 changes. While the same explanation as for the T1 increase could be used - the increase in free versus bound water in the tissue - the effect of an increase in free to bound water could be less on T2 than T1 due to the differing mechanisms involved: T1 is an energy effect with loss of energy from the

RF pulse to the surroundings, whereas T2 relaxation is an entropy effect of loss of phase coherence due to inhomogeneity of the magnetic field environment of the protons [76]. One would not necessarily expect the same magnitude of effect on the relaxation times from these differing mechanisms.

## **B) Diffusion**

The observation from this data that the water diffusion increased after compression is directly opposite to the observation by Burstein et al. [67] and the observation on two specimens that were tested in the preliminary work for this study. This difference can be explained by the difference in the method of applying the compression to the specimens. In the Burstein study, the cartilage samples were compressed by a device that applied a step in displacement and held this position, allowing the load to decrease. Similarly, in the preliminary specimen measurements, the device had a step displacement applied through a screw mechanism.

Prior to beginning the study on the group of specimens in this study, the compression device was rebuilt to apply a step load to the discs (see Materials and Methods section for details). This change was done to allow the specimens to be loaded in the same method that the mechanical testing was then to be performed: creep (a step load), rather than stress relaxation (a step displacement).

The measurement of diffusion in this study, then, is more dynamic than that measured under stress relaxation. Considering that the diffusion measurements were started within five minutes after application of the step load, the measured diffusion is not yet at equilibrium. In fact, even after four hours of load application in the mechanical testing apparatus, the specimens were still creeping (decreasing in height for the static load). Therefore, the measured diffusion for this project's specimens includes forced flow of water (unlike the situation where a step in displacement is applied and a new equilibrium state develops with denser tissue and smaller diffusion distances), and the diffusion would

be expected to increase after compression, not decrease as in the stress relaxation experiments.

The observation of faster diffusion in the nucleus pulposus than the annulus fibrosus makes sense given the known higher water content in the nucleus and the greater tissue structure of the annulus (layers of annular fibers with higher collagen content). The significant difference in the diffusion by direction correlates with the known diffusion pathways that are through the endplates and radially through the annulus [16]: the larger changes in diffusion with compression were found in the anatomic A/P and S/I directions, the scanner x and y directions, respectively.

The faster diffusion in the Thompson grade 1 was expected due to the higher water content and smaller degree of organization that occurs with degeneration and aging. It was not expected, however, that the more degenerated Thompson grade 4 would also show faster diffusion. As will be discussed in the section on the relationship between the diffusion and the biochemical parameters (section E), there may be an effect with degeneration of forming more areas within the tissue that behave as pools of free water and have longer diffusion distances, while water in close association with the proteins and proteoglycans will have shorter diffusion coefficients [108, 109]. The relaxation times are also found to increase with age, and this again could be due to more free water in pockets within the organizing tissue leading to lengthening of the relaxation times.

### **C) High Resolution Midsagittal Images**

The expected difference of inner annular fiber bulging centrally in degenerated discs was not seen in this set of specimens. There were certainly discs representative of higher grades of degeneration, as well as some normally hydrated discs for comparison. It may be that a combination of annular fiber damage in conjunction with loss of nuclear hydration is necessary to see this inward annular bulge, or, that it is a part of the degeneration process that becomes replaced with fibrosis as the disc continues to degenerate. Interestingly, specimen 2, which had the tumor infiltrating the inferior vertebral body and acute loss of

the disc's support, did show inward annular bulging. This disc's nucleus pulposus therefore lost its ability to behave as a supportive pressure vessel that would provide forces radially outward on the annular fibers in compression.

The lack of a trend of the change in heights and AP diameters with Thompson grade was interesting. Except for the Thompson grade 5, which had a larger percentage decrease in height, all the other grades of discs were similar. Given the differences in sizes of the discs, perhaps the use of an overall creep model then is a more accurate way to compare the discs than these simpler measures of change in geometry. Also, the MR measurements of height before and after compression were single points in time that, due to the changes and difficulties, at times, with scanning setups, were not taken at the same time intervals in the creep period for all specimens. Another MR factor was that there was averaging in the high resolution image over the 30 minute acquisition period.

These factors of averaging and different sampling points were expected prior to the scanning; however, the qualitative differences in the deformations of the disc were the desired information from these scans. The MTS data gives the accurate assessment of the disc change in height with applied compression.

#### **D) Creep Models**

The early portion of the creep curve is often not fit in the published studies, perhaps due to difficulties in sampling this data [39, 40]. If the first 30 seconds of data is not included, the three parameter solid model then fits the data well.

Ekström et al. [45] found very similar curve fits to this project's data. The qualitative lack of fit for the 3 parameter model in the early part of the curve, with the acute "corner" of the curve for the 4 parameter model and progressive undershoot of the model were the same in their data. They used the Burger's linear model for the best fit, and it has been shown that this model is mathematically equivalent to the water transport model. Thus, the fact that this project's creep data was best fit by the water transport model is consistent with their findings.

Koeller et al. [48] did not find a correlation between creep behavior and the grade of degeneration. Their study used dynamic loading with a static 950 N. and a sinusoid of  $\pm$  540 N. For the creep measurements, however, only the first five minutes of data were used, as they felt from a previous study that this was a long enough time period to predict long-term deformation.

The creep data in this study correlated quite well with the Thompson grade of degeneration. In fact, the parameters of the water transport model changed with degeneration in the direction that one would predict qualitatively from this type of model. The permeability term,  $K$ , increased with increasing degeneration - consistent with the decrease in integrity of cartilage with aging.  $D$ , the system parameter that relates to the magnitude of the strain dependence of the osmotic pressure, decreased with increasing degeneration - consistent with the known decrease in osmotic pressure with degeneration, probably due to degeneration of the proteoglycans that attract the water. The term  $G$ , which relates to the time dependence of the collagen, decreased with increasing degeneration - consistent with less resistance to creep and relaxation as the tissue is older and more degenerated.

The values for  $K$ ,  $D$  and  $G$  from the 8 human specimens differed from the values for canine specimens in the Cassidy study [42], which were loaded to 2 MPa. (compared with 0.35 MPa. for this study).  $K$  in the human data was about 100 times larger than the canine data,  $D$  was about half that of the canine values and  $G$  was about 10 times smaller than the Cassidy data. When specimen 8 was refit to the model with only the first 60 minutes of data, to make it consistent with the Cassidy experiments, the value of  $K$  increased by a factor of 10 (to  $2.4 \times 10^{-15}$ ),  $D$  increased by a factor of 10 (to  $1.9 \times 10^7$ ) and  $G$  increased by a factor of 5 (to 116). Comparing these values to the Cassidy data showed that  $K$  was now almost 1000 times larger than the canine values,  $D$  was very consistent with the canine data and  $G$  was of the same magnitude as the Cassidy data.



The value of K calculated is obviously very dependent on the time period that is used for fitting the creep data, so any comparisons between studies will have to account for these differences. Also, the loading condition in the Cassidy study was almost 6 times larger than that in this study, and comparable loading conditions would be necessary for direct comparisons between studies.

The permeability of bovine cartilage has been estimated at between  $0.58$  and  $2.5 \times 10^{-15}$  [110], which is comparable to the human data in this study. A study in baboon lumbar spine specimens found a permeability of  $14.3 \times 10^{-14}$  [111], which is much larger (1000x's) than that calculated in this study. Setton et al. mention that this value is, in fact, large compared to measured values of  $0.03 \times 10^{-14}$  for human annulus fibrosus and  $0.08 \times 10^{-14}$  for bovine meniscus [111], which are comparable to this study's data.

Given the nature of this test system - the intervertebral disc with the vertebral bodies above and below, one could visualize the actual area of permeability of the disc to include the trans-annular pathway also. Radioactive tracer studies have found diffusion occurs both across the endplates and radially across the annular fibers [16]. Perhaps the permeability factor, K, is then a reflection of an overall disc system permeability, which is an average of that across the two cartilage surfaces of the disc end-plates and the annular route of diffusion.

The initial osmotic pressure for the water transport model was assumed to be 0.2 MPa. for all specimens. For specimen 11, which was a Thompson grade 5, the model was refit with a the osmotic pressure set to 0.1 MPa to represent a value at the lower range of normal [17]. The effect of this change on the parameters was that K decreased by about 30%, D increased about 50% and G increased about 50%. This change in K actually would give it a permeability more similar to the less degenerated specimens, so the implications of assuming the same initial osmotic pressure in this model must be considered. If one could measure the swelling pressure of disc tissue from each specimen,

then one could more accurately fit the parameters to the disc system. This change in protocol should be considered for further specimen testing.

#### **E) Effect of Tissue Biochemistry on MR Parameters**

This part of the study considered the grade of degeneration and tissue location, annulus or nucleus, together with the biochemical factors of hydration, collagen and proteoglycan content of lumbar disc specimens, to determine which affected the MR-measured parameters diffusion, D, 1/T1 and 1/T2.

The average proteoglycan and collagen contents were consistent with published values [31, 53, 73, 74], and the variation in collagen and proteoglycan was greater between specimens than within individual specimens, as would be expected.

The trends of decreasing GAG with increasing Thompson grade for both nuclear and annular specimens, decreasing collagen in the annulus, but no trend in the nucleus pulposus, compare with the work of Thompson et al. [112]. They found decreasing GAG in both nucleus and annulus with increasing Thompson grade, with decreasing collagen in the annulus. Their data differed in finding an increase in nuclear collagen, where our data found no trend. Lyons [73] and Terti [53] also found decreases in GAG with degeneration, and little change in collagen. Pearce et al. [31] found decreasing GAG with degeneration, and some increase in collagen.

In agreement with this study's MR relaxation results, Weidenbaum, et al., [79] found that 1/T2 correlated negatively with hydration in their study. 1/T2 vs. collagen had moderate correlation ( $r = 0.67$ ), and our data showed no significant correlation after accounting for the correlation with hydration. If 1/T2 vs. collagen was considered alone, a low ( $r = 0.27$ ,  $p < 0.001$ ) correlation was found. 1/T2 showed no correlation to proteoglycan in their study. Our data showed no significant correlation after accounting for the correlation with hydration. If graphed alone for all specimens, 1/T2 had a mild correlation with GAG content,  $r = -0.30$ ,  $p < 0.001$ .

The differences in our study from the Weidenbaum study included 1) that they used only grade II disc tissue: specimens without signs of degeneration, while our study had tissue from Thompson grades I through V, 2) a lower field MR scanner, 0.5 Tesla vs. 1.5 Tesla, and 3) a smaller range of tissue hydrations, about 58 to 78%, while our study increased the range of hydration to from 51 to 90% using PEG solutions. The larger range of degeneration of our specimens may explain the larger degree of scatter in our data.

Terti et al. [53] found increasing linear relationships between T1 and T2 and tissue water content ( $r = 0.68$  and  $0.66$ , respectively,  $p < 0.001$ ). Their data also showed a decreasing trend in T1 and T2 with increasing age, though histologic analysis did not show any distinct differences between discs with bright and dark signal intensity. Gross morphologic grading of specimens was not used, and severely degenerated discs were not included.

Majors et al. [74] found T2 correlated linearly with water, GAG and hydroxyproline contents ( $r = 0.79, 0.81, -0.72$ , respectively,  $p < .001$ ). The apparent diffusion coefficient also correlated significantly with these factors ( $r = 0.73, 0.73, -0.72$ ,  $p < 0.001$ ). Table 13 summarizes the univariate correlations for our data. It would be interesting to see Majors' data in a multiple regression, as it is very possible that due to the relationships between increasing GAG and water, and increasing collagen and decreasing water, that the hydration alone might explain most of the variation in the MR parameters.

The measured tissue diffusion, normalized to saline diffusion, was in the range of published values [67, 72]. The lack of difference in diffusion by direction was expected in this experimental setup. The tissue, enclosed in dialysis membranes, is not confined from swelling as it would be *in vivo*, or even as in an intact specimen. The ordered laminations of annular fibers are swelled by proteoglycans absorbing water, and a more isotropic diffusion resulted. Diffusion measurements of intact specimens have shown significant directional dependence [113] consistent with known diffusion pathways [16].

Given the complex nature of the MR signals, one would actually be surprised if the MR parameters correlated with the gross morphologic Thompson grade. Theories of the MR signal of tissue water see water in multiple compartments with fast exchange between the compartments [58]. Water molecules closely associated with the tissue matrix will have shorter relaxation times than the water molecules in between - the free, or bulk, water.

For the intervertebral disc, one has a complex structure of water-holding proteoglycan with structural collagen fibers. As the tissue is allowed to uptake water, it will expand, with an increase in free water and longer relaxation times. If there is more collagen present, water uptake will be limited, as well as more water being in closer association with matrix and having shorter relaxation times.

Our data showed that D,  $1/T_1$  or  $1/T_2$  did not correlate linearly with the Thompson grade. For diffusion,  $1 > 4 > 3 > 2 > 5$ . For  $1/T_1$ ,  $2 > 5 > 3 > 4 > 1$ . For  $1/T_2$ ,  $4 > 3 > 2 > 5 > 1$ . The ordering of the values obviously does not follow that of the gross changes. Perhaps at the microscopic level, degeneration involving decreasing GAG and increasing collagen would decrease  $T_1$ ,  $T_2$  and D as the water decreased; then, as degeneration progressed, pockets of free water could develop as the matrix organized - with increases in  $T_1$ ,  $T_2$  and D from these regions. The effect of compression, of course, would be very complex, as water would be shifted from bound to free regions, and relaxation times could change from this process also.

Crooks, et al. [57] made the observation that relaxation times are complex functions of the underlying components, so complex that we may never truly be able to model and predict the relaxation times beginning from the tissue composition. Since we are not sure about the tissue parameters: water content, fat content, molecular weight, molecular size, paramagnetic ions, viscosity, etc. that would be needed in a model to predict tissue MR parameters, the goal of achieving predictive power may be impossible.

*In vivo* we do not usually know the tissue biochemical contents; however, we can examine across an individual's multiple discs for comparison purposes, and we can

observe changes over time and with different symptoms in the same individual. By studying the biochemistry as was done in this project, an attempt was made to find out what changes occur with degeneration that lead to the changes in signal intensity observed in clinical scans.

#### **F) Predicting Creep Parameters from MR Parameters**

Overall, the ability of the MR parameters to predict the creep behavior of the disc tested in this study was not good. There were certainly trends of the creep parameters relating to the MR parameters but not strong enough to be able to predict the creep parameters from the MR images. Also, the trends were seen only after using each disc's subspecimen graphs to estimate a precompression water content. This obviously is not available to us in the clinical realm (we cannot get subspecimens of an individual's disc for hydration and biochemistry). Again, one might consider that the complex factors that are involved in the generation of the MR signal may be too difficult to make conclusions about underlying biochemistry based upon relaxation or diffusion, though changes within an individual with time or compared to an adjacent disc could be useful.

### **X. CONCLUSIONS**

This project set out to study the human intervertebral disc under compression with MRI followed by mechanical testing. Relaxation times, water diffusion and high resolution images were acquired, followed by creep testing. In the second part of the project, tissue biochemistry was studied for its relationship to the relaxation times and diffusion coefficients.

For the MR relaxation times, significant differences ( $p < 0.05$ ) were found by region of the specimen (nucleus vs. annulus), before and after loading, and by Thompson grade. For the diffusion coefficients, significant differences were found by region, loading state, diffusion direction and Thompson grade. High resolution images resolved the annular fiber deformation in some specimens, though in the more degenerated specimens the fibers could not be seen.

The method of loading is an important difference in technique when measuring tissue diffusion before and after compression. Stress relaxation in the preliminary specimens showed a decrease in tissue diffusion; however, creep loading in the project specimens showed an increase in diffusion.

To quantify the dynamic creep data, the viscoelastic and water transport models were used. Very good fits ( $r = 0.999$ ) were found for the water transport model, which then allowed comparison of parameters across the specimens. Significant trends ( $r_s = 0.65$  to  $0.80$ ) were found between the creep parameters and the Thompson grade, no trends were found directly between the creep parameters and the MR parameters, and weak trends ( $r = 0.43$  to  $0.55$ ) were found between creep parameters and the MR derived water contents.

While the goal of predicting the disc's mechanical behavior directly from the MR parameters was not achieved, good models were developed to quantify the creep behavior that correlated with the grade of degeneration and weak trends were found with the MR derived water content. Within a given individual, MRI would be most useful in following the course of disc degeneration with diffusion sequences and comparing one disc to others. It will also be interesting to examine discs clinically with diffusion sequences to see if changes in diffusion correlate with symptoms.

For the biochemical analysis, an analysis of covariance was used to find which of the factors (region, water content, proteoglycan and collagen contents) most affected the MR parameters (diffusion, T1 and T2), and tissue hydration was found to be the most consistent predictor. For  $1/T1$ , collagen was an additional factor; and for  $1/T2$ , the location of the tissue - annulus or nucleus - was an additional factor.

## **XI. FUTURE WORK**

Given the ability of MRI to measure water diffusion in the intervertebral disc, with values in the range of published tissue water diffusion, and sensitive to differences by

region and grade of degeneration, extension of disc water diffusion measurements to *in vivo* applications will be the next step.

The lumbar intervertebral disc sits anatomically next to the aorta *in vivo*. This large pulsatile blood flow next to the area being imaged will lead to large artifacts and prevent the use of spin-echo techniques. Fast imaging techniques, such as EPI, or echo planar imaging, can acquire images very quickly and avoid this flow artifact. These sequences are being modified to include diffusion sensitizing gradients by the same principles used in this project. Imaging of the human brain has been done with EPI-diffusion sequences, looking for anisotropy in brain structures and changes after infarcts. The limitations to this technique are the resolution; however, as higher resolution is achieved, application to the human intervertebral disc is becoming feasible.

Most clinical scanners image the patient laying supine, and this position does not allow for gravitational loading of the discs as in the actual standing or sitting positions that are the most symptomatic clinically. After finding significant differences in diffusion before and after loading *in vitro*, plans are being made to design a compression apparatus for use in the horizontal bore scanner on human subjects in order to measure both changes in diffusion and in anatomy with loading.

It will be very interesting to measure water diffusion *in vivo* before and after loading, in symptomatic and asymptomatic discs in the same individual, as well as in the same patient with and without back pain. Once the ability to measure disc water diffusion *in vivo* is developed, the addition of these measurements to MR imaging may well prove to be clinically useful.

### **XIII. REFERENCES**

1. Burton, C.V. and Cassidy, J.D., *Economics, epidemiology and risk factors, in Managing low back pain*, W.H. Kirkaldy-Willis, Editor. 1992, Churchill Livingstone: New York. p. 1-6.
2. Salkever, D.S., *Morbidity Costs: National Estimates and Economic Determinants*. 1986, Department of Health and Human Services:

3. Praemer, A., Furner, S., and Rice, D.P., *Musculoskeletal Conditions in the United States*. First ed. 1992, Park Ridge, Illinois: American Academy of Orthopaedic Surgeons.
4. Frymoyer, J.W. and Cats-Baril, W.L., *An overview of the incidences and costs of low back pain*. *Orthop Clin North Am*, 1991. **22**(2): p. 263-271.
5. Johannig, E., Wilder, D.G., Landriagn, P.J., and Pope, M.H., *Whole-body vibration exposure in subway cars and review of adverse health effects*. *J Occup Med*, 1991. **33**(5): p. 605-612.
6. Damkot, D.K., Popoe, M.H., Lord, J., and Frymoyer, J.W., *The relationship between work history, work environment and low-back pain in men*. *Spine*, 1984. **9**: p. 395.
7. Broman, H., Pope, M.H., Benda, M., Svensson, M., Ottoson, C., and Hansson, T., *The impact response of the seated subject*. *J Ortho Res*, 1991. **9**(1): p. 150-154.
8. Pope, M.H. and Hansson, T.H., *Vibration of the spine and low back pain*. *Clin Orthop*, 1992. **279**: p. 49-59.
9. Nachemson, A.L., *Disc pressure measurements*. *Spine*, 1981. **6**(1): p. 93-97.
10. Ballard, W.T. and Weinstein, N., *Biochemistry of the intervertebral disc*, in *Managing low back pain*, W.H. Kirkaldy-Willis and C.V. Burton, Editor. 1992, Churchill Livingstone: New York. p. 39-48.
11. Saunders, J.B. and Inman, V.T., *Pathology of the intervertebral disk*. *Arch Surg*, 1940. **40**: p. 389-416.
12. Inoue, H., *Three-dimensional architecture of lumbar intervertebral discs*. *Spine*, 1981. **6**(2): p. 139-146.
13. White, A.A. and Panjabi, M.M., *Clinical Biomechanics of the Spine*. Second ed. 1990, Philadelphia: J.B. Lippincott Co.
14. Hukins, D.W.L., *Disc structure and function*, in *The Biology of the Intervertebral Disc*, P. Ghosh, Editor. 1988, CRC Press, Inc.: Boca Raton, Florida. p. 1-39.
15. White, A.A. and Gordon, S.L., *Synopsis: Workshop on idiopathic low back pain*. *Spine*, 1982. **7**(2): p. 141-149.
16. Maroudas, A., *Nutrition and metabolism of the intervertebral disc*, in *The Biology of the Intervertebral Disc*, P. Ghosh, Editor. 1988, CRC Press, Inc.: Boca Rotan, Florida. p. 1-38.
17. Urban, J.P.G. and McMullin, J.F., *Swelling pressure of the intervertebral disc: influence of proteoglycan and collagen contents*. *Biorheology*, 1985. **22**: p. 145-157.
18. Melrose, J. and Ghosh, P., *The noncollagenous proteins of the intervertebral disc*, in *The biology of the intervertebral disc*, P. Ghosh, Editor. 1988, CRC: Boca Raton, Fl. p. 189-239.



19. Adams, M.A., Dolan, P., Hutton, W.C., and Porter, R.W., *Diurnal changes in spinal mechanics and their clinical significance*. J Bone Joint Surg, 1990. **72-B(2)**: p. 266-270.
20. Panagiotacopoulos, N.D., Knauss, W.G., and Bloch, R., *On the mechanical properties of human intervertebral disc material*. Biorheology, 1979. **16**: p. 317-330.
21. Adams, M.A. and Hutton, W.C., *The effect of posture on the fluid content of lumbar intervertebral discs*. Spine, 1983. **8(6)**: p. 665-671.
22. Adams, M.A. and Hutton, W.C., *The effect of posture on diffusion into lumbar intervertebral discs*. J Anat, 1986. **147**: p. 121-34.
23. Boos, N., Wallin, A., Ch. Boesch, and Aebi, M. *Quantitative MR imaging of diurnal water content variations in lumbar intervertebral disc*. in *38th Annual Meeting, Orthopaedic Research Society*. 1992. Washington, D.C.: The Orthopaedic Research Society.
24. Ohshima, H., Tsuji, H., Hirano, N., Ishihara, H., Katoh, Y., and Yamada, H., *Water diffusion pathway, swelling pressure, and biomechanical properties of the intervertebral disc during compression load*. Spine, 1989. **14(11)**: p. 1234-1244.
25. McNally, D.S. and Adams, M.A., *Internal intervertebral disc mechanics as revealed by stress profilometry*. Spine, 1992. **17(1)**: p. 66-73.
26. Shirazi-Adl, A., Ahmed, A.M., and Shrivastava, S.C., *A finite element study of a lumbar motion segment subjected to pure sagittal plane moments*. J Biomech, 1986. **19**: p. 331-350.
27. Adams, M.A., Morrison, H.P., and Dolan, P. *Internal disruption of an intervertebral disc can be caused by previous minor damage to an adjacent vertebral body*. in *International Society for the Study of the Lumbar Spine*. 1995. Helsinki, Finland:
28. Kazarian, L.E., *Creep characteristics of the human spinal column*. Orthop Clin North Am, 1975. **6(1)**: p. 3-18.
29. Yasuma, T., Makino, E., Saito, S., and Inui, M., *Histological development of intervertebral disc herniation*. J Bone Joint Surg, 1986. **68-A(7)**: p. 1066-1072.
30. Andersson, G.B.J. and Schultz, A.B., *Effects of fluid injection on mechanical properties of intervertebral discs*. J Biomech, 1979. **12**: p. 453-458.
31. Pearce, R.H., Grimmer, B.J., and Adams, M.E., *Degeneration and the chemical composition of the human lumbar intervertebral disc*. J Orthop Res, 1987. **5**: p. 198-205.
32. Farfan, H.F., *Biomechanics of the lumbar spine*, in *Managing low back pain*, W.H. Kirkaldy-Willis, Editor. 1988, Churchill Livingstone: New York. p. 15-27.
33. Skaggs, D.L., Iatridis, J.C., Gibbons, J.M., Richardson, L.C., Foster, R.J., and Weidenbaum, M. *Regional variation in tensile properties and biochemical composition of single lamellae of human annulus fibrosus*. in *39th Annual Meeting, Orthopaedic Research Society*. 1993. San Francisco, California: The Orthopaedic Research Society.
34. Galante, J.O., *Tensile properties of the human lumbar annulus fibrosus*. Acta Orthop Scand Suppl., 1967. (100).

35. Wilder, D.G., Pope, M.H., and Frymoyer, J.W., *The biomechanics of lumbar disc herniation and the effect of overload and instability*. J Spinal Disord, 1988. 1(1): p. 16-32.
36. Fung, Y.C., *Biomechanics: Mechanical properties of living tissues*. 2nd ed. 1993, New York: Springer-Verlag.
37. Broberg, K.B. and von Essen, H.O., *Modeling of intervertebral discs*. Spine, 1980. 5(2): p. 155-167.
38. Broberg, K.B., *On the mechanical behaviour of intervertebral discs*. Spine, 1983. 8(2): p. 151-165.
39. Burns, M.L., Kaleps, I., and Kazarian, L.E., *Analysis of compressive creep behavior of the vertebral unit subjected to a uniform axial loading using exact parametric solution equations of Kelvin-solid models - part 1. Human intervertebral joints*. J Biomech, 1984. 17(2): p. 113-130.
40. Keller, T.S., Spengler, D.M., and Hansson, T.H., *Mechanical behavior of the human lumbar spine. I. Creep analysis during static compressive loading*. J Orthop Res, 1987. 5(4): p. 467-478.
41. Li, S., Patwardhan, A.G., Amirouche, F.M.L., Havey, R., and Meade, K.P., *Limitations of the standard linear solid model of intervertebral discs subject to prolonged loading and low-frequency vibration in axial compression*. J Biomech, 1995. 28(7): p. 779-790.
42. Cassidy, J.J., Silverstein, M.S., Hiltner, A., and Baer, E., *A water transport model for the creep response of the intervertebral disc*. J Mater Sci: Mater Med, 1990. 1: p. 81-89.
43. Flugge, W., *Viscoelasticity*. 2nd ed. 1975, New York: Springer-Verlag.
44. Laible, J.P., Pflaster, D.S., Krag, M.H., Simon, B.R., and Haugh, L.D., *A poroelastic-swelling finite element model with application to the intervertebral disc*. Spine, 1993. 18(5): p. 659-670.
45. Ekström, L., Kaigle, A., Hult, E., Holm, S., Rostedt, M., and Hansson, T., *Intervertebral disc response to cyclic loading - an animal model*. Proceedings of the Institution of Mechanical Engineers; Journal of Engineering in Medicine, Proceedings Part H, 1996. 210(H4): p. 249-258.
46. Hasberry, S. and Percy, M.J., *Temperature dependence of the tensile properties of interspinous ligaments of sheep*. J Biomed Eng, 1985. 8: p. 62-66.
47. Adams, M.A., *Spine update: Mechanical testing of the spine, An appraisal of methodology, results and conclusions*. Spine, 1995. 20(19): p. 2151-2156.
48. Koeller, W., Muehlhaus, S., Meier, W., and Hartmann, F., *Biomechanical properties of human intervertebral discs subjected to axial dynamic compression - Influence of age and degeneration*. J Biomech, 1986. 19(10): p. 807-816.

49. Smeathers, J.E. and Joanes, D.N., *Dynamic compressive properties of human lumbar intervertebral joints: A comparison between fresh and thawed specimens*. J Biomech, 1988. **21**(5): p. 425-433.
50. Panjabi, M.M., Drag, M., Summers, D., and Videman, T., *Biomechanical time-tolerance of fresh cadaveric human spine specimens*. J Orthop Res, 1985. **3**: p. 292-300.
51. Bass, E.C., Duncan, N.A., Hariharan, J.S., Dusick, J., Bueff, H.U., and Lotz, J.C., *Frozen storage affects the compressive creep behavior of the porcine intervertebral disc*. Spine, 1997. **22**(24): p. 2867-2876.
52. Yu, S., Sether, L.A., Ho, P.S.P., Wagner, M., and Haughton, V.M., *Tears of the annulus fibrosus: Correlation between MR and pathologic findings in cadavers*. AJNR, 1988. **9**: p. 367-370.
53. Terti, M., Paajanen, H., Laato, M., Aho, H., Komu, M., and Korman, M., *Disc degeneration in magnetic resonance imaging: A comparative biochemical, histologic, and radiologic study in cadaver spines*. Spine, 1991. **16**(6): p. 629-634.
54. Gunzburg, R., Parkinson, R., Moore, R., Cantraine, F., Hutton, W., Vernon-Roberts, B., and Fraser, R., *A cadaveric study comparing discography, magnetic resonance imaging, histology and mechanical behavior of the human lumbar disc*. Spine, 1991. **17**(4): p. 417-423.
55. Tencer, A.F., Ahmed, A.M., and Burke, D.L., *Some static mechanical properties of the lumbar intervertebral joint, intact and injured*. J Biomech Eng, 1982. **104**(3): p. 193-201.
56. Kasra, M., Shirazi-Adl, A., and Drouin, G., *Dynamics of human lumbar intervertebral joints*. Spine, 1992. **17**(1): p. 93-102.
57. Crooks, L.E., Hylton, N.M., Ortendahl, D.A., Posin, J.P., and Kaufman, L., *The value of relaxation times and density measurements in clinical MRI*. Invest Radiol, 1987. **22**: p. 158-169.
58. Fullerton, G.D. and Cameron, I.L., *Ch 3: Relaxation of biological tissues, in Biomedical Magnetic Resonance Imaging: Principles, Methodology, and Applications*, F.W. Wehrli, D. Shaw, and J.B. Kneeland, Editor. 1988, VCH Publishers, Inc: New York. p. 115-155.
59. Modic, M.T., Masaryk, T.J., Ross, J.S., and Carter, J.R., *Imaging of degenerative disc disease*. Radiology, 1988. **168**(177-186).
60. Sether, L.A., Yu, S., Haughton, V.M., and Fischer, M.E., *Intervertebral disk: Normal age-related changes in MR signal intensity*. Radiology, 1990. **177**: p. 385-388.
61. Gundry, C.R. and Fritts, H.M., *Magnetic resonance imaging of the musculoskeletal system. Part 8. The spine, section 1*. Clin Ortho Rel Res, 1997. **338**: p. 275-287.
62. Modic, M.T., Pavlicek, W., Weinstein, M.A., Boumpfrey, F., Ngo, F., Hardy, R., and Duchesneau, P.M., *Magnetic resonance imaging of intervertebral disc disease: Clinical and pulse sequence considerations*. Radiology, 1984. **152**: p. 103-111.

63. Modic, M.T., Masaryk, T., Boumphrey, F., Goormastic, M., and Bell, G., *Lumbar herniated disk disease and canal stenosis: Prospective evaluation by surface coil MR, CT and myelography*. AJNR, 1986. 7: p. 709-717.
64. Jenkins, J.P.R., Hickey, D.S., Zhu, X.P., Machin, M., and Isherwood, I., *MR Imaging of the intervertebral disc: a quantitative study*. Br J Radiol, 1985. 58: p. 705-709.
65. Hickey, D.S., Aspden, R.M., Hukins, D.W.L., Jenkins, J.P.R., and Isherwood, I., *Analysis of magnetic resonance images from normal and degenerate lumbar intervertebral discs*. Spine, 1986. 11(7): p. 702-708.
66. Boos, N., Dreier, D., Hilfiker, E., Schade, V., Kreis, R., Hora, J., Aebi, M., and Boesch, C., *Tissue characterization of symptomatic and asymptomatic disc herniations by quantitative magnetic resonance imaging*. J Orthop Res, 1997. 15: p. 141-149.
67. Burstein, D., Gray, M.L., Hartman, A.L., Gipe, R., and Foy, B.D., *Diffusion of small solutes in cartilage as measured by nuclear magnetic resonance (NMR) spectroscopy and imaging*. J Orthop Res, 1993. 11: p. 465-478.
68. Koh, K., Kusaka, Y., and Hase, H. *Self diffusion coefficient of water in human intervertebral discs analyzed by pulsed gradient NMR method*. in *Transactions of the 39th Annual Meeting*. 1993. San Francisco: Orthopaedic Research Society.
69. Koh, K., Kusaka, Y., Mifune, T., Hase, H., and Hirasawa, Y., *Self diffusion coefficient of water and its anisotropic property in bovine intervertebral discs analyzed by pulsed gradient NMR method*. Orthopaedic Transactions, 1991. 15(2): p. 483.
70. Boos, N. and Boesch, C., *Quantitative magnetic resonance imaging of the lumbar spine. Potential for investigations of water content and biochemical composition*. Spine, 1995. 20(21): p. 2358-2366.
71. Bottomley, P.A., Foster, T.H., Argersinger, R.E., and Pfeifer, L.M., *A review of normal tissue hydrogen NMR relaxation times and relaxation mechanisms from 1-100MHz: Dependence on tissue type, NMR frequency, temperature, species, excision, and age*. Med. Physics, 1984. 11(4): p. 425-448.
72. Beall, P.T., Amtey, S.R., and Kasturi, S.R., *States of water in biology*, in *NMR Data handbook for biomedical applications*. 1984, Pergamon Press: New York. p. 1-10.
73. Lyons, G., Eisenstein, S.M., and Sweet, M.B.E., *Biochemical changes in intervertebral disc degeneration*. Biochim. Biophys. Acta, 1981. 673: p. 443-453.
74. Majors, A.W., McDevitt, C.A., Silgalis, I., and Modic, M.T. *A correlative analysis of T2, ADC and MT ratios with water, hydroxyproline and GAG content in excised human intervertebral disk*. in *Transactions of the 40th Annual Meeting*. 1994. New Orleans, LA: Orthopaedic Research Society.
75. Ghosh, P., *The Biology of the Intervertebral Disc*. 1988, Boca Raton, FL: CRC Press, Inc.
76. Shaw, D., *Ch 1: The fundamental principles of nuclear magnetic resonance, in Biomedical Magnetic Resonance Imaging*, F.W. Wehrli, D. Shaw, and J.B. Kneeland, Editor. 1988, VCH Publishers, Inc.: New York. p. 1-46.

77. Boos, N., Wallin, A., Harms, S., Vock, P., Ch. Boecsh, and Aebi, M. *Tissue characterization of normal and herniated lumbar intervertebral discs by quantitative MRI*. in *Transactions of the 39th Annual Meeting*. 1993. San Francisco, California: Orthopaedic Research Society.
78. Ke, J.H., Zong, L.B., Natarajan, R.N., Andersson, G.B.J., Chen, I.H., Wang, J.Z., and Turner, D.A. *Relationship between MRI relaxation time and water content in intervertebral discs*. in *Transactions of the 39th Annual Meeting*. 1993. San Francisco, California: Orthopaedic Research Society.
79. Weidenbaum, M., Foster, R.J., Best, B.A., Saed-Nejad, F., Nickoloff, E., Newhouse, J., Ratcliffe, A., and Mow, V.C., *Correlating magnetic resonance imaging with the biochemical content of the normal human intervertebral disc*. *J Orthop Res*, 1992. **10**: p. 552-561.
80. Chatani, K., Kusaka, Y., Mifune, T., and Nishikawa, H., *Topographic differences of H1-NMR relaxation times (T1, T2) in the normal intervertebral disc and its relationship to water content*. *Spine*, 1993. **18**(15): p. 2271-2275.
81. Furo, I., Bobset, M., Pocsik, I., and Tompa, K., *In vitro 1H NMR "mapping" of human intervertebral discs*. *Mag Reson Med*, 1986. **3**: p. 146-149.
82. Scholz, T.D., Fleagle, S.R., Burns, T.L., and Skorton, D.J., *Nuclear magnetic resonance relaxometry of the normal heart: Relationship between collagen content and relaxation times of the four chambers*. *Mag Res Imag*, 1989. **7**: p. 643-648.
83. Scholz, T.D., Fleagle, S.R., Burns, T.L., and Skorton, D.J., *Tissue determinants of magnetic resonance relaxation times; Effect of water and collagen content in muscle and tendon*. *Invest Radiol*, 1989. **24**: p. 893-898.
84. Einstein, A., *Investigations on the theory of the Brownian movement*. 1956, New York: Dover Publications.
85. Stejskal, E.O. and Tanner, J.E., *Spin diffusion measurements: spin-echoes in the presence of a time-dependent field gradient*. *J Chem Phys*, 1965. **42**: p. 288-292.
86. Stejskal, E.O. and Tanner, J.E., *Use of spin echo in pulsed magnetic-field gradient to study anisotropic, restricted diffusion and flow*. *J Chem Phys*, 1965. **43**: p. 3579-3603.
87. Abragam, A., *The Principles of Nuclear Magnetism*. 1961, London: Oxford University Press. 60.
88. Cussler, E.L., *Diffusion: Mass transfer in fluid systems*. Vol. 525. 1984, Cambridge: Cambridge University Press.
89. Sze, G., Merriam, M., Oshio, K., and Jolesz, F.A., *Fast spin-echo imaging in the evaluation of intradural disease of the spine*. *Am J Neuroradiol*, 1992. **13**(5): p. 1383-92.
90. Zoarski, G.H., Mackey, J.K., Anzai, Y., Hanafee, W.N., Melki, P.S., Mulkern, R.V., Jolesz, F.A., and Lufkin, R.B., *Head and neck: initial clinical experience with fast spin-echo MR imaging*. *Radiology*, 1993. **188**(2): p. 323-7.

91. Jolesz, F.A. and Jones, K.M., *Fast spin-echo imaging of the brain*. *Mag Res Imag*, 1993. **5**(1): p. 1-13.
92. Basser, P.J., Mattiello, J., and LeBihan, D., *Estimation of the effective self-diffusion tensor from the NMR spin echo*. *J Mag Reson*, 1994. **Series B 103**: p. 247-254.
93. Basser, P.J., Mattiello, J., and LeBihan, D., *MR diffusion tensor spectroscopy and imaging*. *Biophys J*, 1994. **66**: p. 259-267.
94. Mattiello, J., Basser, P.J., and LeBihan, D., *Analytical expressions for the b matrix in NMR diffusion imaging and spectroscopy*. *J Mag Reson*, 1994. **Series A 108**: p. 131-141.
95. Thompson, J.P., Pearce, R.H., Schechter, M.T., Adams, M.E., Tsang, I.K.Y., and Bishop, P.B., *Preliminary evaluation of a scheme for grading the gross morphology of the human intervertebral disc*. *Spine*, 1990. **15**(5): p. 411-415.
96. Nachemson, A. and Morris, J., *In vivo measurements of intradiscal pressure*. *J Bone Joint Surg*, 1964. **46A**(5): p. 1077-1092.
97. Nachemson, A., *The load on lumbar disks in different positions of the body*. *Clin Orthop*, 1966. **45**: p. 107-122.
98. Farndale, R.W., Buttle, D.J., and Barrett, A.J., *Improved quantitation and discrimination of sulphated glycosaminoglycans by use of dimethylmethylene blue*. *Biochim Biophys Acta*, 1986. **883**(2): p. 173-177.
99. Burleigh, M.C., Barrett, A.J., and Lazarus, G.S., *Cathepsin B1. A lysosomal enzyme that degrades native collagen*. *Biochem J*, 1974. **137**(2): p. 387-398.
100. Hollander, A.P., Heathfield, T.F., Webber, C., Iwata, Y., Bourne, R., Rorabeck, C., and Poole, A.R., *Increased damage to type II collagen in osteoarthritic articular cartilage detected by a new immunoassay*. *J Clin Inv*, 1994. **93**(4): p. 1722-1732.
101. Nimni, M.E., *Collagen: structure, function and metabolism in normal and fibrotic tissues*. *Sem Arthr Rheum*, 1983. **13**(1): p. 1-86.
102. Young, I.R., Hand, J.W., Oatridge, A., and Prior, M.V., *Modeling and observation of temperature changes in vivo using MRI*. *Mag Reson Med*, 1994. **32**: p. 358-369.
103. Glantz, S.A., *Primer of Biostatistics*. 3rd ed. 1992, New York: Mc Graw - Hill, Inc., Health Professions Division.
104. Ahn, C.B., Lee, S.Y., Nalsioglu, O., and Cho, Z.H., *An improved nuclear magnetic resonance diffusion coefficient imaging method using an optimized pulse sequence*. *Med Phys*, 1986. **16**(6): p. 789-793.
105. Wesby, G.E., Moseley, M.E., and Ehman, R.L., *Translational molecular self-diffusion in magnetic resonance imaging*. *Invest Radiol*, 1984. **19**: p. 491-409.
106. Uemura, O., Kusaka, Y., Mikami, Y., Hase, H., Morimoto, T., and Hirasawa, Y., *Water retention in the loaded human intervertebral disc and its correlation with deformation*

*of end-plate.* in *Transactions of the 43rd Annual Meeting.* 1997. San Francisco, CA: Orthopaedic Research Society.

107. Mikami, Y., Kusaka, Y., Morita, Y., Uemura, O., Chatani, K., Hase, H., and Tanaka, C. *MRI analysis of water molecule kinetics during and after compression of intervertebral discs.* in *Transactions of the 39th Annual Meeting.* 1993. San Francisco, CA: Orthopaedic Research Society.

108. Chang, D.C., Rorshach, H.E., Nichols, B.L., and Hazlewood, C.F., *Implications of diffusion coefficient measurements for the structure of cellular water.* Ann of N.Y. Acad Sci, 1973. **204**: p. 434-443.

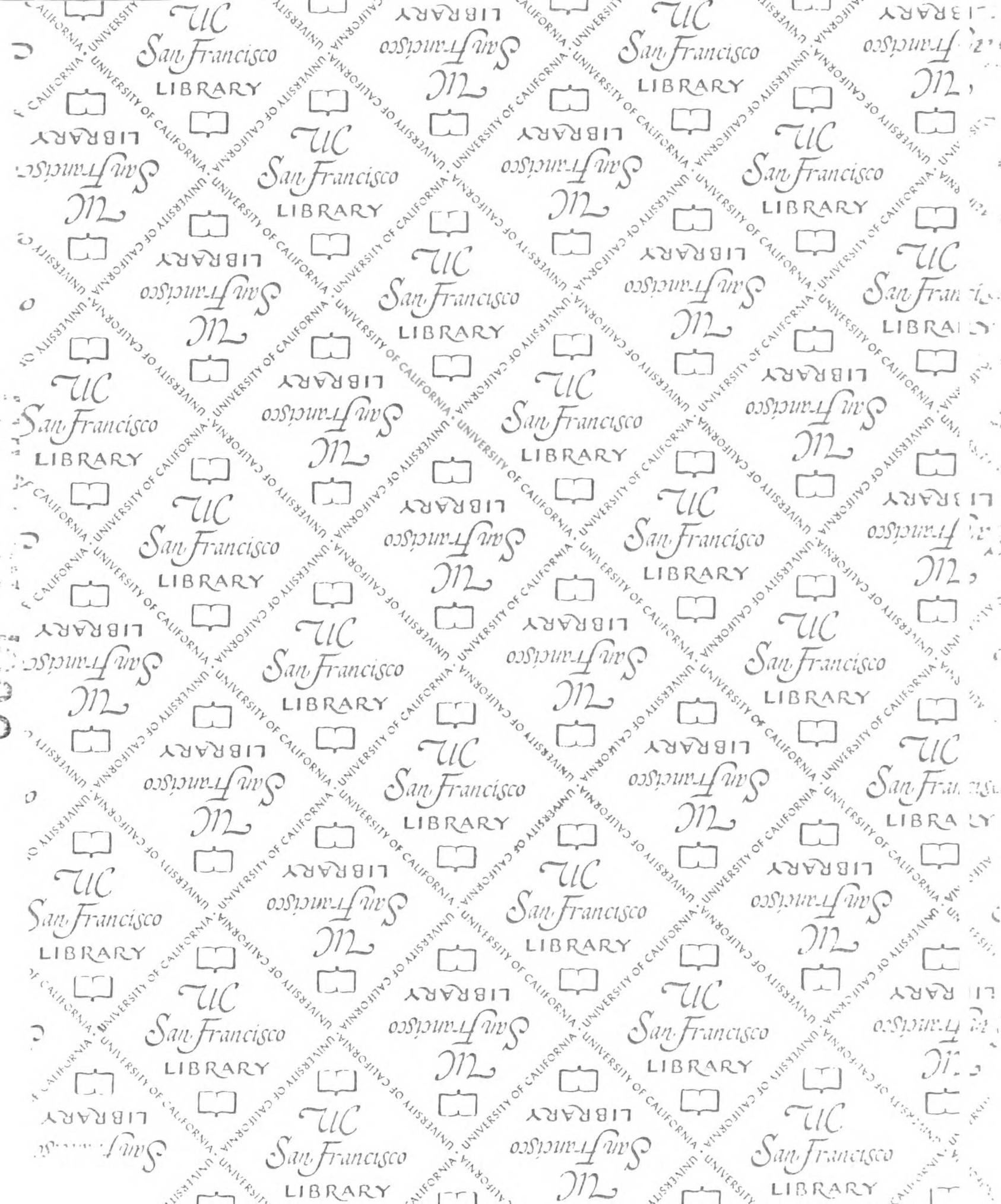
109. Rorschach, H.E., Change, D.C., Hazlewood, C.F., and Nichols, B.L., *The diffusion of water in striated muscle.* Ann of N.Y. Acad Sci, 1973. **204**: p. 444-452.

110. Mow, V.C., Holmes, M.H., and Lai, W.M., *Fluid transport and mechanical properties of articular cartilage: A review.* J Biomech, 1984. **17**(5): p. 377-394.

111. Setton, L.A., Zhu, W., Weidenbaum, M., Ratcliffe, A., and Mow, V.C., *Compressive properties of the cartilaginous end-plate of the baboon lumbar spine.* J Orthop Res, 1993. **11**(2): p. 228-239.

112. Thompson, J.P., Pearce, R.H., and Ho, B. *Correlation of gross morphoogy and chemical composition with magnetic resonance images of human lumbar intervertebral discs.* in *Transactions of the 34th Annual Meeting.* 1988. Atlanta, GA: Orthopaedic Research Society.

113. Chiu, E.J., Newitt, D.C., Hu, S.S., Lotz, J.C., and Majumdar, S. *MRI measurement of water diffusion in the human intervertebral disc with compression.* in *Transactions of the 43rd Annual Meeting.* 1997. San Francisco, CA: Orthopaedic Research Society.





# For reference

Not to be taken from the room.

